Interplay of Histone Methyl Writers and Erasers in the Brain

by

Christina N. Vallianatos

A dissertation submitted in partial fulfillment
of the requirements for the degree of
Doctor of Philosophy
(Human Genetics)
in the University of Michigan
2019

Doctoral Committee:

Assistant Professor Shigeki Iwase, Chair
Professor Sally Camper
Professor Yali Dou
Assistant Professor Kenneth Kwan
Assistant Professor Stephen Parker

Christina N. Vallianatos

cvallia@umich.edu

ORCID iD: 0000-0003-3159-3200

Dedication

To my parents, who have given me everything.

None of this would be possible without you.

To the KDM5C families, who have given my work meaning.

None of this would matter without you.

Acknowledgements

This has all been possible because of the cumulative efforts of so many people. Scientifically, to those who came before me and helped pave the way with their findings. Professionally, to those who gave me a chance and supported me along my journey. Personally, to those who believed in me and showed me kindness. Thank you.

To the University of Michigan, my home for the last 13 years. I'm grateful for the opportunities and experiences I've had in Ann Arbor that have shaped me into the person, leader, and scientist that I am today. To Rackham Graduate School for their constant support of graduate students. Their exceptional programming, robust funding, and generous services, including professional development workshops, grants, and counseling sessions, have been invaluable resources for me throughout my graduate studies. To PIBS and OGPS for uniting the biomedical trainees. I've been impressed at the growth of their expanding career, wellness, and outreach events, all of which have helped me tremendously. To the Department of Human Genetics for being my home department even before grad school. I value the excellent education I received, the opportunities for scientific growth, the engagement of the faculty, the fellowship with student peers, the support from the administrative staff, and the general comradery within the department.

To the many funding sources who made this research possible. It's a privilege to be paid to go to school and do what you love, and I'm extremely grateful. To the collaborators who elevated our research. I appreciate the opportunities to learn new things and expand our research questions. To the students I've trained, for their contributions to this research. Thanks for your commitment and motivation, and especially for being patient with me through poorly planned

experiments. To the KDM5C families for sharing your stories. Working with you has given my research new meaning, and I've gained valuable perspectives I'll carry with me forever. To my thesis committee for their insight, expertise, and guidance on my research projects. To Dr. Sally Camper for always going above and beyond in your support, professionally and personally. To Dr. Miriam Meisler for training me as an undergrad and continuing to support me all these years later. To Dr. Guy Lenk for always being someone I could come to for advice, support, coffee, and lols.

To the Iwase lab, past and present, for being my lab family. Thank you for creating a collaborative, fun, and supportive work environment. I'm grateful for the teamwork on projects, endless help with experiments, (too) many late night and weekend lab sessions, coffee dates, birthday treats, clever Halloween costumes, happy hours, holiday parties, celebrations for grants and papers, and so much more. Thank you all for the precious memories. I couldn't ask for better colleagues and friends, and I'm so excited to see where each of you goes in life.

To my friends and family, near and far. I feel extremely fortunate to have you as my support system. To Adrian for always believing in me. Thank you for making me laugh, letting me be myself, and being on my team. To my parents for giving me everything I could hope for. Your encouragement, support, and love mean the world to me.

Last but certainly not least, to Shigeki, for being my PhD advisor, mentor, and scientific guide. Truly none of this would be possible without you. Thank you for trusting me with the projects you've worked on for so long. It has been a privilege to be your first student, to see your ideas evolve and watch the lab grow, to work with you and learn from you. You have an enthusiasm for your work that can be contagious, and your drive to push the limits of human knowledge is inspiring. I admire your creative way of thinking, and I look forward to seeing more successes come from you and the lab. Thank you for introducing me to the world of

chromatin biology, for training me in a wide variety of techniques from biochemistry to genomics, for being patient with me through failed experiments and difficult moments, for encouraging my scientific growth, for supporting every single opportunity I pursued, and for giving me the flexibility to find my place in the science world and pursue my passion.

Table of Contents

List of Tables

List of Figures

Abstract

Dysregulation of histone methylation has emerged as a major contributor of neurodevelopmental disorders (NDDs) such as autism and intellectual disability. Methylation of histone H3 lysine 4 (H3K4me) is an extensively regulated post-translational modification with 13 writer and eraser enzymes modulating this mark, nine of which are mutated in human NDDs to date. However, roles of H3K4 methylation and demethylation in the central nervous system are not well understood. My thesis research aims to address this gap in knowledge and gain insight into the interplay of H3K4me-specific chromatin regulators in normal and pathologic brain development. We propose that H3K4me balance is critical for proper cognitive development, and that H3K4me-regulators orchestrate developmental programs in the brain by fine-tuning methylation at key genomic loci. We also posit the opposite nature of writer-eraser enzymes reveals a potential for enzyme activity modulation to "neutralize" histone methylation and serve as a therapeutic.

The work in this dissertation focuses on H3K4me writer and eraser duo *KMT2A* and *KDM5C*, responsible for human NDDs Wiedemann-Steiner Syndrome (WDSTS) and mental retardation, X-linked, syndromic, Claes-Jensen type (MRXSCJ), respectively. Mouse models of each recapitulate the cognitive and behavioral impairments characteristic of the respective human disorders, yet mechanistic studies of how *KDM5C* and *KMT2A* affect the brain are lacking. I reported a new MRXSCJ-associated human mutation in *KDM5C* that specifically compromises gene-regulatory function but not enzymatic activity or stability, suggesting non-enzymatic roles for KDM5C and a new pathological mechanism for loss-of-function mutations.

To explore the roles of KMT2A and KDM5C in the brain, I systematically characterized *Kmt2a*- and *Kdm5c*-deficient mice at molecular, cellular, and behavioral levels. We show similar phenotypes between *Kmt2a*- and *Kdm5c*-mutant male mice, including altered transcriptomes and impaired dendritic morphology in amygdala, and increased aggressive behaviors, revealing commonalities despite loss of opposite H3K4me regulators. I generated *Kmt2a-Kdm5c*-double-mutant mice to determine if pairwise relationships between opposing enzymes could "neutralize" histone methylation and specifically combat loss of the opposite enzyme to ameliorate disease phenotype(s). We observed a clear reversal in double mutant male mice of neuron morphology and behavior deficits, and partially corrected H3K4me3 landscapes and transcriptomes. Female double mutant mice exhibited exacerbated fear memory deficits, and rescued social behaviors.

Together, the studies in this dissertation reveal functional consequences of altered KMT2A and KDM5C function, both individually and in concert, in the central nervous system, and provide the field with a proof-of-principle concept of opposing enzyme dual modulation to combat their associated disorders.

Chapter 1 — Introduction

Overview of dissertation

Recent large-scale exome sequencing studies led to the discovery that mutations of histone methyl regulators are overrepresented in neurodevelopmental disorders (NDDs) including autism and intellectual disability. Yet we still know very little about how histone methyl dysregulation leads to such cognitive and behavioral deficits. This dissertation focuses on regulators of histone H3 lysine 4 methylation (H3K4me) and their molecular functions in the brain.

H3K4me is an intricately regulated post-translational modification of active chromatin, with eleven associated enzymes mutated in several neurodevelopmental disorders (NDD). Chapter 1 provides an introduction to H3K4me regulators in the context of NDDs and summarizes major progress in identification of mutations and functional investigations of these genes in the central nervous system. Chapter 2 characterizes a new human mutation in eraser gene *KDM5C* and discusses enzymatic activity-independent roles for such enzymes in transcriptional regulation. Chapter 3 investigates the effects of loss of writer-eraser duo KMT2A and KDM5C, both individually and together, at molecular, cellular, and behavioral levels in male mice, and reveals dual modulation as a proof-of-principle therapeutic strategy. Chapter 4 explores KMT2A and KDM5C in female mouse behavior. Finally, Chapter 5 offers conclusions and perspectives on how this work has shaped the field, and suggestions for future experiments.

Introduction to H3K4me regulators in the brain

Histone proteins are the spools to the thread of DNA, allowing our genetic code to become compact and organized inside the nucleus (Figure 1.1). Chromatin remodeling is a dynamic process that regulates gene expression via changes in DNA accessibility, where post-translational modifications on N-terminal tails of histone proteins are an integral element influencing chromatin structure. Advent of next-generation sequencing led to a rapid growth of the list of histone modifiers that are mutated in human neurodevelopmental disorders (NDDs). These disorders include a plethora of intellectual disability (ID) syndromes (Najmabadi et al., 2011) and schizophrenia (Takata et al., 2014). Additionally, recent large-scale exome sequencing studies highlighted dysregulation of histone methylation as a major contributing factor of autism spectrum disorders (ASD) (De Rubeis et al., 2014b; Iossifov et al., 2014). Therefore, regulation of histone modifications appears to be essential for the development and function of the central nervous system. However, the roles of these mutated histone modifiers in the brain are not well understood.

Methylation of lysine 4 of histone H3 (H3K4me) is one such modification, which is associated with gene activation. Three statuses of lysine methylation, namely mono-, di-, and tri-methyl groups (me1/2/3), confer an additional layer of complexity in chromatin remodeling events. Using technologies such as chromatin immunoprecipitation coupled with next-generation sequencing (ChIP-seq), the genomic signatures of these epigenetic marks can be uncovered for specific cell types and developmental stages. Early genome-wide studies using cultured cell lines revealed that H3K4me1 is a hallmark of enhancers (Heintzman et al., 2009; Heintzman et al., 2007), while H3K4me2/3 mark promoters of actively transcribed genes (Barski et al., 2007; Zhu et al., 2013). Mono- and di-methylated H3K4 appear as broad ChIP-seq peaks, marking stretches of open chromatin throughout the genome (Barski et al., 2007). In the human brain, similar to the

observations in cell cultures, tri-methylated H3K4 is concentrated in sharp peaks 1-2 kilobases (kb) in length at transcription start sites of regulatory sequences such as proximal gene promoters (Cheung et al., 2010). These neuron-specific H3K4me3 peaks are enriched at promoters of genes that control synaptic function (Cheung et al., 2010). Additionally, unmethylated H3K4 (me0) also recruits a distinct set of proteins with transcriptional repressors (Lan et al., 2007; Ooi et al., 2007), including *DNMT3L*, which tethers CpG DNA methylation enzymes (Ooi et al., 2007).

Two families of proteins serve as primary regulators of H3K4me: histone lysine methyltransferases (KMTs) are the "writers" which place the methyl marks onto histones; and histone lysine demethylases (KDMs) are the "erasers" which remove them. An additional class of proteins recognizes and "reads" H3K4me status, serving as effectors to recruit chromatin remodeling proteins and regulate transcriptional state. Remarkably, among other methylation sites on histones, H3K4 appears to be the most extensively targeted position by the largest number of writer and eraser enzymes. To date, in higher eukaryotes, at least seven KMTs and six KDMs have been shown to regulate H3K4me with differential substrate preference to me0-3 (Greer and Shi, 2012; Ruthenburg et al., 2007; Zhou et al., 2016). This intricate balancing act at H3K4 by opposing mechanisms might have evolved to sculpt epigenetic landscapes that achieve delicate developmental and cellular processes in complex organs such as brain. Indeed, pioneering work has shown dynamic gain and loss of H3K4me3 throughout the genome in the neurons of developing human prefrontal cortex (Cheung et al., 2010; Shulha et al., 2013). While H3K4me regulation has been unequivocally shown to be crucial for normal development in metazoans through *HOX* gene regulation (Soshnikova and Duboule, 2008), the function and regulation of this methylation mark in the developing nervous system is not fully understood. The dynamics of chromatin regulation in the brain is the focus of the emerging field of neuroepigenetics.

Among the 13 enzymes that target H3K4me in humans, mutations in five KMT and four KDM genes have been associated with neurodevelopmental disorders to date (Figure 1.2). An excellent review summarized the implications of H3K4 demethylases in neurodevelopmental disorders with a focus on regulatory mechanisms of the demethylases (Wynder et al., 2010). Shen *et al*. provided a comprehensive view on writer and eraser enzymes for H3K4me in brain disorders from a clinical perspective, including data from human samples and animal models (Shen et al., 2014). More recently, alterations of *KMT2F* in schizophrenia (Takata et al., 2014), *KDM1A* in Kabuki/KBG-syndrome (Tunovic et al., 2014), and *KDM5A* and *KDM5B* in ID (Athanasakis et al., 2014; Najmabadi et al., 2011) have been reported, which were not covered by these earlier reviews. New exome sequencing of a large cohort of individuals with ASD also identified *KMT2C* and *KDM5B* (De Rubeis et al., 2014b; Iossifov et al., 2014). It may only be a matter of time before alterations in the remaining enzymes are identified in neurological disorders. Furthermore, genetic mutations in two reader proteins for H3K4me status, PHF21A and PHF8, have been associated with ID syndromes (Kim et al., 2012; Laumonnier et al., 2005) (Figure 1.2). Here, we aim to summarize the recent progress in understanding the molecular and cellular consequences of mutations in H3K4me regulators. Although very limited reports described the function of H3K4me regulators at a genomic level in the brain, by reviewing the data obtained from non-brain tissues and cell types, we further discuss how intricate balancing and readout of H3K4me can be engaged in brain development genome-wide.

H3K4 methyltransferases

Methylation of H3K4 is generated primarily by the lysine (K)-specific methyltransferase 2 (KMT2) family of enzymes (Allis et al., 2007; Shilatifard, 2012). This class of proteins is characterized by the presence of a catalytic Su(var), Enhancer of Zeste, Trithorax (SET) domain,

conferring lysine-specific methyltransferase function. While each writer enzyme has been shown to generate all three methylation marks on H3K4 (Greer and Shi, 2012), specific substrate preference is often conferred by additional cofactor proteins. For example, while KMT2A itself can generate mono- and di-methyl marks on H3K4, physical contact with cofactors including RbBP5, Ash2L, and WDR5 allows tri-methylation by KMT2A (Dou et al., 2006). Additionally, PRDM16, whose PR domain shares high homology to the SET domain, was recently identified as having H3K4 methyltransferase activity (Zhou et al., 2016).

The six KMT2 family members can be broken into three subclasses of protein pairs that have evolved distinct features and functions (Rao and Dou, 2015). *KMT2A* and *KMT2B* are homologs of *Trithorax* (*Trx*) gene found in lower organisms such as fly, whereas *KMT2C* and *KMT2D* are thought to be duplicated from the common ancestor gene *Trithorax-related* (*Trr*) in fly (Shilatifard, 2012). *KMT2F* and *KMT2G* are structurally distinct from the KMT2A-D enzymes. Similar to the *KMT2A/B* and *KMT2C/D* pairs, mammalian *KMT2F* has a cognate paralog, *KMT2G*, and both share a common ancestor gene *SET1* in budding yeast (Shilatifard, 2012). Four of these six KMTs have been found mutated in neurodevelopmental disorders thus far. Remarkably, evidence suggests that within each protein pair, one enzyme cannot compensate for a mutation in the other, indicating that each KMT in the duo has non-redundant functions.

KMT2A in a developmental disorder with neurological symptoms

The human *KMT2A* gene (also known as *MLL, ALL-1*) was first discovered for its involvement in chromosomal translocations in acute leukemia (Cimino et al., 1991; Zieminvanderpoel et al., 1991). As discussed above, *KMT2A* is responsible for generating mono-, di-, and tri-methylated H3K4 through its SET domain and by interaction with cofactors (Dou et al., 2006). Recently, dominant *de novo* mutations in *KMT2A* have been identified in individuals

with Wiedemann-Steiner syndrome (*Mendelian Inheritance in man* (MIM) no. 605130), a developmental disorder with clinical features including intellectual disability, microcephaly, and short stature (Jones et al., 2012; Strom et al., 2014). The majority of identified mutations are heterozygous *de novo* mutations predicting a premature truncation of the protein product (Figure 1.3), suggesting haploinsufficiency of *KMT2A* is responsible for these clinical phenotypes. Since the catalytic SET domain is located at the C-terminal end of the protein, the truncations most likely result in a loss of enzymatic activity. Given that H3K4me is a signature of actively transcribed chromatin, the pathogenic mechanism may be insufficient transcription of key genes in the central nervous system. However, several lines of evidence suggest the molecular etiology can be much more complex than this simplistic scenario.

KMT2A harbors both transcriptional activator and repressor activities. These two opposite functions appear to be located at the SET-containing C-terminal portion and the PHD-containing N-terminal segment, respectively (Zeleznik-Le et al., 1994). A cluster of three plant homeodomain (PHD) fingers, located in the middle of the KMT2A molecule (PHD1-PHD3 in Figure 1.3), plays an important role in demarcating the two opposite activities. PHD fingers are one of the major modules that can recognize specifically modified histones, and thus can act as "readers" of chromatin modifications (Musselman and Kutateladze, 2011; Wysocka et al., 2006). Interestingly, KMT2A PHD3 binds to both H3K4me3, a reaction product of KMT2A itself, as well as the transcriptional corepressor protein Cyp33 (Wang et al., 2010). While the role of PHD1 remains unknown, PHD2 appears to have ubiquitin ligase activity towards both histones and KMT2A itself (Wang et al., 2012), facilitating the degradation of KMT2A (Wang et al., 2012). Thus, beyond the canonical function of PHD fingers as reader modules, the KMT2A-PHD cluster represents a novel regulatory hub, which defines the balance between transcriptional activator and repressor functions. Notably, some of the Wiedemann-Steiner syndrome mutations,

including a missense mutation, fall within this PHD finger cluster (Figure 1.3). Therefore, these mutations can potentially lead to both down- and up-regulation of KMT2A-target genes in Wiedemann-Steiner syndrome. Future studies can address these possibilities using cells harboring these mutations.

Additionally, alternative splicing events have been reported in the PHD3-encoding area (Rossler and Marschalek, 2013). Yeast two-hybrid experiments revealed that these PHD3 isoforms differ in their ability to interact with Cyp33-containing corepressor complex, suggesting an influence in the transcriptional regulatory activities of KMT2A (Rossler and Marschalek, 2013). Perhaps each transcript type has a unique expression pattern in the developing nervous system. It is plausible that different *KMT2A* isoforms function as either an activator or a repressor in a cell-type-dependent manner in neurons and glia cells within the central nervous system. Functional studies in developing brains are necessary to determine to what extent this alternative splicing event exists and how it contributes to molecular etiology *in vivo*.

Expression of KMT2A peaks in the neocortex in human fetal brains, declining slightly through early stages of postnatal development but then gradually increasing into adulthood (Johnson et al., 2009). This expression signature hints at the importance of KMT2A during neocortical development. Consistently, *KMT2A* plays an essential role in mouse postnatal neurogenesis (Lim et al., 2009). Lim *et al.* demonstrated that important neurogenesis-promoting genes have bivalent chromatin domains carrying both activating H3K4me3 and repressive H3K27me3 marks, and that presence of *KMT2A* at these poised loci is necessary to promote an active transcription state (Lim et al., 2009). Therefore, impaired neurogenesis by *KMT2A* mutations might be responsible for the cognitive deficits observed in Wiedemann-Steiner syndrome.

On a genomic scale, KMT2A has been shown to be required for generating 5 % of the active H3K4me3 marks on promoters in mouse embryonic fibroblasts (Wang et al., 2009b). Relatively weak impact on global H3K4me3 landscape upon the loss of *KMT2A* suggests a redundant, if not completely redundant, function of paralog *KMT2B* and the four other KMT2 family members. Recent studies in mouse embryonic stem cells (mESCs) re-confirmed the functional redundancy between *KMT2A* and *KMT2B* in generating global H3K4me3, whereas removal of *KMT2B* alone lead to a 2.5-fold reduction in H3K4me levels at bivalent promoters (Denissov et al., 2014). Reconciling these findings with previous evidence of *KMT2A* at bivalent promoters in neural precursor cells (Lim et al., 2009), it is plausible that KMT2A and KMT2B are responsible for generating neural precursor- and mESC-specific bivalent promoters, respectively. Heterozygous *de novo* mutations in Wiedemann-Steiner syndrome indicate that alteration of H3K4me levels at only limited genomic loci is sufficient to attenuate proper brain development. Further studies to identify direct gene targets of KMT2A during central nervous system development will be imperative in elucidating a functional role for this writer enzyme in the brain.

<u>*KMT2C*: a new gene for Kleefstra syndrome and ASD</u>

KMT2C (also known as *MLL3*, *HALR*) contributes to the implementation of mono- and di- methylation marks on H3K4 in mammalian cells (Hu et al., 2013; Lee et al., 2013). KMT2C was originally discovered as a human homologue of *Drosophila* gene *Trr* in the chromosomal region lost in individuals with developmental defects of the forebrain and myeloid leukaemia (Ruault et al., 2002; Tan and Chow, 2001). In recent years *KMT2C* variants have been found in two neurodevelopmental disorders. Kleefstra *et al.* identified a *KMT2C* mutation in an individual with Kleefstra syndrome (MIM no. 610253), a neurodevelopmental spectrum disorder with

hallmarks including severe intellectual disability, brachy(micro)cephaly, and epileptic seizures. The female individual carries a heterozygous *de novo* nonsense mutation, p.Arg1481X (Kleefstra et al., 2012) (Figure 1.3), resulting in loss of more than half of the KMT2C protein. This truncation of the C-terminal segment includes loss of the enzymatic SET domain, which likely results in the loss of histone methyltransferase activity. Additionally, five mutations were identified in recent large-scale exome sequencing of individuals with autism spectrum disorder (ASD) (Figure 1.3) (De Rubeis et al., 2014b; Iossifov et al., 2014). These new variants will require further studies to examine their consequences on protein function and pathogenic contribution to neurodevelopment. Clearly, disruption of *KMT2C* and its contribution to a delicate epigenetic regulatory network may underlie broad neurodevelopmental abnormalities including cognitive and social anomalies.

While neuron-specific targets of KMT2C regulation have yet to be discovered, it is known that this writer is highly expressed in the human brain (Nagase et al., 2000; Tan and Chow, 2001). *KMT2C* expression levels peak during human fetal development and remain steady into adulthood (Johnson et al., 2009). Notably, expression in the adult brain is stronger in the hippocampus, caudate nucleus, and substantia nigra, regions of the brain associated with learning, memory, and social behaviors (Nagase et al., 2000). These data implicate roles for *KMT2C* in the developing brain as well as in mature neuronal circuitries.

Genome-wide functional studies found that KMT2C contributes to installation of mono- and di-methylation of H3K4 at gene enhancers (Hu et al., 2013; Lee et al., 2013). H3K4me1/2 at enhancers is required for full activation of genes. Interestingly, KMT2C can also be found at gene promoters, where promoter-bound KMT2C functions to repress gene transcription (Cheng et al., 2014). These studies raise a possibility that KMT2C can both activate and repress gene transcription depending on localization along chromatin. Studying the chromatin regulatory

network involving KMT2C will lead to a better understanding of the tight gene regulation in brain development, and can pave the way towards targeted therapeutic approaches.

KMT2D mutations are a major cause of Kabuki syndrome

The human histone lysine methyltransferase *KMT2D* (also known as *ALR*, *MLL2 or MLL4*) is partially functionally redundant to *KMT2C*, and the two enzymes are responsible for a majority of the H3K4me1/2 marks in mammalian cells (Hu et al., 2013; Lee et al., 2013). Exome sequencing revealed *KMT2D* to be a major cause of Kabuki syndrome (*MIM* no. 147920) (Ng et al., 2010), an autosomal dominant congenital intellectual disability disorder characterized by unique facial features. Over 100 unique mutations in *KMT2D* have been identified in Kabuki syndrome individuals, a majority of which result in premature termination of the protein product (Banka et al., 2013; Banka et al., 2012; Bogershausen and Wollnik, 2013; Hannibal et al., 2011; Li et al., 2011; Micale et al., 2011; Ng et al., 2010; Paulussen et al., 2011) (Figure 1.3). Though most mutations occur *de novo*, many are recurrent in unrelated individuals, indicating the importance of these repeatedly mutated amino acids in KMT2D function and/or suggesting the nature of the DNA is particularly mutable.

The large number of mutations appears to cluster into three distinct locations along the protein (Figure 1.3). One mutation group surrounds a triple PHD finger cluster (PHD4-PHD6 in Figure 1.3). These three PHD fingers bind unmethylated arginine 3 on histone H4 (H4R3me0), thereby promoting the access of the SET domain to its substrate, namely the histone H3 N-terminus (Dhar et al., 2012). This trans-tail crosstalk enables KMT2D to efficiently methylate H3K4 in a nucleosomal context (Dhar et al., 2012). Importantly, two missense mutations in Kabuki syndrome, p.Cys1430Arg and p.Cys1471Tyr in the PHD4-6 cluster, showed decreased binding affinity to H4 and reduced H3K4 methylation activity, when nucleosomes were used for

the methyltransferase assays (Dhar et al., 2012). Thus, Kabuki syndrome mutations in this cluster ultimately result in loss-of-function of KMT2D methyltransferase activity. The second mutation cluster occurs in an area of the protein lacking a characterized functional domain, yet this region may be significant for the 3-dimentional structure and function of the enzyme. The third mutation group occurs around the C-terminal PHD finger, whose function remains unknown. Similar to *KMT2A* and *KMT2C* mutations, over 30 variants in *KMT2D* lead to truncation of C-terminal SET catalytic domain, likely resulting in the loss of enzymatic function.

A role for *KMT2D* in neuronal differentiation has been suggested from recent *in vitro* studies. Using human pluripotent NT2/D1 carcinoma cells, which commit to a neuronal state upon retinoic acid treatment, Dhar *et al.* showed that shRNA knockdown of *KMT2D* results in attenuation of morphological changes and impaired activation of neural differentiation hallmark genes including *HOXA1-3* and *NESTIN* (Dhar et al., 2012). The insufficient expression of these *KMT2D* target genes was associated with decreased H3K4me levels. Thus, loss-of-function mutations in *KMT2D* in Kabuki syndrome likely result in a decrease in these methyl marks necessary to promote expression of key neuronal differentiation genes, and ultimately hinder commitment of stem cells to a neuronal state. These data suggest a critical role for *KMT2D* in neuronal differentiation. Whether this writer enzyme also contributes to maintenance of neuronal function later in life remains to be seen.

Several lines of evidence suggest a cooperation of KMT2C and KMT2D in neuronal differentiation. First, knockdown of *KMT2C* in the NT2/D1 system resulted in down-regulation of KMT2D-target genes, although to a lesser extent compared to *KMT2D* knockdown (Dhar et al., 2012). Second, KMT2C and KMT2D can be co-purified in the same protein complex (Cho et al., 2007). Third, both KMT2C and KMT2D are found at gene enhancers and are required for enhancer activation (Hu et al., 2013; Lee et al., 2013). These results raise a possibility that

deficiency in common molecular pathways, including enhancer activation of specific genes, impinge on Kabuki and Kleefstra syndromes, though they were originally described as distinct conditions.

KMT2F: a new schizophrenia susceptibility gene

KMT2F (also known as *SET1*, *SETD1A*) encodes an H3K4 writer enzyme capable of generating mono-, di-, and tri-methylation marks *in vitro* (Hu et al., 2013; Lee and Skalnik, 2005). Notably, in cells, KMT2F/G and Set1 appear to be responsible for bulk H3K4me3 (Ardehali et al., 2011; Hallson et al., 2012; Mohan et al., 2011; Wu et al., 2008).

Recently, Takata *et al*. have identified *KMT2F* as a risk gene for schizophrenia (*MIM* no. 181500), a common and severe psychiatric disorder characterized by delusions, hallucinations, and disorganized thinking (Takata et al., 2014). It is significant that two loss-of-function mutations (Figure 1.3) were found in two phenotypically similar but unrelated schizophrenia individuals with a secondary diagnosis of obsessive-compulsive disorder (OCD) (*MIM* no. 164230). It is possible that individuals with *KMT2F* mutations define a new subset of schizophrenia with OCD comorbidity (Takata et al., 2014). The first mutation is a *de novo* frameshift resulting in the introduction of a premature stop codon and likely leads to the loss of enzymatic activity carried in the C-terminal SET domain. The second individual harbors a *de novo* indel that alters a canonical splice acceptor site. This change is expected to cause a loss of exon 16 and disruption of the N-SET domain, which is critical for proper H3K4 methyltransferase function of the neighboring SET domain *in vitro* (Mersman et al., 2012).

As previously discussed, KMT2F contributes to deposition of the activating H3K4me3 mark, which shows sharp peaks near transcription start sites of active genes (Barski et al., 2007). While H3K4me1 is enriched at gene enhancers, H3K4me3 levels at enhancers appear to be low

(Heintzman and Ren, 2007; Heintzman et al., 2007). Hence, KMT2F acts as an H3K4me3 writer enzyme at promoters, in sharp contrast to KMT2C/D function at enhancers. Indeed, a KMT2F-interacting protein, Cfp1, recruits H3K4me3 activity, likely mediated by KMT2F/G, at CpG islands which are prevalent in mammalian gene promoters (Clouaire et al., 2012). Recent studies found that loss of Cfp1 in mESCs lead to global loss of DNA-damage induced accumulation of H3K4me3 at the promoters of DNA-damage responsive genes (Clouaire et al., 2014). However, induction of genes was mildly affected in Cfp1-mutant mESCs except for few dramatically affected genes, suggesting a role for KMT2F in context-dependent transcriptional activity (Clouaire et al., 2014). H3K4me3 plays a crucial part in recruiting the general transcription machinery, TFIID, through an interaction between H3K4me3 and the PHD finger of TAF3, a TFIID component (Lauberth et al., 2013; Vermeulen et al., 2007). Thus, the KMT2F mutations may lead to insufficient gene transcription of important neural circuitry genes via impaired placement of H3K4me3 at their promoters.

Psychiatric disorders are often characterized by disorganization of neuronal networks, where alteration of these networks from an early time point leads to life-long disorders. The inability to activate the correct genes at the correct time during brain development due to a loss of KMT2F function could lead to improper establishment of neuronal networks and, ultimately, impaired brain function manifested by schizophrenia. However, brain-specific roles of KMT2F or specific genomic loci that are targets of KMT2F in brain cells have yet to be defined. The aforementioned genetic studies open an avenue for interrogating chromatin regulatory mechanisms that underlie pathogenesis of psychiatric disorders.

H3K4 demethylases

Histone methylation was thought to be an irreversible epigenetic mark, thereby serving as memory of cellular identities. The identification and characterization of histone demethylases revealed that methylation is not a permanent event but rather a dynamic process. Four H3K4me eraser enzymes, KDM1A, KDM5A, KDM5B, and KDM5C, are mutated in neurodevelopmental disorders, evidence that the balance between methylation and demethylation is intricately regulated during brain development and function.

KDM1A in a unique neurodevelopmental syndrome

KDM1A (also known as *LSD1*, *BHC110*) was the first histone lysine demethylase gene to be identified (Shi et al., 2004). A flavin-containing amine oxidase homolog, KDM1A catalyzes the oxidative demethylation of H3K4me1/2. Recently, a mutation in *KDM1A* has been identified in a new neurodevelopmental disorder. Tunovic *et al*. describe two *de novo* variations in one male with mixed features of Kabuki syndrome and KBG syndrome (Tunovic et al., 2014). As discussed above, Kabuki syndrome is a developmental and cognitive disorder frequently associated with mutations in other histone lysine regulators, *KMT2D* (Ng et al., 2010) or *KDM6A* (Miyake et al., 2013). KBG syndrome (MIM no. 148050) is characterized by macrodontia, craniofacial dysmorphism, and delay in brain development (Sirmaci et al., 2011). One identified variation was p.Tyr785His in the C-terminal amine oxidase domain of KDM1A. The other alteration was a deletion of three nucleotides in *ANKRD11,* which lead to the loss of an evolutionally conserved lysine residue. Haploinsufficiency of the *ANKRD11* gene, which encodes an ankyrin-repeat containing a transcription coactivator, was previously identified as a causative agent for KBG syndrome (Sirmaci et al., 2011). Based on the new mixed features of Kabuki and KBG syndromes found in the individual, the authors postulated that the *KDM1A*

mutation might be responsible for the Kabuki-related symptoms such as ptosis and downturned month corners.

How could mutations in counteracting enzymes over H3K4me, namely KMT2D and KDM1A, both result in Kabuki-related syndromes? The majority of KMT2D mutations appear to result in loss of enzymatic activity by truncation of the catalytic SET domain (Ng et al., 2010). One possibility is that the identified p.Tyr785His variant may be a gain-of-function mutation. In this scenario, both loss-of-function mutations in a writer and gain-of-function mutations in an eraser would lead to decreased H3K4me levels. Alternatively, developmental change in expression of key genes might require temporal coordination of KMT2D and KDM1A at specific time points. Deletion of *Kdm1a* in mouse confers embryonic lethality (Wang et al., 2007), as *Kdm1a* is required for gastrulation and differentiation of embryonic stem cells (Wang et al., 2009a; Whyte et al., 2012). Thus, if the *KDM1A* mutation is a loss-of-function one, it is likely hypomorphic. Further studies including identification of additional mutations in *KDM1A* are needed to understand this interesting observation from human genetics studies.

While only one *KDM1A* mutation has been described in a human developmental disorder thus far, studies have demonstrated pivotal roles of this eraser in neurodevelopment. KDM1A was originally discovered as a key subunit of the CoREST complex, which is responsible for the repression of neuronal genes such as Synapsin I (*SYN1*) in non-neuronal cells (Andres et al., 1999; Ballas et al., 2001; Hakimi et al., 2003). The CoREST complex is recruited to neuron-specific genes via an interaction with REST, a sequence-specific DNA binding factor (Andres et al., 1999). Thus, it is possible that the loss of KDM1A function causes aberrant expression of neuron-specific genes in neural precursor and/or glia cells, thereby eventually perturbing proper brain development. Consistently, leaky expression of neuron-specific genes in HeLa cells was observed upon *KDM1A*-knockdown (Shi et al., 2004).

In addition to its involvement in neuronal gene repression, cell-autonomous functions of KDM1A in neurons have also been described. Neuron-specific isoforms of *KDM1A* have been shown to modulate neurite morphogenesis in zebrafish (Zibetti et al., 2010). The first functional study of *KDM1A* in the mammalian nervous system demonstrated that the presence of alternatively-spliced exon E8a dynamically regulates neurite maturation. Loss of *KDM1A* upon shRNA knockdown resulted in decreased dendritic arborizations, secondary branches, and average neurite width, while overexpression lead to an increase in these morphological features in mouse cortical neurons (Zibetti et al., 2010). Inclusion of exon E8a generates a small protruding loop near the catalytic site, which may provide a site for posttranslational modifications and thus confer an additional regulatory element. Taken together, current knowledge supports the idea of a significant role for *KDM1A* in neurodevelopment.

On a genomic level, ChIP studies on individual genes show that KDM1A localizes to active promoters in HeLa and MCF7 cells, suggesting the enzyme is a locus-specific demethylase (Garcia-Bassets et al., 2007; Shi et al., 2004). Additionally, a ChIP-seq study has found that removal of KDM1A from enhancers of pluripotency genes influences commitment of ES cells to differentiate (Whyte et al., 2012). Thus, KDM1A may regulate developmental expression of neuronal genes by controlling methylation of promoters and enhancers. What factors recruit KDM1A in specific regulatory regions in neurons remains unanswered.

KDM5 family: a second class of demethylases

The finding that *KDM1A* is unable to demethylate tri-methylated H3K4 (Shi et al., 2004) raised the possibility that additional demethylases had yet to be discovered. This lead to the identification and characterization of a second class of H3K4 demethylases, the lysine (K)-specific demethylase 5 (KDM5) family proteins (formerly JARID1 family), comprising

KDM5A, KDM5B, KDM5C, and KDM5D (Christensen et al., 2007; Hayakawa et al., 2007; Iwase et al., 2007; Klose et al., 2007; Xiang et al., 2007; Yamane et al., 2007). The enzymatic activity of these erasers lies in two Jumonji domains, JmjN and JmjC. This demethylation signature requires Fe(II) and α-ketoglutarate as cofactors to perform the hydroxylation reaction to remove methylation (Tsukada et al., 2006). Notably, to date three of the four KDM5 family members, KDM5A, KDM5B, and KDM5C, are reported mutated in neurodevelopmental disorders, revealing non-redundant functions of this class of enzymes in the brain.

KDM5A: a candidate intellectual disability gene

KDM5A (also known as *RBP2*, *JARID1A*) was first identified as a binding factor of retinoblastoma RB gene product (Defeojones et al., 1991). Further studies revealed it to be an H3K4me3-specific demethylase from the JmjC-domain-containing family (Christensen et al., 2007; Hayakawa et al., 2007; Iwase et al., 2007; Klose et al., 2007). A mutation in *KDM5A* was recently identified in an individual with autosomal recessive intellectual disability (ARID) (Najmabadi et al., 2011). The homozygous *de novo* missense mutation causes a p.Arg719Gly change, substituting a nonpolar amino acid for a positively charged one. The mutation was predicted to be damaging to KDM5A function (Najmabadi et al., 2011), as it is located within a zinc-finger motif likely responsible for DNA-binding and possibly contributes to enzymatic activity (Chen et al., 2006) (Figure 1.3). It is unknown whether this single amino acid substitution would affect overall stability, DNA-binding property, and/or enzymatic activity of KDM5A. Functional characterization of this missense mutation is necessary to determine its effects on protein function and contribution to intellectual disability.

Little work has been done experimentally to investigate the neuron-specific functions of *KDM5A*, however a role for this demethylase has been described in early embryonic

development (Lopez-Bigas et al., 2008), cellular differentiation (Shao et al., 2014), senescence (Chicas et al., 2012), and circadian gene regulation (DiTacchio et al., 2011). Genome-wide analysis in mammalian cell lines revealed KDM5A is bound at proximal promoter regions, about half of which are H3K4me3-positive, suggesting an inhibitory role for *KDM5A* on many genes via direct action on promoters (Lopez-Bigas et al., 2008). *KDM5A* mRNA levels are high during human prenatal brain development and plateau postnatally, with cortical expression levels remaining slightly elevated throughout adulthood (Johnson et al., 2009). Considering the homozygous mutation in ARID, and the expression data showing *KDM5A* peaks at a very specific prenatal window, it is plausible that *KDM5A* serves as an "off" switch for a subset of genes at significant developmental time points.

KDM5B mutations in ID and ASD

KDM5B (also known as *PLU1*, *JARID1B*) encodes an H3K4-specific eraser enzyme that directly catalyzes the demethylation of mono-, di-, and tri-methylated H3K4 (Iwase et al., 2007; Xiang et al., 2007; Yamane et al., 2007). Until recently, all variants in *KDM5B* had been described in cancer. Next-generation sequencing has since revealed a *de novo* splicing mutation (c.283A>G) in *KDM5B* in an individual with nonsyndromic intellectual disability (ID) (Athanasakis et al., 2014) (Figure 1.3). Six additional variants were newly identified in exome sequencing of a large cohort of individuals with autism spectrum disorder (ASD) (De Rubeis et al., 2014b; Iossifov et al., 2014). These mutations include missense, nonsense, and frameshift variants found all along the protein, many of which lie in key functional domains (Figure 1.3). Further studies are necessary to assess the functional effects of these mutations and the pathogenicity of mutated *KDM5B* in ID and ASD.

KDM5B has been shown to regulate cell fate decisions (Dey et al., 2008) in mouse embryonic stem cells (mESCs) to neuronal lineage (Schmitz et al., 2011). Knockdown of *KDM5B* in mESCs resulted in failure to differentiate to neurons, whereas knockout mouse neural stem cells (mNSCs) revealed that loss of *KDM5B* at this later stage does not affect differentiation to mature neurons (Kidder et al., 2014; Schmitz et al., 2011). Knockout of *KDM5B* in mouse is embryonic lethal (Catchpole et al., 2011), and, remarkably, overexpression also leads to impaired neural differentiation (Dey et al., 2008). This suggests tight control of this demethylase is critical for cell fate determination. Loss of *KDM5B* may result in activation of genes that drive proliferation, while overexpression of KDM5B could lead to aberrant demethylation of differentiation genes in uncommitted cells to hinder neural differentiation. Therefore, either loss- or gain-of function mutations could lead to inefficient neuronal differentiation, which can result in cognitive deficiencies. Identification of additional human mutations in neurological disorders would advance our knowledge about the significance of precise *KDM5B* regulation in neural differentiation.

How *KDM5B* regulates neuronal differentiation has become less of a mystery through recent genome-wide studies. ChIP-seq in mESCs show KDM5B bound to transcription start sites of genes encoding developmental regulators (Schmitz et al., 2011). KDM5B can be recruited to target genomic loci via association with transcription factors such as androgen receptor (Xiang et al., 2007), and act as a transcriptional repressor by stopping H3K4me spreading at gene promoters (Kidder et al., 2014; Scibetta et al., 2007; Yamane et al., 2007). Loss of *KDM5B* in mESCs results in a global increase in H3K4me3 levels and a failure to silence germ cell genes (Schmitz et al., 2011), suggesting that KDM5B is a major H3K4me3 eraser in stem cells. Additionally, KDM5B depletion leads to H3K4me spreading into promoters and gene bodies, revealing a role for KDM5B in restricting H3K4me to specific genomic areas (Kidder et al.,

2014; Xie et al., 2011). Which specific genes' misregulation affects neural differentiation will be a focus of future studies.

Additionally, *KDM5B* has been suggested to regulate genomic stability by dictating the cell's response to DNA damage (Li et al., 2014). This critical function in DNA repair is likely a fundamental aspect of the pathogenicity of *KDM5B* mutations in cancer, however if and how this function could contribute to neurological disorders remains open to investigation.

KDM5C mutations are frequent in X-linked intellectual disability

In 2005, the first mutations in *KDM5C* (also known as *SMCX*, *JARID1C*) were identified as a frequent cause of X-linked intellectual disability (XLID) (Figure 1.3) (Jensen et al., 2005b). Currently, mutations in *KDM5C* are estimated to account for roughly 0.7 to 2.8 % of all XLID (Goncalves et al., 2014; Jensen et al., 2005b; Ropers and Hamel, 2005). The function of this gene's product remained unknown until in 2007 *KDM5C* was discovered as a specific demethylase for di- and tri-methylated H3K4 (Iwase et al., 2007; Tahiliani et al., 2007b). To date, 26 mutations have been reported in individuals with XLID, a majority of which are missense or nonsense variants (Figure 1.3). Of the mutations characterized thus far, functional studies indicate these human variants cause a decrease in *KDM5C* enzymatic activity, suggesting a loss-of-function pathogenic mechanism (Iwase et al., 2007; Tahiliani et al., 2007b). In addition to cognitive deficits, aggressive behaviors are frequently observed in affected individuals (Jensen et al., 2005b; Tzschach et al., 2006) and autistic features have been noted in one case(Adegbola et al., 2008). Along with developmental abnormalities in males, KDM5C variants have also been found in females with short term memory deficits (Simensen et al., 2012).

KDM5C was originally identified as a gene that escapes X-inactivation (Agulnik et al., 1994; Kent-First et al., 1996), and both *KDM5C* and Y-chromosome paralog *KDM5D* are

expressed in a sex-specific manner in mouse brain (Xu et al., 2002). These findings suggest a non-redundant function for KDM5C and KDM5D, and that dosage differences between males and females may underlie differential consequence of KDM5C loss between the sexes. Thus, KDM5C appears to be essential for development of a broad spectrum of cognitive and adaptive functions both in males and females.

KDM5C is broadly expressed, with higher levels in human brain and skeletal muscle (Jensen et al., 2005b). Expression levels of *KDM5C* remain relatively unchanged throughout human brain development, from prenatal to adult stages, suggesting a life-long critical role of this demethylase (Johnson et al., 2009). Within the mouse brain, *Kdm5c* is expressed in areas important for cognitive and emotional behaviors such as the prefrontal cortex, hippocampus, and amygdala (Aguilar-Valles et al., 2014; Xu et al., 2002; Xu et al., 2008). Additionally, this eraser enzyme has been shown to affect dendritic outgrowth in rat cerebellar granule neurons and neuronal survival in developing zebrafish (Iwase et al., 2007). Together, these data may help reveal the pathogenic mechanism for mutations in *KDM5C* leading to neurodevelopmental defects.

Genetic and biochemical interactions of KDM5C with other molecules have provided insights into molecular mechanisms of intellectual disability. *KDM5C* is directly regulated by *ARX*, a homeobox gene frequently mutated in XLID and epilepsy (Poeta et al., 2013). A majority of the *ARX* variants cause a hypomorphic *ARX* allele, leading to a decrease in *KDM5C* expression, thus possibly altering the regulation of H3K4me. *KDM5C* also physically interacts with the transcriptional repressor REST (Tahiliani et al., 2007b). As discussed above, REST represses neuronal genes in non-neuronal cells. Loss of KDM5C was shown to impair REST-mediated repression of neuronal genes, such as *SCN2A* and *SYN1* (Tahiliani et al., 2007b). Defective repression of REST-target genes in KDM5C may be a non-cell autonomous

mechanism of impaired cognitive development. XLID mutations in *KDM5C* may cause dysregulation of REST-target genes due to the impaired H3K4me demethylase activity. Further studies will be necessary to understand functions of KDM5C in different cell types in the brain.

Interestingly, KDM5C appears to have dual function depending on its localization along chromatin in mouse embryonic stem cells, namely transcription corepressor activity at promoters and transcriptional coactivator activity at enhancers (Outchkourov et al., 2013). Thus, it is possible that KDM5C serves as not only a repressor of REST-target genes, but also a coactivator for yet unidentified genes in the brain. Jensen *et al.* recently identified a dozen genes that are commonly dysregulated in multiple lymphocyte lines derived from individuals with *KDM5C* mutations (Jensen et al., 2010). However, it is unclear if gene expression changes in lymphocytes can be translated to the cognitive deficits in individuals with *KDM5C* mutations. Identifying the KDM5C-target genes and mechanisms of their regulation in a genomic context, especially in relevant cell types in the brain, will greatly advance our understanding of molecular mechanisms underpinning this frequent form of ID and ultimately provide hope for therapeutic interventions.

H3K4me reader molecules

Histone methylation itself does not seem to have an impact on higher-order chromatin structure. In addition to writer and eraser enzymes, reader molecules act at H3K4 by recognizing specific methylation states and recruiting effector proteins to influence transcription. Here we discuss two H3K4me-specific reader proteins, PHF21A and PHF8, which have been found mutated in intellectual disabilities. Both genes encode for proteins that belong to the PHD finger (PHF) family.

PHF21A: A methyl "zero" reader in intellectual disability

PHF21A (also known as BHC80) was the first reader molecule discovered to recognize unmethylated H3K4 (HeK4me0) (Lan et al., 2007), introducing unmodified H3K4 as an important addition to the histone code in regulating chromatin state. Recognition of unmodified histone H3 tail by PHF21A PHD finger is specifically inhibited by H3K4 methylations (Lan et al., 2007). Recently, three unrelated individuals with ID and craniofacial anomalies have been identified harboring *de novo* balanced translocations disrupting *PHF21A* (Kim et al., 2012). Two of these translocations, t(11;19)(p11.2;p13.2)dn and t(1;11)(p13;p11)dn, are predicted to lead to truncated protein products resulting in loss of the PHD finger (Figure 2) (Kim et al., 2012). The translocation breakpoint of the third, t(X;11)(p22.2;p11.2)dn, has not been characterized, yet it is likely that loss of protein function is also the pathogenic mechanism at play (Kim et al., 2012). Therefore, H3K4me0 recognition by PHF21A PHD finger appears to be essential for cognitive and craniofacial development. Notably, Potocki-Shaffer syndrome (MIM no. 601224) is a contiguous gene deletion syndrome of the chromosomal region where *PHF21A* is located, namely chromosome 11p11.2 (Potocki and Shaffer, 1996; Shaffer et al., 1993). Potocki-Shaffer syndrome has hallmark clinical features including multiple exostoses, parietal foamina, ID, and craniofacial anomalies. While *EXT2* and *ALX4* have been identified to be responsible for multiple exostoses and parietal foamina, respectively, it remained unknown which gene(s) deletion leads to ID and craniofacial anomalies. The discovery of heterozygous translocations and resulting truncations of *PHF21A* strongly suggests that haploinsufficiency of *PHF21A* is responsible for ID and craniofacial deficits in Potocki-Shaffer syndrome (Kim et al., 2012).

Transcript levels of *PHF21A* are high during early stages of human embryonic development, and remain steady throughout development into adulthood (Johnson et al., 2009). Accordingly, *in situ* hybridization and immunofluorescence experiments in mouse show *Phf21a*

is expressed highly in both the central nervous system as well as in cranial bones of embryonic and adult mice (Iwase et al., 2004; Kim et al., 2012), suggesting an important role for this reader protein in both development and function of nervous tissue and craniofacial bones.

To test whether a loss of *PHF21A* results in defects in neuronal and craniofacial development, Kim *et al*. studied the effects of *phf21a* knockdown by morpholino injection in zebrafish (Kim et al., 2012). Injection of morpholino resulted in pronounced deficiencies in head development including facial dysmorphism. These abnormalities were rescued upon injection of wild-type human *PHF21A* mRNA, supporting the specificity of knockdown effect. Interestingly, *Phf21a* knockout mice show neonatal lethality with an insufficient ability to suckle (Iwase et al., 2006). *Phf21a*-null mice were not closely examined for craniofacial defects; therefore it is also plausible that failure to suckle was a result of craniofacial anomalies, as suggested by the zebrafish studies (Kim et al., 2012). In addition, *PHF21A* appears to be involved in pituitary function through modulation of neurosecretion based on *in vitro* studies using mammalian cells (Klajn et al., 2009). Taken together, these functional studies in model organisms and cells support a critical role for *PHF21A* in neuro- and craniofacial development and function. It would be informative to generate conditional knockout mice in order to assess the effects of loss of *Phf21a* specifically in neurons or cranial bones.

PHF21A is a key subunit of the CoREST complex (Hakimi et al., 2002), as is demethylase KDM1A, discussed above. This protein complex functions to mediate repression of neuron-specific genes (Hakimi et al., 2002), and thus it may not be surprising that loss of *PHF21A* leads to neurodevelopmental phenotypes. Significantly, RNAi knockdown of *PHF21A* in HeLa cells results in a derepression of neuron-specific KDM1A-target genes including *SCN1A* and *SYN1*, suggesting PHF21A occupancy at unmethylated H3K4 is required for sufficient gene repression (Lan et al., 2007; Shi et al., 2005). A neuron-specific CoREST/KDM1A target gene,

SCN3A, showed increased mRNA expression in the lymphoblastoid cell lines from individuals with the translocations mentioned above (Kim et al., 2012). Additionally, ChIP results indicated decreased occupancy of KDM1A at the promoter of *SCN3A* in the PHF21A-translocation cell lines (Kim et al., 2012). Together these findings demonstrate that PHF21A is necessary for KDM1A recruitment and the generation of a repressive chromatin state. It remains unknown what aspects of neurodevelopment are perturbed by PHF21A deficiency and whether the role of PHF21A as a neuronal gene repressor contributes to pathogenesis of ID and craniofacial abnormality.

PHF8, another XLID-associated demethylase, reads H3K4me3

Mutations in X-linked gene *PHF8* were thought to be responsible for Siderius X-lined intellectual disability (XLID) (MIM no. 300263), a syndromic form of ID often associated with facial anomalies such as cleft palate (Abidi et al., 2007; Koivisto et al., 2007; Laumonnier et al., 2005; Qiao et al., 2008; Siderius et al., 1999). In 2010, PHF8 was discovered to be a histone demethylase that mainly targets H3K9me1/2 and H4K20me1 (Feng et al., 2010; Fortschegger et al., 2010; Kleine-Kohlbrecher et al., 2010; Loenarz et al., 2010; Qi et al., 2010; Qiu et al., 2010). Further studies identified that PHF8 contains a PHD finger that specifically recognizes H3K4me3 (Feng et al., 2010; Fortschegger et al., 2010; Horton et al., 2010; Kleine-Kohlbrecher et al., 2010). Thus, PHF8 represents an intriguing example of histone methylation crosstalk engaged in brain development.

All three human *PHF8* mutations in XLID are predicted to truncate the entire or large portion of the JmjC domain, which is responsible for demethylase activity (Figure 1.3). Therefore, loss of histone demethylase function likely underlies pathogenesis of Siderius XLID. Indeed, one missense mutation, p.Phe279Ser, which is located within the JmjC domain (Figure

1.3), leads to dramatic decrease in the histone demethylase activity (Fortschegger et al., 2010; Loenarz et al., 2010). Although any mutation in the PHF8 PHD finger has not yet been clinically observed, the H3K4me3 recognition by this PHD finger appears be significant in fulfilling PHF8 function. The presence of H3K4me3 substantially enhances enzymatic activity of PHF8 via increasing affinity between the histone H3 tail and PHF8 (Horton et al., 2010). Thus, this PHD finger domain is critical for optimal demethylase activity of PHF8. Future human genetic studies may identify loss-of-function mutations in this PHD finger.

Significantly, neuronal functions of *PHF8* have been shown in model systems. Qi *et al*. demonstrated that *PHF8* is essential for brain and craniofacial development, as well as neuronal survival in zebrafish (Qi et al., 2010). PHF8 has also been shown to regulate neuronal differentiation in mouse carcinoma P19 cells, which differentiate into neurons after exposure to retinoic acid. Additionally, knockdown of *PHF8* in primary mouse cortical neurons results in down-regulation of cytoskeleton genes and deficient neurite outgrowth (Asensio-Juan et al., 2012). *PHF8* expression levels sharply decline during early stages of human embryonic development, and plateau at this reduced level throughout development into adulthood (Johnson et al., 2009). Together, these studies support a role for PHF8 in either proliferation of neural progenitor cells or gene expression changes during early differentiation stages in embryonic development.

Genome-wide, PHF8 has been found at the transcription start sites of more than 7,000 RefSeq genes, as well as in gene bodies and intergenic regions (Kleine-Kohlbrecher et al., 2010; Qi et al., 2010), indicating participation of PHF8 in broad epigenome regulation. PHF8-binding sites consist of approximately one-half of total H3K4me3 peaks across the genome. The PHF8 PHD finger, whose reader function permits recognition of H3K4me2/3, likely contributes to recruitment of this reader protein to gene promoters. Additionally, PHF8 interacts with ZNF711,

which is also mutated in XLID, and together the two activate reporter gene expression synergistically (Kleine-Kohlbrecher et al., 2010). Since ZNF711 contains multiple C2H2 zinc-finger domains, ZNF711 may also participate in recruiting PHF8 onto target loci cooperatively with the H3K4me3/PHD interaction. Qi *et al.* showed PHF8 to be a positive regulator of gene expression, dependent on its H3K4me3-binding PHD and catalytic domains (Qi et al., 2010). The function of PHF8 as a transcriptional activator is consistent with its enzymatic activity, which removes repressive histone methylation marks H3K9me1/2 and H4K20me1. Direct PHF8 target genes are involved in various signaling pathways including retinoic acid and Notch, both of which play pivotal roles in neural and craniofacial development (Cau and Blader, 2009; Lupo et al., 2006; Qi et al., 2010).

Interestingly, KDM5C, an XLID-associated H3K4 demethylase discussed above, appears to be a PHF8 target gene, and consequently is down-regulated upon the loss of PHF8. Moreover, PHF8 is localized at nucleoli and required for full activation of rRNA genes (Feng et al., 2010). Given the high demand of protein synthesis in rapidly dividing stem cells, it is plausible that insufficient ribosome biogenesis by PHF8 deficiency may underlie impaired maintenance of developing brain cells observed in zebrafish (Qi et al., 2010). These findings highlight a role for a novel network of chromatin regulators controlling expression of critical neurodevelopmental genes across the genome.

Conclusion & future perspective

The field of neuroepigenetics is rapidly changing as we continue to define roles for chromatin regulating proteins in the central nervous system. As the cost of DNA sequencing declines, the number of mutations discovered in neurodevelopmental disorders is dramatically increasing. We believe it is only a matter of time before many more chromatin regulators are

added to the growing list of proteins implicated in neurological disorders. Functional studies of the molecular consequences of mutations, alongside thorough investigations of cellular and behavioral abnormalities in animal models of these neurodevelopmental disorders, are essential to uncovering the pathophysiology of brain dysfunction.

We mainly discussed consequences of human mutations in the context of enzymatic activity and protein-protein interactions. It is noteworthy that both writer and eraser enzymes have recently been shown to physically interact with long non-coding RNAs (lncRNAs) (Tsai et al., 2010; Wang et al., 2011). Long ncRNAs appear to play roles in recruitment of associated chromatin modifiers to specific genomic loci (Tsai et al., 2010; Wang et al., 2011) and stability of protein complexes (Yang et al., 2014). Thus, an important direction is to test if mutations affect physical interaction of H3K4me modifiers to lncRNAs. At the epigenomic level, pioneering comparative studies of human and primate brain samples have demonstrated that human-specific H3K4me3 exist in the neurons of the cerebral cortex (Bell et al., 2014; Shulha et al., 2012b). Given that neurodevelopmental disorders affect higher-order cognitive and adaptive functions, it will be highly informative to test if such human-specific H3K4me landscapes are altered by the mutations.

As summarized in earlier work (Shen et al., 2014), animal models for neurodevelopmental disorders associated with H3K4me dysregulation will be invaluable tools to dissect molecular and cellular mechanisms, as well as for drug development. Thus far, knockout mouse lines of three H3K4me enzymes, KMT2A (Gupta et al., 2010; Kerimoglu et al., 2017), KMT2B (Kerimoglu et al., 2013; Kerimoglu et al., 2017), and KDM5C (Iwase et al., 2016; Scandaglia et al., 2017; Vallianatos et al., 2019) have been reported to exhibit deficits in learning and memory. Harnessing the contemporary mouse genetics approach, one of the important questions that should be addressed is when the cognitive and adaptive deficits originate. One

possibility is that a given chromatin modifier may play roles both in brain development and plasticity of mature circuitry. In such cases, therapeutic intervention would still hold a hope to ameliorate cognitive deficits even after affected individuals reach adulthood.

Great strides are being made with small-molecule inhibitors of writers and erasers in order to modulate H3K4me status (Cao et al., 2014; Grembecka et al., 2012; Helin and Dhanak, 2013). While these strategies are currently being targeted for cancers, a therapeutic potential for these drugs in brain disorders is evident. Clearly, understanding the intricate nature of H3K4me dynamics, as well as other chromatin modifications, in the developing brain will form the groundwork necessary for targeted therapeutics and prevention for these neurodevelopmental disorders in the future.

Notes & Acknowledgements

This chapter was previously published in *Epigenomics* (Volume 7, Issue 3) (Vallianatos *et al.*, 2015), with the following additions: overview section, PRDM16 as an H3K4 methyltransferase, Figure 1.1, and updated Figures 1.2-1.3.

Figures

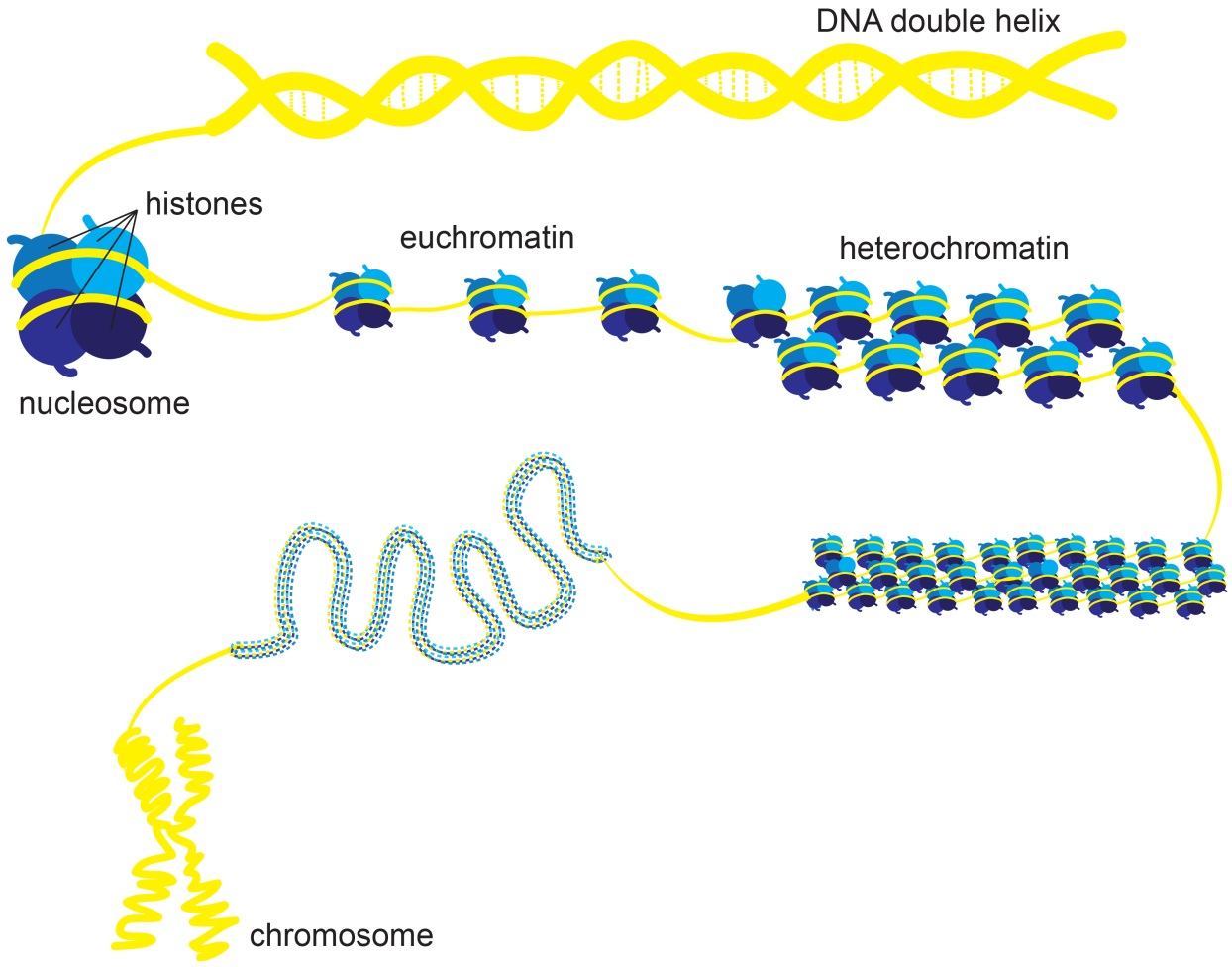

Figure 1.1 Chromatin organization.

DNA (yellow) wraps around histone proteins (blue), allowing precise and dynamic genomic organization.

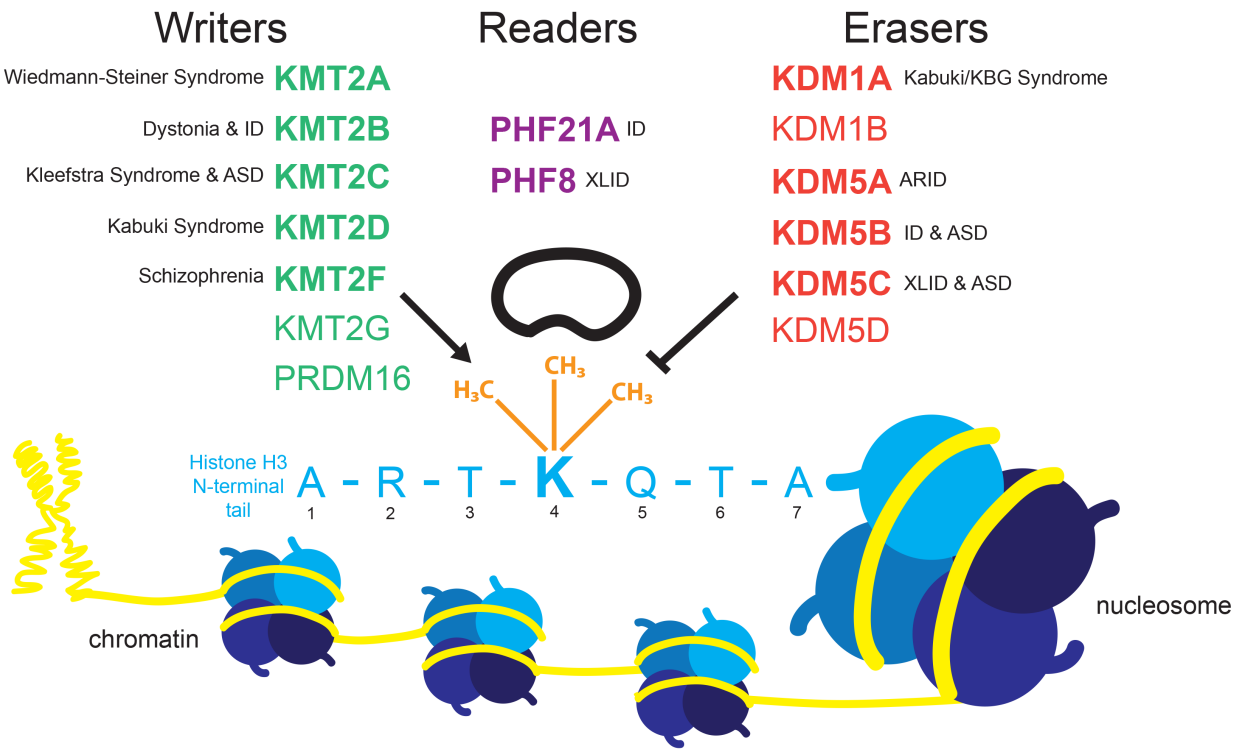

Figure 1.2 H3K4me writer, eraser, and reader genes in neurodevelopmental disorders.

The first seven amino acids of the N-terminal tail of histone H3 (light blue) are extending from a representative nucleosome. The fourth lysine (K) can be differentially methylated (orange) by the writer and eraser proteins shown above. Methyltransferases (green) "write" methyl marks, whereas demethylases (red) "erase" methyl marks. Reader enzymes (purple) recognize and "read" methylation status. Mutations in many of these enzymes leads to neurodevelopmental disorders, indicated in black next to each gene name. ASD, autism spectrum disorder; ID, intellectual disability; XLID, X-linked intellectual disability; ARID, autosomal recessive intellectual disability.

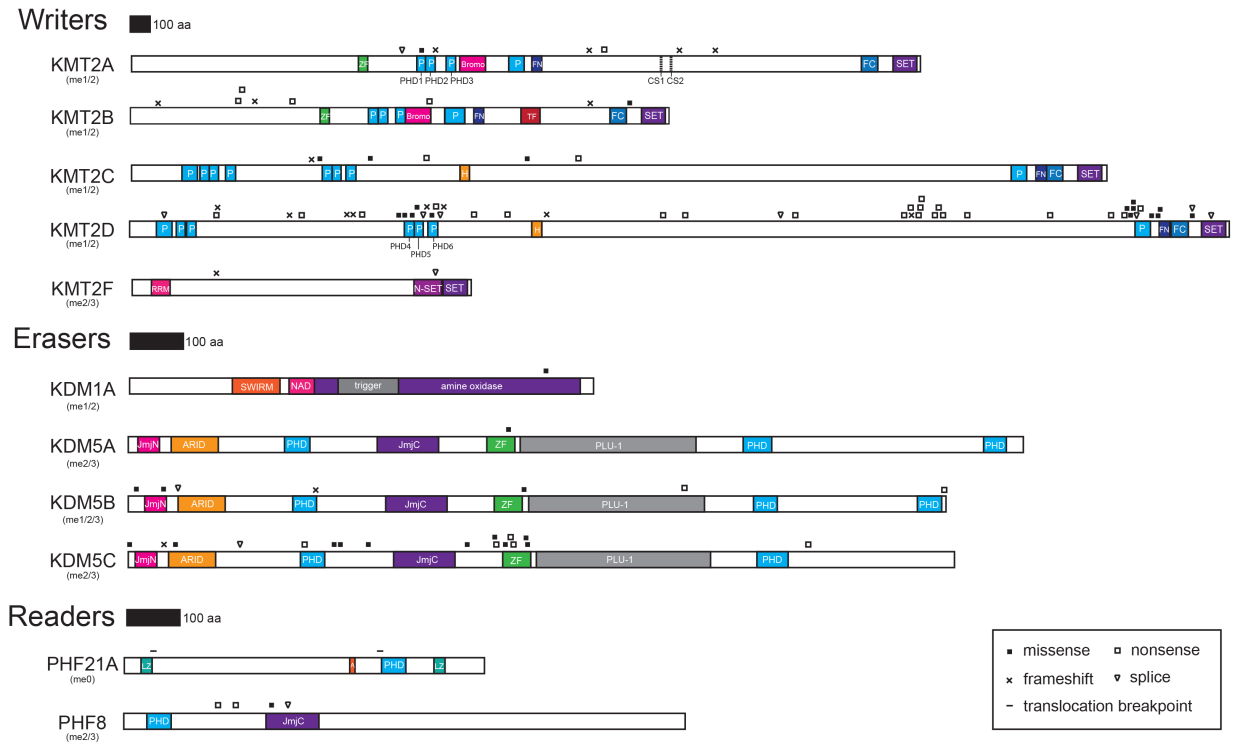

Figure 1.3 Domain organization of H3K4me regulators mutated in neurodevelopmental disorders.

Protein schematics of H3K4me proteins mutated in human neurodevelopmental disorders. Colored blocks correspond to functional protein domains found within each gene. Substrate preference is indicated below each gene name. Mutation types and corresponding symbols are summarized in inset key. KMT2D mutations are limited to a subset based on Miyake *et al*. (Miyake et al., 2013). Scale is provided for each category of enzymes. ZF, zinc finger; P or PHD, plant homeodomain (PHD) finger; FN, FY-rich N-terminal domain; CS, cleavage site; FC, FY-rich C-terminal domain; SET, Su(var)3-9 Enhancer-of-zeste Trithorax methyltransferase domain; TF, precursor of transcription factor II A (TFIIA) alpha and beta subunits; H, High Mobility Group (HMG) box; RRM, RNA recognition motif; LZ, leucine zipper; A, AT-hook, JmjN, jumonji N-terminal; ARID, AT-rich interaction domain; JmjC, jumonji C-terminal; PLU-1, PLU1-like domain.

Chapter 2 — Altered Gene-Regulatory Function of KDM5C By a Novel Mutation Associated With Autism and Intellectual Disability

Introduction

Intellectual disabilities (ID) affect 1.5-2% of the population world-wide (Leonard and Wen, 2002). Clinical features of ID include significant deficiencies in cognitive function and adaptive behaviors beginning before 18 years of age (American Psychiatric Association. et al., 1994). ID syndromes are often accompanied with other comorbidities, including autism spectrum disorders (ASD), which are characterized by impaired speech, hindered social development, and repetitive behaviors. X-linked intellectual disability (XLID) is a monogenic form of cognitive deficits, and has been thought to account for the higher frequency of ID in males compared to females (Chiurazzi et al., 2008). *KDM5C* is one of the most frequently mutated genes in XLID and estimated to explain approximately 0.7-2.8% of all XLID cases. *KDM5C*-deficiency is characterized by frequent autistic and aggressive behaviors (Jensen et al., 2005b; Ropers and Hamel, 2005) and is currently referred to as Mental Retardation, X-linked, Syndromic, Claes-Jensen type (MRXSCJ: OMIM#300534). The *KDM5C* gene, located at Xp11.22-p11.21, encodes a histone demethylase, which specifically targets di- and tri-methylated histone H3 lysine 4 (H3K4me2 and H3K4me3) (Iwase et al., 2007; Tahiliani et al., 2007a).

KDM5C is ubiquitously expressed, with the highest expression levels in human skeletal muscle and brain tissues (Jensen et al., 2005b). Within the brain, KDM5C is also broadly expressed in key areas for cognitive function, such as the hippocampus, the cortex, and the amygdala, and both neurons and astrocytes contain KDM5C protein (Iwase et al., 2016; Xu et

al., 2008). In mouse models, loss of *Kdm5c* led to defective development of dendrites and dendritic spines (Iwase et al., 2016; Iwase et al., 2007), which are often observed in human individuals with ID/ASD. *Kdm5c*-deficient mice displayed impaired fear memory, spatial learning, increased aggression, and reduced social preference. In sum, both human genetics and mouse models have highlighted important roles of KDM5C in cognitive development.

H3K4me2/3, the substrates of KDM5C, are generally associated with promoters of transcriptionally active or poised genes, and play important roles in gene transcription (Barski et al., 2007; Kouzarides, 2007; Vallianatos and Iwase, 2015). KDM5C has been reported to repress transcription in post-mitotic neurons and breast cancer cells (Iwase et al., 2016; Shen et al., 2016), whereas KDM5C can promote gene expression when it acts on specific transcriptional enhancers in mouse embryonic stem cells (Outchkourov et al., 2013). In the *Kdm5c*-deficient brain, H3K4me2/3 levels were increased at the promoters of genes that encode key synapse-related genes, and some KDM5C-target genes were aberrantly expressed in the mutant mice. Despite this circumstantial evidence, it still remains elusive whether or not H3K4me2/3 demethylase activity is the sole mechanism of KDM5C-mediated gene regulation.

Both truncation and missense mutations of *KDM5C* have been found in MRXSCJ patients. The majority of missense mutations functionally tested to date result in reduced demethylation activity of KDM5C (Brookes et al., 2015a; Iwase et al., 2007; Rujirabanjerd et al., 2010; Tahiliani et al., 2007a). Moreover, most mutations occur in the N-terminal to mid regions of the protein, an area that has been shown to be sufficient for enzymatic activity (Vinogradova et al., 2016). Thus, the predominant molecular mechanism underlying MRXSCJ appears to be loss of function of histone H3K4 demethylation. Here, we report a novel ID/ASD-associated *KDM5C* mutation, which compromises KDM5C's gene-regulatory function but not enzymatic activity or stability. This new mutation lies in the C-terminal end of the protein, the most distally

located missense mutation identified to date. Our results suggest non-enzymatic roles of KDM5C and a novel pathogenic mechanism contributing to MRXSCJ.

Results

KDM5C p.Arg1115His is identified in family UM1

The proband of family UM1 was first clinically examined at 26 months for developmental delay and microcephaly, after observing delays in developmental milestones from one year of age. He was diagnosed with an autism spectrum disorder (ASD) due to cognitive impairment and behavioral concerns, including severe tantrums, aggression, and anxiety (for the full clinical description, please visit the family profile on MyGene2 as family 1600 https:www.mygene2.org/MyGene2). Clinical whole exome sequencing revealed a missense mutation in the *KDM5C* gene, c.3344G>A, in the proband (Figure 2.1A). This variant results in a histidine-arginine substitution at amino acid position 1115 (p.R1115H), and was inherited from the maternal grandmother. The carrier mother was phenotypically normal, and the variant was not present in the unaffected siblings or maternal uncle. We isolated genomic DNA from lymphoblastoid cell lines from father (UM1 II-1) and proband (UM1 III-3), and confirmed by Sanger sequencing that the variant is present specifically in the proband (Figure 2.1B).

The R1115H variant lies in a region of high conservation and is itself highly conserved among vertebrates (Figure 2.1C). KDM5C belongs to a family of histone H3K4 demethylases, in which KDM5A, KDM5B, and KDM5D are the additional members (Iwase et al., 2007). The R1115 residue in KDM5C is conserved in the family members, though it is substituted with lysine, another basic amino acid, in KDM5A, implicating a conserved functional role (Figure 2.1D). Consistently, multiple genetic variant assessment algorithms predict this variant to be pathogenic (Table 2.1). We did not find any homozygous or hemizygous substitutions of R1115

in the Genome Aggregation Database (gnomAD, http://gnomad.broadinstitute.org/), indicating that variation in this amino acid residue is intolerant in the population. To date, 25 *KDM5C* mutations have been identified in MRXSCJ patients (Abidi et al., 2008; Adegbola et al., 2008; Brookes et al., 2015a; Jensen et al., 2005b; Ounap et al., 2012; Rujirabanjerd et al., 2010; Santos et al., 2006; Santos-Reboucas et al., 2011; Tzschach et al., 2006). Most of them tend to cluster around the JmjC catalytic core domain (Figure 2.1E). The R1115H variant lies within the C-terminal segment of the KDM5C protein, making it the most distal missense mutation in KDM5C reported to date.

X-chromosome inactivation skewing predicts a pathogenicity of KDM5C R1115H

In female mammals, one of the two X chromosomes is randomly chosen to be silenced during early embryogenesis; therefore, females are chimeras of cells that silenced either the paternally- or the maternally-inherited X (Augui et al., 2011). Female carriers of recessive X-linked disorders often display skewed X-inactivation, i.e. a higher percentage of silencing in either the paternal or the maternal X chromosome over the other (Brown, 1999). Skewed X-inactivation might be due to (dis)advantage of carrying the X-linked mutation in cell proliferation and/or survival. Multiple MRXSCJ cases are reported to have highly-skewed X-inactivation in carrier mothers ((Ounap et al., 2012) and Table 2.2). When we tested the X-inactivation status of the carrier mother (UM1 II-2), we observed highly-skewed inactivation (95:5, Table 1), and moderate skewing in the grandmother (UM1 I-2). In the carrier mother, the X-chromosome passed on to the proband is dominantly CpG-methylated at the *androgen receptor* (*AR*) locus. *AR* and *KDM5C* are located nearby (~14.5 Mb), flanking the centromere, and no meiotic recombination site is known between the two loci (Kong et al., 2002); therefore, *KDM5C* is very likely mutated on the inactive X-chromosome of the carrier mother. These

results indicate that KDM5C-R1115H mutation might have an impact on cell proliferation/survival during development (also see *Discussion*).

Enzymatic activity is largely retained in KDM5C R1115H

A majority of *KDM5C*-MRXSCJ mutations that have been tested for enzymatic activity exhibit a decrease in histone demethylase activity, suggesting a loss-of-function pathogenic mechanism (Brookes et al., 2015a; Iwase et al., 2007; Rujirabanjerd et al., 2010; Tahiliani et al., 2007a). We set out to test whether the R1115H variant affects histone demethylation capabilities of the KDM5C protein. WT and R1115H mutant KDM5C proteins containing an N-terminal Strep-tag were expressed at equal levels in insect cells and affinity purified (Figure 2.2A). We performed *in vitro* demethylation assays using purified KDM5C and two synthetic histone H3 N-terminal tail peptides carrying the following modifications: K4me3, the direct substrate for the KDM5C catalytic subunit; or K4me3 and K9me3, which is recognized by the first PHD domain of KDM5C (Iwase et al., 2007). Our results showed that the R1115H mutation did not dramatically reduce H3K4me3 demethylase activity on peptides carrying either H3K4me3 alone or both H3K4me3 and K9me3 (Figure 2.3A-B). These data indicate intrinsic demethylation ability of the KDM5C R1115H protein is largely retained.

We next tested demethylation activities in cells. We over-expressed Strep-tagged human *KDM5C* cDNA in U2OS cells and examined H3K4me3 levels using immunofluorescence (Figure 2.3C). Cells expressing KDM5C WT showed dramatically reduced H3K4me3 staining. Similar to WT, KDM5C R1115H-expressing cells exhibited a marked reduction in H3K4me3 signal. In contrast, cells expressing the catalytically-inactive KDM5C H514A mutant (Iwase et al., 2007) retain high H3K4me3 levels. While we observed cytoplasmic signal more frequently in R1115H-expressing cells than WT, this potential mislocalization does not seem to impair

demethylation activity of KDM5C R1115H. We also over-expressed Strep-tagged human *KDM5C* cDNA in primary mouse neurons and examined H3K4me1/2/3 levels using immunofluorescence (Figure 2.2B). Cells expressing KDM5C WT often showed reduced H3K4me2 and H3K4me3 staining, and no effect on H3K4me1, as predicted. Similar to WT, KDM5C R1115H-expressing cells frequently exhibited a marked reduction in H3K4me2/3 signal. In contrast, cells expressing the catalytically-inactive KDM5C H514A mutant (Iwase et al., 2007) retain high H3K4me2/3 levels. When we examined global H3K4me levels of lymphoblastoid cell lines from father (WT) and proband (R1115H) by quantitative Western blot analysis, proband-derived cells were indistinguishable from father-derived cells (Figure 2.3D). Taken together, these data strongly suggest that KDM5C R1115H substitution does not lead to substantial reduction in histone demethylation activity.

Protein stability of KDM5C R1115H is largely unaffected

Some *KDM5C*-MRXSCJ mutations have been shown to destabilize KDM5C protein, representing another potential loss-of-function effect. To test the stability of KDM5C R1115H, we treated the lympoblastoid cells from the father and the proband with cycloheximide, an inhibitor of protein synthesis, for 0-28 hours. Reduction kinetics of endogenous KDM5C levels were not dramatically different in proband compared to father throughout the time course, suggesting protein stability is largely unaffected by the R1115H mutation (Figure 2.4).

Ubiquitination of proteins, via the post-translation addition of ubiquitin to a substrate protein, is a common mechanism for proteolysis. We found that the R1115H mutation lies six amino acids upstream of a KDM5C ubiquination site, K1121ub (Figure 2.5A). To test if R1115H affected mono- or poly-ubiquination of KDM5C, we performed immunoprecipitation of Strep-tagged KDM5C and measured ubiquination via Western blot (Figure 2.6). Using full-length

KDM5C (1560 amino acid) or PHD2 fragment (135 amino acids) (Figure 2.5B) we observed no detectable difference in total ubiquination between WT or R1115H mutation conditions (Figure 2.6). These data confirm R1115H has no detectible effect on protein stability, and suggest that KDM5C R1115H does not alter total ubiquitination of the KDM5C protein.

RNA-seq reveals impact of the R1115H variant on gene expression

We previously reported that *Kdm5c* regulates neurodevelopment genes in cultured mouse forebrain neurons and multiple brain regions *in vivo* including the cortex and the amygdala (Iwase et al., 2016). To test consequences of the R1115H substitution on KDM5C gene regulatory behavior, we over-expressed KDM5C WT and KDM5C R1115H in primary mouse forebrain neuron culture and performed RNA-seq analysis on three biological replicates. To assess the impact of H3K4 demethylation activity on the transcriptome, we also overexpressed KDM5C H514A as a representative of other mutations that reduce enzymatic activity (Iwase et al., 2007). As outlined in Figure 2.7A, transduced neurons were selected by puromycin and subjected to RNA-seq. Expression of intended mutants was confirmed by examining the nucleotide sequence of reads mapped to the human *KDM5C* cDNA (Figure 2.8A). Mapping the sequencing reads to the human *KDM5C* cDNA also allowed us to validate similar levels of human *KDM5C* WT and R1115H mutant cDNAs, while we noted moderately higher level of H514A mutant expression compare to the other two *KDM5C* cDNAs (Figure 2.8B-C). We compared the sequencing reads mapped to human *KDM5C* cDNA and mouse *Kdm5c* gene without allowing any mismatch, and estimated that each *KDM5C* cDNA was expressed approximately 15- to 30-fold higher than endogenous *Kdm5c* mRNA (Figure 2.8B-C). The expression of endogenous *Kdm5c* does not appear to be largely affected by human *KDM5C* overexpression Figure 2.8C).

Compared to the vector control, overexpression of KDM5C-WT resulted in 42 differentially-expressed (DE) genes (7 up-regulated, 35 down-regulated). KDM5C R1115H expression resulted in 64 DE genes (16 up-regulated, 48 down-regulated) compared to WT, while KDM5C H514A gave 99 DE genes (45 up-regulated, 54 down-regulated) ($p < 0.01$; Figure 2.7B). Consistent with its role as a transcriptional repressor in primary neuron culture (Iwase et al., 2016), we observe a majority (83%) of these DE genes are down-regulated by KDM5C-WT overexpression. KDM5C R1115H expression similarly led to predominant down-regulation of genes (75% down, 25% up), while KDM5C H514A expression resulted in a near even split between up- and down-regulated genes (54% down, 46% up). To test if R1115H and/or H514A mutations affect gene-regulatory function of KDM5C, we plotted the fold change and *P*-values of 42 DE genes, whose expression was altered by WT overexpression, in the R1115H- or H514A-overexpression datasets (Figure 2.7C). Both KDM5C R1115H and H514A failed to fully repress this group of genes, suggesting that the two mutations interfere with KDM5C's gene-regulatory function (Figure 2.7C). The partial deficiency of H514A mutant despite of the higher level of KDM5C-H514A mRNAs implicates that demethylation activity is not the sole mechanism for KDM5C-mediated gene control. It is noteworthy that KDM5C R1115H mutant showed a similar level of deficiency compared to H514A mutant in regulating the 42 genes.

We then compared identity of DE genes upon overexpression of KDM5C-WT, R1115H, and H514A. Interestingly, overlap between DE genes in each condition were limited, suggesting that R1115H and H514A mutants can regulate different sets of genes compared to KDM5C-WT and the two mutants are functionally distinct each other (Figure 2.7D). Representative genes for the following four expression patterns across conditions are shown in Figure 2.8D-G: (1) genes repressed by KDM5C WT but not by mutants include *PWWP domain containing 2b (Pwwp2b)* and *Zinc finger protein 198 (Zfp189)*; (2) genes that show unique response to KDM5C-H514A

include *Protein kinase C, theta (Prkcq)* and *Trichoplein, keratin filament binding (Tchp)*; (3) genes strongly repressed by KDM5C-R1115H include *TATA-box binding protein associated factor 5 like (Taf5l)* and *coordinator of PRMT5, differentiation stimulator (Coprs)*; and finally (4) genes uniquely up-regulated by KDM5C-R1115H including *Transmembrane protein 251 (Tmem251)* and *Keratin associated protein 4-8 Krtap4-8)*.

Having observed both common and unique impacts of R1115H and H514A substitutions, we sought to gain biological insights associated with the mutations by using the database for annotation, visualization, and integrated discovery (DAVID) (Huang da et al., 2009a, b). Given that KDM5C primarily acts as a transcriptional repressor, we reasoned that down-regulated genes reflect direct impact of KDM5C overexpression more likely than up-regulated genes; therefore, here we primarily analyzed down-regulated genes. Genes down-regulated by WT were enriched in developmental processes and cell signaling gene ontology (GO) terms (Figure 2.9A). These GO terms are absent from both R1115H (Figure 2.9B) and H514A (Figure 2.9C) down-regulated genes, pointing to the inability of the mutant KDM5Cs to regulate the relevant genes as WT. Meanwhile, down-regulated genes by R1115H and H514A were enriched in largely distinct sets of GO terms compared to WT, and these GO terms are also different between the two mutants. For example, KDM5C-R1115H mutant down-regulated and “membrane-bound organelle” and “muscle structure development”, while KDM5C-H514A down-regulated “gliogenesis” and “protein binding”. Distinct sets of genes appear to contribute the diverse GO term enrichments between the conditions. Taken together, these data suggest that KDM5C R1115H is less potent in suppressing WT-regulated genes, yet the mutant gains unique gene regulatory roles, which may lead to deleterious and distinct consequences in neuronal development and functions.

R1115H lies near PHD2 domain

The proximity of the R1115H substitution to the second PHD domain (PHD2) of KDM5C lead us to speculate whether this nearby mutation could affect the function of this domain (Figure 2.5). PHD2 has yet unreported function, despite a shared conservation across all four KDM5A-D family members (Klein et al., 2014). PHD domains are often found in chromatin regulators, and many bind histone tails with high specificity due to their zinc-finger-like structure (Musselman and Kutateladze, 2011). We first sought to determine whether KDM5C PHD2 binds to any histone tails and utilized the histone peptide microarray to allow the unbiased identification of interactions (Cornett et al., 2016; Rothbart et al., 2012). Using recombinant KDM5C PHD2 protein fragment, containing PHD2 and flanking regions (Figure 2.5) we performed this microarray assay. Top five candidate interacting histones were selected from the list, and to validate interactions, we performed a binding assay with PHD2 and each of the candidates (Figure 2.10). Binding assay results were inconsistent with microarray, making the results inconclusive. Our attempts to perform bulk histone binding assay were unsuccessful despite stringent conditions (see *Methods*), as the GST we used to tag our recombinant proteins was able to pull-down histones to the same detectible degree as either PHD2 WT or R1115H, or PHD1 (Figure 2.10).

We next performed a histone binding assay with unmodifiend histone peptide tails (Figure 2.11) We observed that KDM5C PHD2 did not bind any of the six tested peptides, at least not to the affinity of ATRX ADD, a known H3 binidng domain (Iwase et al., 2011).

It was previously reported that KDM5C harbors a PIP-box, a motif known for PCNA binding (Liang et al., 2011) (Figure 2.5). We identified that this motif occurs within PHD2 itself, unlike previous reporting of this motif lying upstream of PHD2 (Liang et al., 2011), and therefore may render PHD2 a putative PCNA binding domain. PCNA and KDM5C have been

shown to interact (Alabert et al., 2014; Liang et al., 2011; Rondinelli et al., 2015), though a direct interaction has not been shown. We performed a binding assay using recombinant His-tagged PCNA and our KDM5C PHD2-containing fragments (Figure 2.11B). We observed PHD2-PCNA interaction. When we tested PHD2 fragment containing the R1115H mutation, we found that the missense mutation did not hinder the ability of PHD2 to bind PCNA (Figure 2.11). We also tested PHD1, which does not harbor any known canonical or non-canonical PIP-box sequence. Surprisingly, we found that PHD1 also interacts with PCNA in our recombinant system (Figure 2.11). This interaction was specific to the PHD fragments, as GST alone was not able to bind PCNA (Figure 2.11). While *in vivo* binding may be different, our *in vitro* results show that KDM5C PHD2 WT and R1115H, as well as PHD1, can bind PCNA in this state. Nevertheless, these studies laid an important foundation for future work to probe PHD2 specialization

Discussion

MRXSCJ has been primarily attributed to either reduced enzymatic activity and/or stability of KDM5C protein by associated mutations. In the present study, we describe a novel KDM5C missense mutation, R1115H, which was identified in an individual with a typical MRXSCJ phenotype. While R1115H substitution does not result in appreciable changes in enzymatic activity or protein stability, this substitution appears to alter the transcriptional regulatory function of KDM5C. Another KDM5C mutation, D87G, was shown to not interfere with the demethylation activity [7]. However, the functional consequence of the D87G substitution remains elusive. Thus, our study implicates a novel mechanism underlying MRXSCJ.

We provide several lines of evidence that support contribution of the KDM5C-R1115H mutation to developmental and behavioral phenotypes of the proband. First, the clinical

phenotypes including short stature, aggressive behavior, and ASD associated with ID align well with previously-described individuals with MRXSCJ (Adegbola et al., 2008; Jensen et al., 2005a; Ounap et al., 2012; Santos et al., 2006; Santos-Reboucas et al., 2011; Tzschach et al., 2006). Second, the mutation clearly segregates with the cognitive impairment, as both unaffected brother and maternal uncle did not carry the R1115H mutation (Figure 2.1). Third, KDM5C-R1115 is highly conserved among vertebrates and the R1115H substitution is predicted to be functionally damaging by multiple prediction algorithms (Figure 2.1 and Supplemental Table 1). Forth, the carrier mother showed highly-skewed X-inactivation (Table 1). KDM5C was originally discovered as an X-linked gene that escapes X-inactivation both in human and mouse although escaping is not complete — KDM5C is expressed at a lower level from the inactive X compared to that of the active X (Wu et al., 1994a; Wu et al., 1994b). We recently reported that KDM5C is necessary and sufficient for initiating X-chromosome inactivation by inducing expression of the Xist non-coding RNA (Gayen et al., 2017). In KDM5C heterozygous knockout female embryos, cells that chose the KDM5C mutant-carrying X as the active X chromosome failed to inactivate one of the two Xs, and these cells were quickly lost during development (Gayen et al., 2017). We speculate that a similar cell selection process took place in the carrier mother, as we determined that KDM5C is very likely mutated on her inactive X-chromosome. These data, together with the observations in mouse models, support the deleterious impact of R1115H substitution on the function of KDM5C. The moderate bias of X-inactivation in the carrier grandmother may imply that additional genetic event(s) in the carrier mother might have contributed to the MRXSCJ-like symptoms in her son. Finally, our RNA-seq data indicate that R1115H alters KDM5C's gene-regulatory function in neurons. Generation and characterization of knock-in mice carrying KDM5C-R1115H will allow us to understand the causal roles of this mutation in cognitive development in the future.

It is important to note that exome sequencing of the proband also revealed a missense mutation in the *CIC (Capicua Transcriptional Repressor)* gene (c.4790C>A, p.Pro1597Gln). Like *KDM5C*, *CIC* encodes a putative transcriptional repressor (Jiménez et al., 2012), and has been associated with a human intellectual disability syndrome (Lu et al., 2017; Vissers et al., 2010). Mouse studies revealed conditional loss of *Cic* in forebrain neurons leads to learning and memory impairments, thinning of cortical layers 2-4, and decreased dendritic arborizations (Lu et al., 2017). As human ID-associated *CIC* mutations show autosomal dominant inheritance, it is especially important for future work to functionally investigate this mutation similar to our study of KDM5C R1115H.

The previously reported missense mutations in KDM5C all fall within the N-terminal half of KDM5C, which harbors JmjC domain, the catalytic core for histone H3K4 demethylation (Figure 2.1). The N-terminal half of KDM5 family demethylases, encompassing JmjN, Bright, PHD1, JmjC, and zinc finger domains, was shown to be sufficient for its catalysis (Figure 2.5) (Johansson et al., 2016; Vinogradova et al., 2016). By contrast KDM5C-R1115 resides outside this catalytic segment, and indeed, the KDM5C-R1115H substitution did not interfere with enzymatic activity. Careful analysis of reported proband phenotype data and both mutation type and mutation location along KDM5C failed to reveal any obvious correlation (Figure 2.12). The C-terminal half of KDM5C contains a PHD finger domain (PHD2) with unknown function, and R1115 is located 73 amino-acid upstream of PHD2. Given that KDM5C-PHD1 recognizes H3K9me (Iwase et al., 2007), it is plausible that this region recognizes specific histone modification(s). Our investigations into PHD2 function as a histone binding domain and/or PCNA binding domain (Figure 2.10), provide important foundations for future work to define PHD2 function. Alternatively, the C-terminal segment may interact with other transcriptional regulators to recruit them to KDM5C-target genes. Interestingly, four truncation mutations that

remove this C-terminal segment have been identified in MRXSCJ patients (Abidi et al., 2008) (Brookes et al., 2015b; Jensen et al., 2005b; Rujirabanjerd et al., 2010). These observations suggest the important roles of the C-terminal segment for KDM5C's gene-regulatory roles. The R1115H substitution may interfere with these uncharacterized roles of the C-terminal regions of KDM5C. A minor population of cells show cytoplasmic signal of KDM5C-R1115H mutant in addition to nuclear signals (Figure 2.2C). Given the intact H3K4 demethylation activity of KDM5C-R1115H and low frequency of its cytoplasmic presence, the mislocalized protein may not have a major impact. However, we cannot rule out the possibility that KMD5C-R1115H could demethylate ectopic target(s) at the cytoplasm. Future studies are needed to determine the roles of the C-terminus in KDM5C-mediated transcriptional regulation, impact of disease mutations in this segment, and the roles of enzymatically-active mutants that can be present outside nuclei.

Our RNA-seq data suggest that the R1115H mutation may not only lead to loss of function of KDM5C but also acquisition of a new gene-regulatory function. It is tempting to speculate that KDM5C neofunctionalization might be involved in the pathophysiology of this specific MRXSCJ-like patient. However, limitations of interpreting the RNA-seq results should be noted. The RNA-seq was carried out upon overexpression of WT- and mutant-KDM5C, 10 days after introducing KDM5C transgenes into neurons. Gene expression changes may therefore involve both direct impact of on KDM5C's target genes as well as indirect consequences, such as alteration in neuronal maturation processes. In addition, gene expression changes upon KDM5C overexpression may not simply reflect the dysregulation of *bona fide* KDM5C target-genes. Nonetheless, KDM5C-R1115H illuminates a novel gene regulatory function of KDM5C, which is independent of its enzymatic activity, and potentially represents a novel molecular etiology contributing to MRXSCJ.

Materials & Methods

Exome sequencing, validation and analysis of the variant

Written informed consent was obtained from all study participants in accordance with approved protocols from the Institutional Review Board at the University of Michigan. Clinical trio whole exome sequencing was performed through GeneDx (XomeDx) on genomic DNA from the proband and both parents. The Agilent SureSelect XT2 All Exon V4 kit was used to target the exon regions of the genomes. The targeted regions were sequenced using the Illumina HiSeq 2000 sequencing system with 100 bp paired-end reads. The DNA sequence was mapped to and analyzed in comparison with the published human genome build UCSC hg19 reference sequence. The targeted coding exons and splice junctions of the known protein-coding RefSeq genes were assessed for the average depth of coverage of 64X and data quality threshold of 95.9%. The XomeAnalyzer was used to evaluate sequence changes in the proband compared to other sequenced family members. All sequence variants in the proband and parental samples were confirmed by Sanger sequencing analysis.

For Sanger sequencing validation, genomic DNA was isolated (Promega) from $3x10^6$ lymphoblastoid cells from proband and his father. A roughly 2kb region surrounding the residue was amplified using the Q5 High-Fidelity Polymerase (NEB) with the following primers: 5'-AGAGGTTGTAGAGGAGGCCG-3' and 5'-CTGTCATGCGAGGACTGTTGGTC-3'. The PCR reaction was purified (Qiagen) and exon 22 was Sanger sequenced using the following primers: 5'-gtgaggcctgggaccttg-3' inside intron 21-22, and 5'-ccccatctgtgtcgaagc-3' inside intron 22-23. Pedigree was made using pedigreedraw.com, from Genial Genetics. Multiple species sequence alignments were made using Clustal Omega.

X-chromosome inactivation

X-inactivation (XI) analysis using the well-characterized CpG methylation site and polymorphic CAG repeats within the Androgen Receptor (AR) locus was performed using standard protocol (Allen et al., 1992). In this assay, digestion with the methylation-sensitive HpaII restriction enzyme followed by PCR amplification was used to determine the ratio of methylation status between the maternal and paternal X chromosome. Parental samples were utilized to delineate allele status.

Plasmid DNA

The R1115H substitution was introduced into pENTR-KDM5C (human) (Iwase et al., 2007) using a PCR-based targeted mutagenesis. WT- and mutant KDM5C cDNA were then moved by LR recombination to a modified pHAGE, a lentivirus compatible mammalian expression plasmid (Murphy et al., 2006). In pHAGE plasmid, cDNA of interest is linked to puromycin-resistant genes via the internal ribosome entry site (IRES), thereby allowing the selection of transduced cells via puromycin. The modifications of pHAGE are insertion of Gateway cassette (Invitrogen) and Strep-tag, and replacement of the CMV promoter with the PGK promoter. The entire KDM5C cDNAs were Sanger-sequenced to validate the single targeted mutagenesis.

KDM5C PHD domains were cloned for protein expression, with flanking regions from human KDM5C cDNA (NP_004178.2) using standard procedures into BamHI/XhoI sites of pGEX4T-1 or pFastBac (Life Technologies). For PHD1, amino acids 261-414 were isolated. For PHD2, amino acids 1147-1281 were isolated using the following primers: 5'-TACTTCCAATCCAATGCAGTTCTCTGCCCATGTGCAGATG-3' and 5'-GCCAACGGCTACAGGCTGAATAACATTGGAAGTGGATAA-3'.

Protein expression and purification

Insect cell expression. Wild-type and mutant KDM5C cDNAs were cloned into a baculovirus expression vector, pFastBac (Life Technologies), and expressed in Sf9 or Hi5 insect cells using the Bac-to-bac baculoviral expression system (Life Technologies). For full-length strep-tagged KDM5C recombinant proteins, cells were lysed in Buffer A (50mM Tris-HCl pH 7.5, 150mM NaCl, 0.05% NP-40) with 0.2mM PMSF and protease inhibitor cocktail (Sigma), proteins were immobilized on Strep-Tactin affinity resin (Qiagen), washed with Buffer A, and eluted in Buffer A containing 2.5 to 25mM desthiobiotin. For GST-tagged PHD fragment recombinant proteins, cells were lysed in Lysis Buffer (1X PBS, 0.1% TritonX-100, 1 mM DTT, 1 mM PMSF, 1X protease inhibitor cocktail), sonicated, cleared by centrifugation at 4°C, proteins were immobilized on glucathione sepharose by rotating incubation 2 hours at 4°C, beads were washed thoroughly with Lysis Buffer, protein was eluted four times with 100 µl GST elution buffer (50 mM Tris pH 8.0, 10 mM glucathione), elutions were combined, and proteins were aliquoted in Storage Buffer (Tris pH 8.0, 150 mM NaCl, 1 mM DTT, 20% glycerol).

Histone demethylase assay

Wild-type and mutant KDM5C recombinant proteins were used from Sf9 (for H3K4me3 assay) or Hi5 (for H3K4me3, K9me3 assay) insect cell expression. Enzymatic activity was assessed using the Histone Demethylase Fluorescent Activity Kit (Arbor Assays, K010-F1). 4-5 µM (for H3K4me3 assay) or 1 µM (for H3K4me3, K9me3 assay) purified KDM5C protein and 4 mM peptides were incubated at 30°C with freshly-prepared 4 mM alpha ketoglutarate, 2 mM ascorbate, 100 µM iron ammonium sulfate. The following synthetic histone N-terminal peptides

were purchased from Anaspec: H3K4me3: H2N-ART(Kme3)QTARKSTGGKAPRKQL-amide, and H3K4me3/K9me3: H2N-ART(Kme3)QTAR(Kme3)STGGKAPRKQL-amide. Reactions were quenched with 4 mM deferoxamaine mesylate at 10, 20, or 30 minutes, and detected with formaldehyde detection reagent according to the kit instructions. Fluorescence end point measurement was performed using the Tecan Safire 2 plate reader and XFluro4 V4.62 software.

Protein binding assays

Histone peptide binding assay: 1 μg biotin-labeled unmodified histone tail peptides (Anaspec) and 1 μg GST-tagged proteins (KDM5C PHD2 WT or R1115H, ATRX ADD) were used. Streptavidin agarose resin (Thermo Fisher). The following synthetic histone N-terminal peptides were purchased from Anaspec: H2A (1-20): SGRGKQGGKARAKAKTRSSRGG-K(biotin); H2B (1-21): PEPSKSAPAPKKGSKKAITKAGG-K(biotin); H3 (1-20): ARTKQTA RKSTGGKAPRKQL-GGK(biotin); H3 (21-44): ATKAARKSAPATGGVKKPHRYRPG-GGK(biotin); H3.3(21-44): ATKAARKSAPSTGGVKKPHRYRPG-GGK(biotin); H4 (1-23): SGRGKGGKGLGKGGAKRHRKVLR-GGK(biotin).

PCNA binding assay. Protocol was adapted from Iwase *et al*. (Iwase and Shi, 2011), with the following conditions. 5 μg His-tagged PCNA protein (Sigma) and 10 μg GST-tagged proteins (KDM5C PHD1, PHD2 WT, PHD2 R1115H) were incubated in Binding Buffer A (50mM Tris-HCl pH8.0, 150 mM NaCl buffer, 0.05% NP-40) rotating overnight at 4 °C. Glucathione sepharose beads were added and allowed to incubate for 1 hour rotating at 4 °C. Samples were washed thoroughly in Binding Buffer A, resuspended in SDS Sample Buffer, boiled and analyzed by Western blot according to standard procedures.

Bulk histone binding assay: Protocol was adapted from Iwase *et al*. (Iwase and Shi, 2011), with the following conditions. 50 μg BSA, 25 μg calf thymus histones, and 1 or 10 μg GST-tagged proteins (KDM5C PHD1, PHD2 WT, PHD2 R1115H) were incubated in Binding Buffer B (50mM Tris-HCL pH 8.0, 500 mM NaCl, 0.05% NP-40) or Buffer B-HS (50mM Tris-HCl pH8.0, 2 M NaCl buffer, 0.05% NP-40) rotating overnight at 4 °C. Glucathione sepharose beads were added incubated for 1 hour rotating at 4 °C. Samples were washed thoroughly in Binding Buffer B or B-HS, resuspended in SDS Sample Buffer, boiled and analyzed by Western blot.

Cell culture, cycloheximide treatment, and transduction

For ubiquitination immunoprecipitation (IP) in HEK 293T cells, Strep-tagged KDM5C full length and PHD-containing expression plasmids (pHAGE) were transfected with Lipofectamine 2000 (Life Technologies) according to manufacturer's instructions.

Lymphoblastoid cell lines from the proband and his father were isolated and cultured under identical conditions as described previously (Burns et al., 2014; Doyle, 1990). Briefly, buffy coat was isolated from citrate (yellow) blood by Ficoll density centrifugation and transformed with Epstein Barr Virus. Lines were maintained in RPMI-1640 media (Gibco) supplemented with 10% FBS, 2mM GlutaMAX, 1% penn-strep, in an incubator set at 37°C with 5% constant CO2. U2OS cells were cultured with DMEM media (Gibco) supplemented with 5% FBS, 2mM GlutaMAX, 1% penn-strep, in an incubator set at 37°C with 5% constant CO_2. Cycloheximide (Sigma) was resuspended in DMSO and used at a final concentration of 100 μg/ml.

For *in situ* demethylation assays in U2OS cells, Strep-tagged KDM5C expression plasmids (pHAGE) were transfected into U2OS cells with Lipofectamine 2000 (Invitrogen)

according to manufacturer's instructions. For *in situ* demethylation assays in neurons, cells were transduced after one day *in vitro* (DIV1) cells with lentivirus of equal titer containing either human KDM5C cDNA (WT, R1115H, or H514A) or vector alone.

Immunofluorescence microscopy

U2OS cells were plated on PDL-coated coverslips in 24-well dishes at $1x10^5$ cells/well and transfected as described above for 48 hours. Mouse forebrain tissue was dissected from embryonic day 16 (E16) CD1 mouse embryos. Cells were dissociated, plated, and cultured as described previously (Iwase et al., 2016), transduced on day *in vitro* 1 (DIV1) as described above, and harvested at DIV3. Cells were fixed with 4% paraformaldehyde, permeabilized with Triton X-100, and blocked with 10% fetal bovine serum. Coverslips were incubated with appropriate primary antibodies overnight at 4°C, washed, and incubated with the corresponding secondary antibodies and DAPI stain for 1 hour at room temperature. Coverslips were then washed, mounted with ProLong Gold Antifade Mountant (Invitrogen). U2OS cells were analyzed on an Olympus BX61 microscope using a 60x oil objective, and images were acquired with cellSens Dimension (1.14) software and processed with ImageJ (1.48) and Adobe Photoshop (CS6). Neurons were analyzed on a Nikon A-1 confocal microscope using a 60x oil objective, and images were acquired with Nikon's Elements software. Primary antibodies were used at the following concentrations: 1:1,000 anti-H3K4me1 (Abcam ab8895), 1:20,000 anti-H3K4me2 (Abcam ab7766), 1:1,000 anti-H3K4me3 (Abcam ab8580), 1:500 (for U2OS) or 1:1,000 (for neurons) anti-Strep (Genscript A01732), 1:1,000 anti-Map2 (Millipore AB5543). Alexa 647-donkey-anti-mouse (for neurons), 594-donkey-anti-rabbit (for U2OS) or -anti-chicken (for neurons), and 488-donkey-anti-mouse (for U2OS) or -anti-rabbit (for neurons) secondary antibodies were all used at 1:1,000. DAPI was used to stain the nucleus at a 1:1,000 dilution.

Immunoprecipitation and ubiquitin assay

48 hours after transfection, cells were washed in 1X PBS, lysed in Buffer A (describe), lightly sonicated, spun, and taken for immunoprecipitation. Lysates were incubated with streptactin resin (Qiagen) rotating overnight at 4 °C. Beads were wash thoroughly, resuspended in SDS Sample Buffer, boiled and analyzed by Western blot.

Western blotting

Lymphoblastoid cells. Cell were lysed in SDS-PAGE sample buffer. Infrared fluorescence-based Western blot was performed using the LI-COR Odyssey Western Blotting RD system according to standard protocol. Primary antibodies were used at the following dilutions: anti-KDM5C (Iwase et al., 2016) at 1:250, anti-GAPDH (G-9, Santa Cruz sc-365062) at 1:50,000, anti-H3K4me1 (Abcam ab8895) at 1:5,000, anti-H3K4me2 (Abcam ab7766) at 1:20,000 or 1:40,000, anti-H3K4me3 (Abcam ab8580) at 1:1,000, anti-H3 (Santa Cruz sc-8654) 1:1,000. Secondary antibodies donkey-anti-goat IRDye 680RD (LICOR 925-68074), donkey-anti-mouse IRDye 680RD (LICOR 926-68072), and donkey-anti-rabbit IRDye 800CW (LICOR 925-32213) were used at 1:10,000. Blots were imaged on the LI-COR Odyssey Clx imager, using Image Studio 3.1 software. Chemiluminescence detection of Western blots was performed as previously described (Iwase et al., 2016).

Binding assays. Chemiluminescence detection of Western blots was performed as previously described (Iwase et al., 2016). The following antibodies were used for detection: anti-GST (Milipore 05-782), in-house anti-KDM5C (Iwase et al., 2016), anti-PCNA (Santa Cruz sc-56), anti-H3 (Santa Cruz sc-8654).

IP and ubiquitination assay. Chemiluminescence detection of Western blots was performed as previously described (Iwase et al., 2016), with the exception that anti-ubiquitin blots were incubated in 1% BSA in PBST. The following antibodies were used for detection: anti-Strep (Genscript A01732), anti-ubiquitin FK2 (Enzo Life Sciences).

RNA-sequencing

Mouse forebrain tissue was dissected from embryonic day 16 (E16) CD1 mouse embryos. Cells were dissociated, plated, and cultured as described previously (Iwase et al., 2016). After one day *in vitro* (DIV1) cells were infected with lentivirus of equal titer containing either human KDM5C cDNA (WT, R1115H, or H514A) or vector alone. Puromycin selection occurred at DIV4 with 0.2 μg/ml puromycin (Sigma). Control puromycin selection with untransduced cultures eliminated nearly all cells, indicating that majority of survived cells carry the KDM5C transgene. Cells were harvested at DIV10 by direct addition of TRI Reagent (Sigma). Samples were subject to total RNA isolation using RNEasy Mini Kit (Qiagen). Ribosomal RNA was depleted using RiboMinus Eukaryotic Kit v2 (Life Technologies). Libraries were prepared using Direct Ligation of Adapters to First-strand cDNA as described previously (Agarwal et al., 2015). Multiplexed libraries were pooled in approximately equimolar ratios and purified from a 1.8% TBE-agarose gel. Libraries were sequenced on the Illumina HiSeq 4000 platform, with paired-end 150 base pair reads, according to standard procedures.

Reads were trimmed to 60bp using BBDuk (35.51) and mapped to the mm9 mouse genome using STAR (2.5.3a) allowing zero mismatches, and only uniquely mapped reads were analyzed further. Due to low mapability of read2, only read1 was used for further analysis. BAM files were indexed and converted to BigWig files in a strand specific manner. BigWigs were normalized to 10 million non-rRNA and non-mitochondrial reads. DESeq2 (1.14.1) was used to

call differential gene expression between conditions, using a cutoff of p-value < 0.01. Cuffdiff (Cufflinks 2.2.1) was used to calculate FPKM. Differentially-expressed genes were examined for functional annotation clustering using DAVID (6.8). To validate overexpression conditions, reads were mapped to a custom genome using STAR, allowing no mismatches, and only uniquely mapped reads were analyzed further. The custom genome contained human *KDM5C* cDNA (NM_001146702.1), where bases were masked with "N" at the H514 (c.1540-1541CA>NN) and R1115 (c.3344G>N) loci to allow for specific mapping under strict no-mismatch conditions.

RNA-seq files can be found at Gene Expression Omnibus GEO:GSE104319.

Multi-species conservation alignment

The following RefSeq sequences were used for alignment for KDM5C: human NP_001140174.1, orangutan NP_001125719.1, rhesus XP_014982969.1, mouse NP_038696.2, rat XP_008771368.1, dog NP_001041497.1, elephant XP_010598233.1, frog NP_001072719.1, fugu XP_003963594.1. The following RefSeq sequences were used for alignment: KDM5A NP_001036068.1, KDM5B NP_006609.3, KDM5C NP_001140174.1, KDM5D NP_001140177.1.

Statistical Analyses

For histone demethylase assays in Figure 2.2A-B, error bars represent standard error of the mean (SEM) of a technical triplicate. For analysis of H3K4me levels in Figure 2.2D, H3K4me signals were normalized to pan-H3 signal and error bars represent SEM of technical triplicate. For RNA-seq data in Figures 2.7-2.8, differentially-expressed genes were determined by DESeq2 using a cutoff of $p < 0.01$. For GO term analysis in Figure 2.9, the modified Fisher

Exact p-value is represented as calculated by the DAVID functional annotation tool (Huang da et al., 2009a, b). For gene expression bar graphs in Supplemental Figure 2.8B-G, error bars represent SEM of three biological replicates.

Notes & Acknowledgements

The data presented in this chapter were previously published in *Frontiers in Molecular Neuroscience* (Volume 11) (Vallianatos *et al.*, 2018), with the following additions: histone tail experiments (peptide microarray, histone binding assays), PCNA binding assay, ubiquitination assay, discussion of phenotype severity and mutation location along KDM5C, discussion of proband mutation in the *CIC* gene.

I performed all of the work presented, with the following exceptions. First, Dr. Catherine Keegan performed the clinical evaluation of the proband and coordinated genetic testing of the proband and family members. Second, Dr. Michael Frieze oversaw the X-chromosome inactivation analyses. Third, Dr. Margit Burmeister oversaw the generation of lymphoblastoid cell lines by Ms. Linda Harper Gates. Fourth, Dr. Shigeki Iwase cloned, expressed, and purified KDM5C PHD1 and PHD2 proteins. Fifth, Dr. Brian Strahl oversaw the histone peptide microarray and binding assay experiments by Dr. Erin Shanle and Ms. Angela Guo. Finally, sequencing was performed at three locations: GeneDx performed clinical exome sequencing of the proband and family, the University of Michigan DNA Sequencing Core performed the genomic DNA resequencing on lymphoblastoid cells, and Genewiz performed RNA-sequencing.

We thank the UM1 family for allowing us to share their story and for their support of our research. We also thank Drs. Raymond Trieval and Robert Fick for their assistance and expertise with the histone demethylase assay, Dr. John Moran and Mr. Trenton Frisbie for their assistance with the fluorescent western blots, Dr. Jacob Mueller for the use of his microscope, Ms. Clara

Farrehi for her assistance with PCNA and histone binding assays, and Dr. Saurabh Agarwal for his assistance and expertise with RNA-sequencing analysis. We also thank Drs. Sally Camper, Yali Dou, Kenneth Kwan, Stephen Parker, Stephanie Bielas, Anthony Antonellis, and Sundeep Kalantry, as well as the members of the Iwase and Bielas labs, for helpful discussions and critical review of the data. We also acknowledge the services of the University of Michigan Microscope and Image Laboratory.

Figures

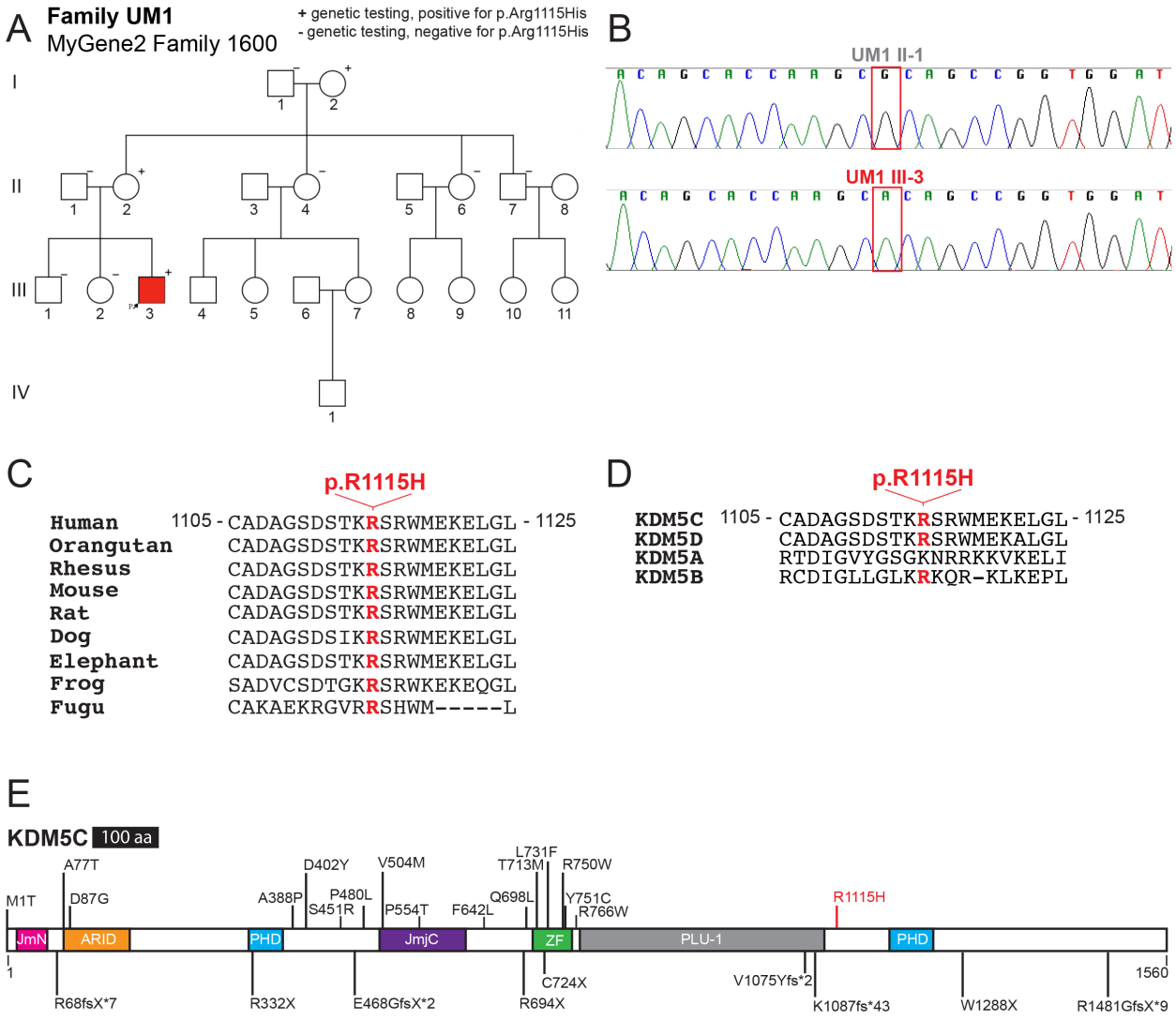

Figure 2.1 KDM5C R1115H mutation in family UM1.

(A) Pedigree of family UM1. (B) Sanger sequencing of genomic DNA from lymphoblastoid cell lines generated from proband (UM1 III-3) and father (UM1 II-1). (C) Multi-species conservation alignment of KDM5C homologs. Multi-species conservation alignment of KDM5C homologs. (D) Conservation alignment of human KDM5 family proteins, KDM5A-D. (E) Schematic of human KDM5C protein and 26 reported mutations associated with KDM5C-XLID. Missense mutations are depicted above the protein, while nonsense and frame-shift mutations are depicted below. Black bar for 100 amino acids (aa) provided as a scale. JmjN, jumonji N-terminal; ARID, AT-rich interaction domain; PHD, plant homeodomain finger; JmjC, jumonji C-terminal; ZF, zinc finger; PLU-1, PLU1-like domain.

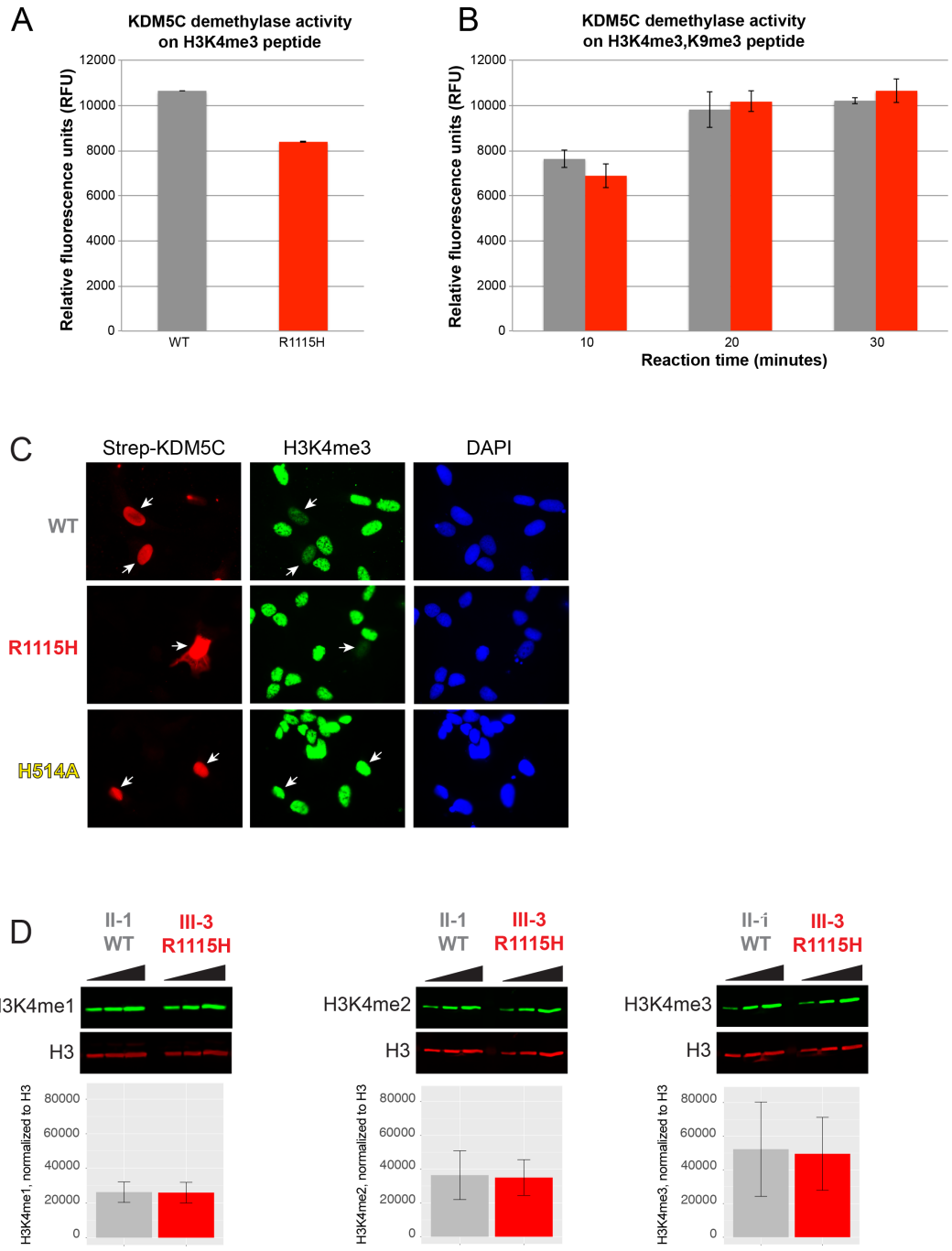

Figure 2.2 KDM5C R1115H has largely intact enzymatic activity.

(A, B) *In vitro* demethylation assay. Full-length KDM5C wildtype (WT) or mutant (R1115H) were subjected to demethylation assay using synthetic histone peptide carrying (A) H3K4me3 or (B) H3K4me3 + K9me3. Relative fluorescence values of formaldehyde, produced by the demethylation reaction, are normalized by the amount of purified proteins in the reaction and plotted. Error bars represent SEM of a technical triplicate. (C) *In situ* demethylation assay. Expression constructs of strep-KDM5C WT, mutant R1115H, or catalytically-inactive H514A were transiently transfected into U2OS cells and stained with antibodies for Strep (red) and H3K4me3 (green). Nuclei were stained with DAPI. (D) H3K4me levels in lymphoblastoid cell lines from proband (UM1-III-3, KMD5C R1115H) and father (UM1-II-1, KDM5C WT) were measured by quantitative Western blot analysis. H3K4me signals were normalized to pan-H3 signal (n=3, Mean ± SEM).

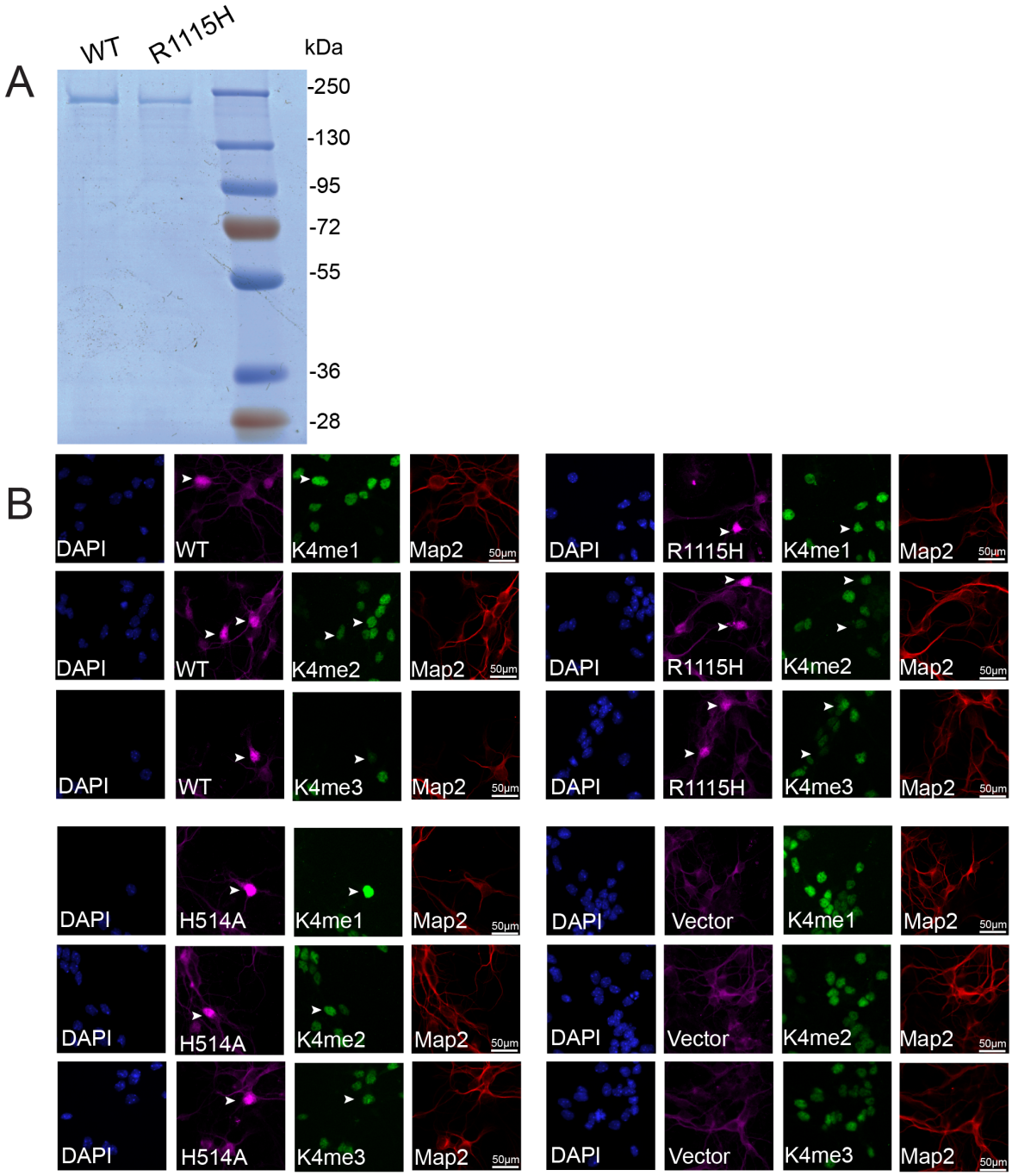

Figure 2.3 Enzymatic activity of KDM5C R1115H is largely retained.

(A) Full-length Strep-tagged KDM5C wildtype (WT) and mutant (R1115H) proteins were expressed in Sf9 cells and purified with Strep-tactin affinity resin. Solubility and equivalence of protein amount was confirmed by SDS-PAGE followed by Coomassie blue staining. (B) *In situ* demethylation assay using primary mouse cortical neuron culture. Expression constructs of strep-KDM5C WT, mutant R1115H, or catalytically-inactive H514A, or vector alone, were transduced into mouse primary neuron cultures and with antibodies for Strep (fuchsia), H3K4me1/2/3 (green), and Map2 (red). Compared to cells transduced with vector alone, significant decrease of K4me2/3 was found in WT- and R1115H over-expressing cells. Demethylation activity was completely abrogated by the H514A mutation. Nuclei were stained with DAPI (blue).

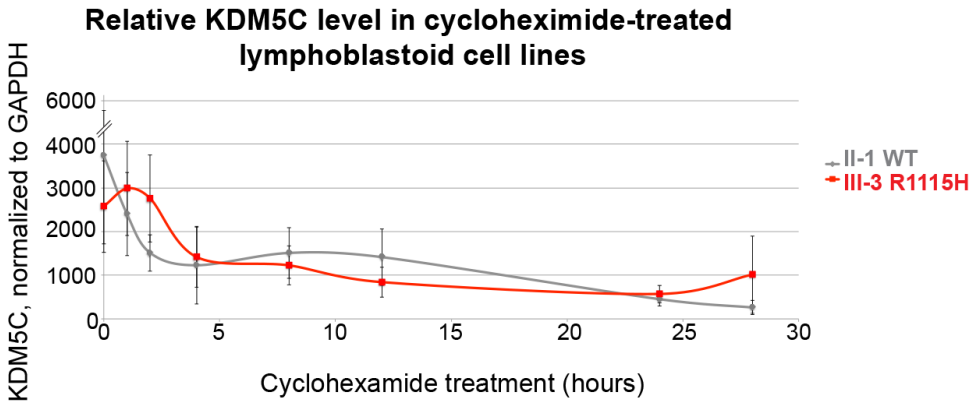

Figure 2.4 *KDM5C* R1115H protein is stable in cells.

(A) Lymphoblastoid cell lines from father (UM1-II-1, KDM5C WT) and proband (UM1-III-3, KDM5C R1115H) were treated with a cycloheximide (CHX) time course from 0-28 hours. The KDM5C levels upon treatment of the cell lines were measured by quantitative Western blot. Relative fluorescence unit normalized by GAPDH signals were plotted (n=3, Mean ± SEM).

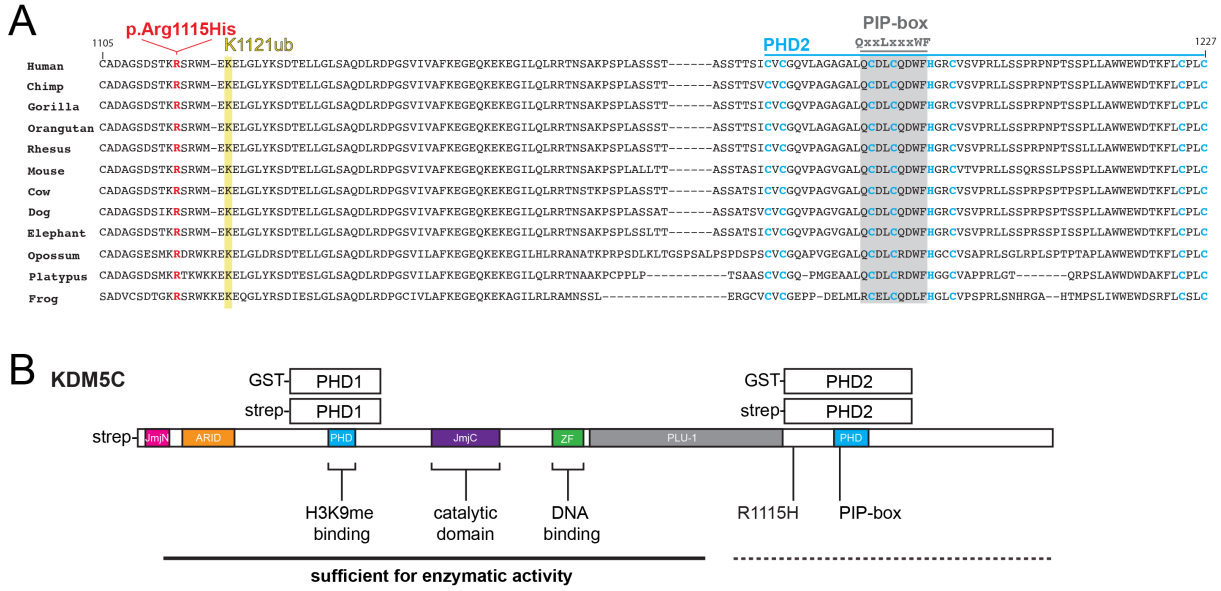

Figure 2.5 KDM5C protein domains.

(A) Location and conservation of the R1115H mutation, nearby ubiquitination site at lysine 1121 (K1121ub), PHD2 domain, and PCNA PIP-box binding site. (B) Protein schematic of KDM5C indicating known functional domains, and protein fragments used in these studies with indicated tags. Solid line indicates N-terminal portion of protein sufficient for enzymatic activity. Dashed line indicates C-terminal portion of protein dispensable for enzymatic activity. JmjN, jumonji N-terminal; ARID, AT-rich interaction domain; PHD, plant homeodomain finger; JmjC, jumonji C-terminal; ZF, zinc finger; PLU-1, PLU1-like domain.

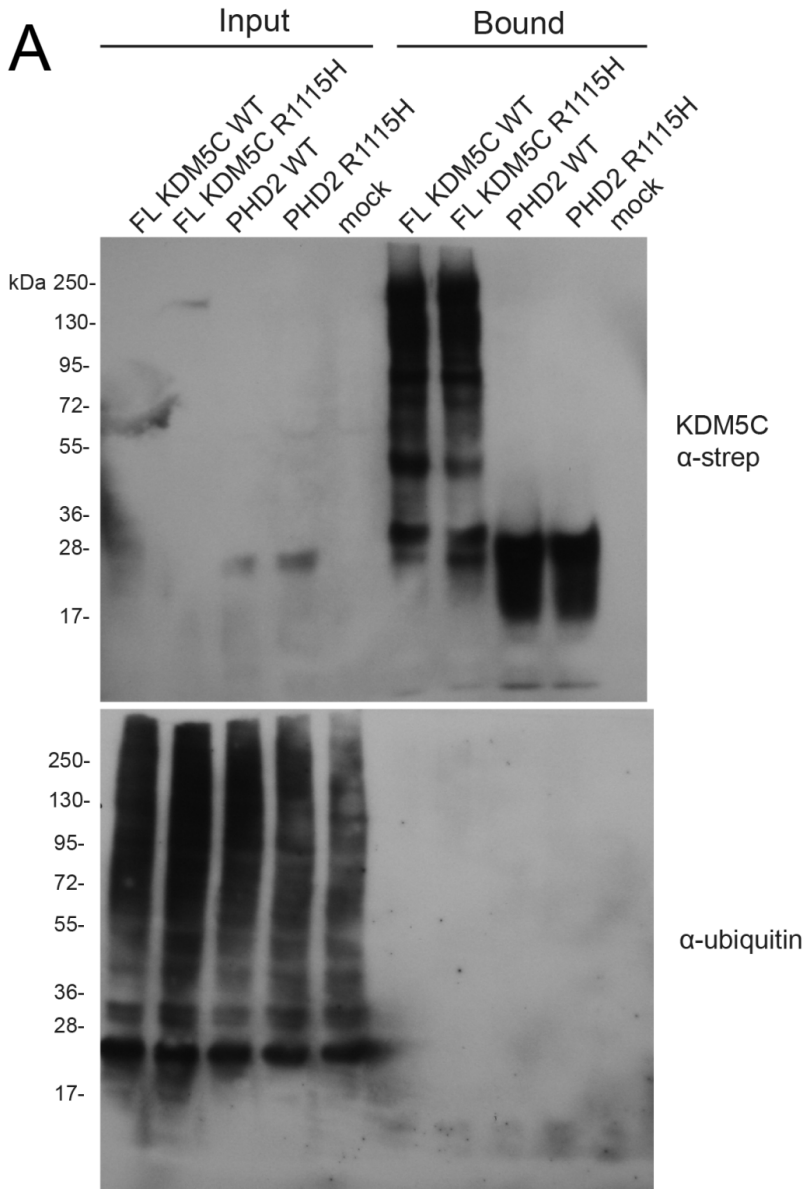

Figure 2.6 Ubiquitination is unchanged by KDM5C-R1115H.

IP of strep-tagged full-length (FL) or PHD fragment KDM5C purified proteins show successful pull-down (top) and no change in ubiquitination levels across conditions (bottom).

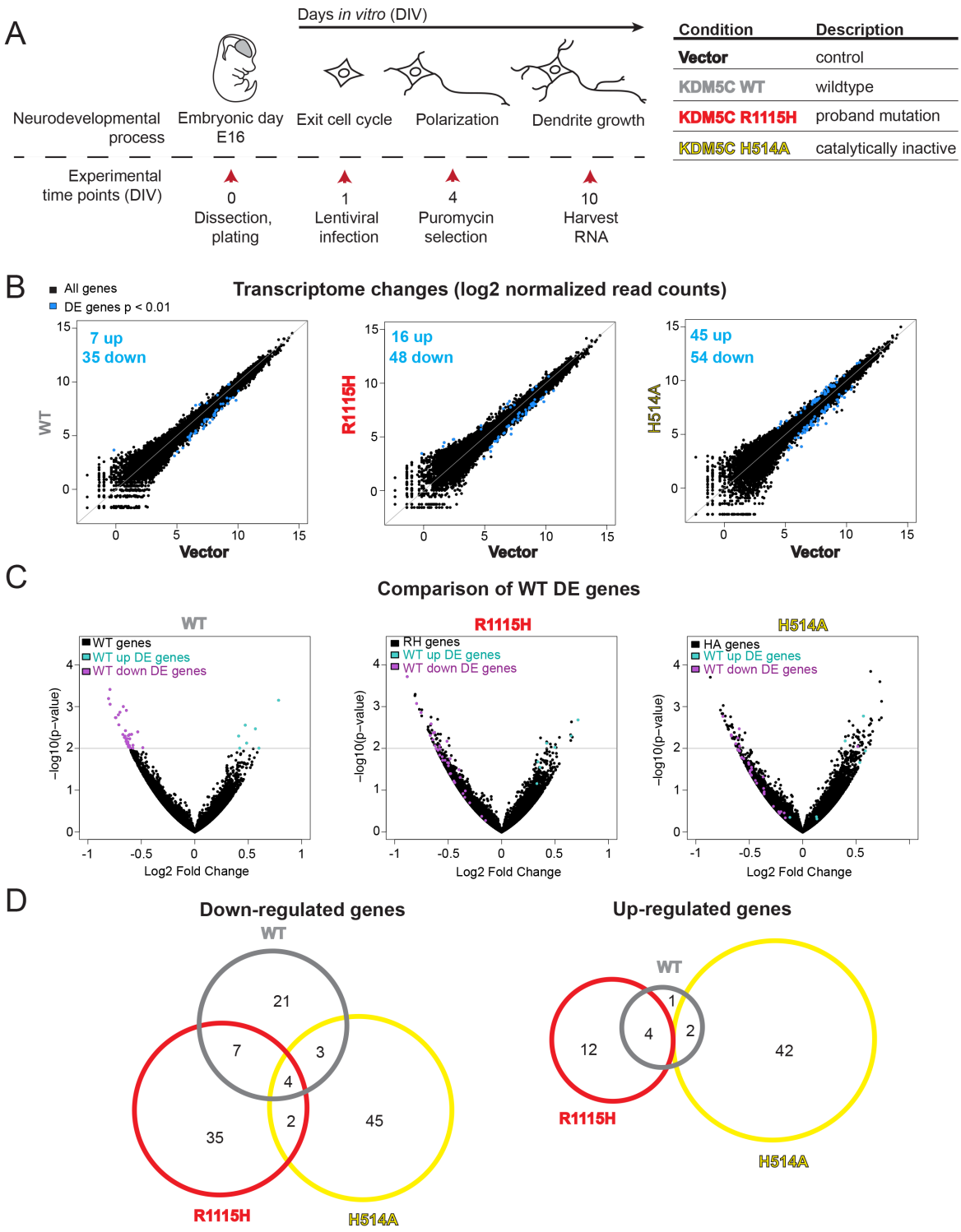

Figure 2.7 RNA-sequencing of primary cultured neurons expressing WT- and mutant-KDM5C.

(A) Schematic of experimental procedures. (B) Normalized expression values of all genes in Vector-WT, Vector-R1115H, and Vector-H514A comparisons. (C) Fold change of down-regulated genes by WT-, R1115H-, and H514A-overexpression plotted against significance. WT up (green) and down (purple) DE genes were plotted for each mutant condition. Horizontal line indicated significance cutoff of $p < 0.01$. (D) Overlap of significantly down- and up-regulated genes ($p < 0.01$).

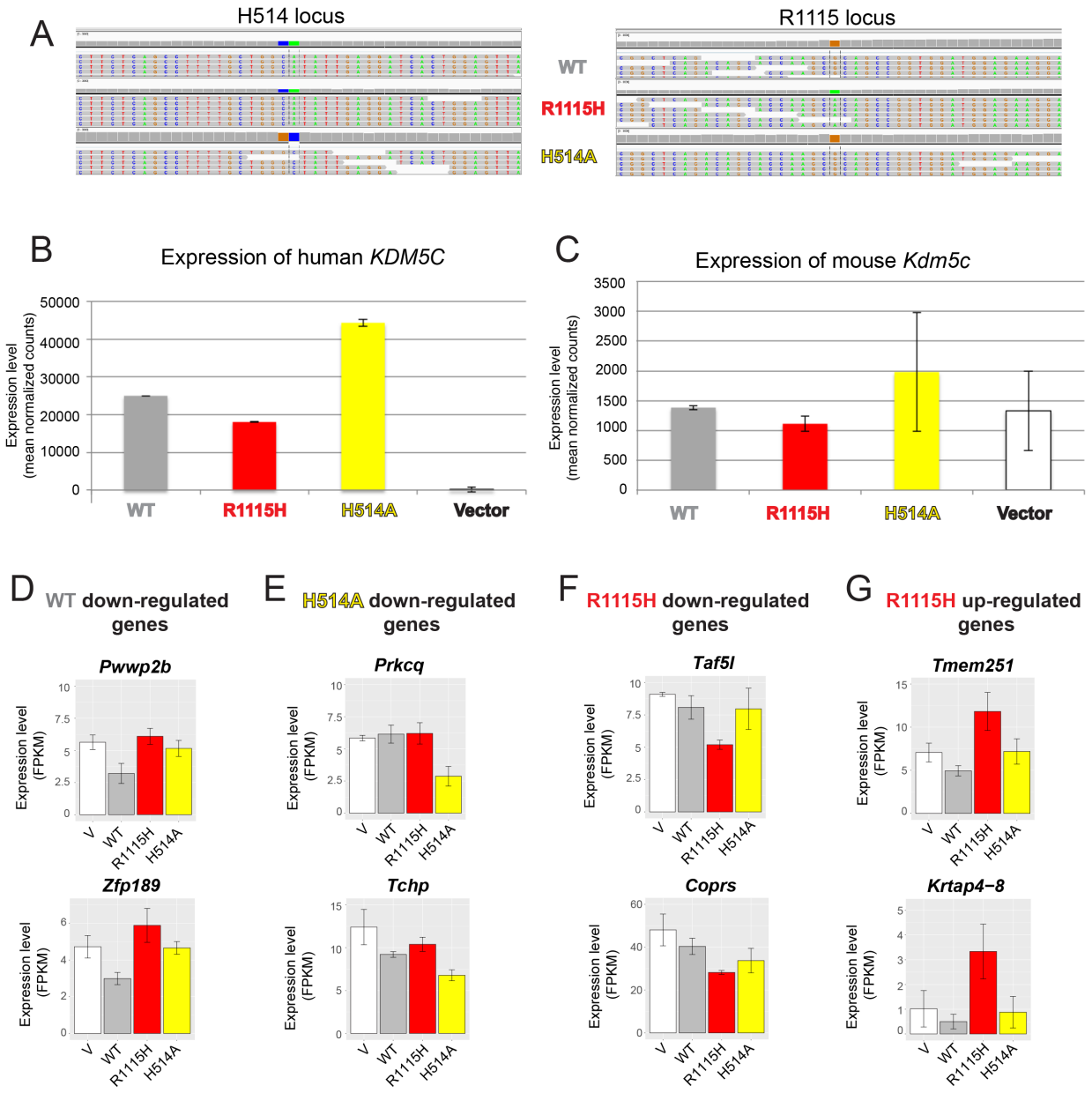

Figure 2.8 RNA-seq validation.

(A) Reads were mapped to human *KDM5C* cDNA the mapped reads for each condition were visualized in IGV. Nucleotide sequences of reads mapped to the regions corresponding H514 and R1115 confirm identity of KDM5C cDNAs overexpressed. (B) Comparison of human *KDM5C* expression levels across conditions, represented as mean normalized read counts. Reads were mapped to human *KDM5C* cDNA sequence. (C) Comparison of mouse *Kdm5c* expression levels across conditions, represented as mean normalized counts. Reads were mapped to mm9 mouse genome. (D-G) Expression patterns of genes that are altered by KDM5C-WT (D), KDM5C-H514A (E), or KDM5C-R1115H (F, G). V, vector control; WT, KDM5C-WT; R1115H, KDM5C-R1115H; H514A, KDM5C-H514A.

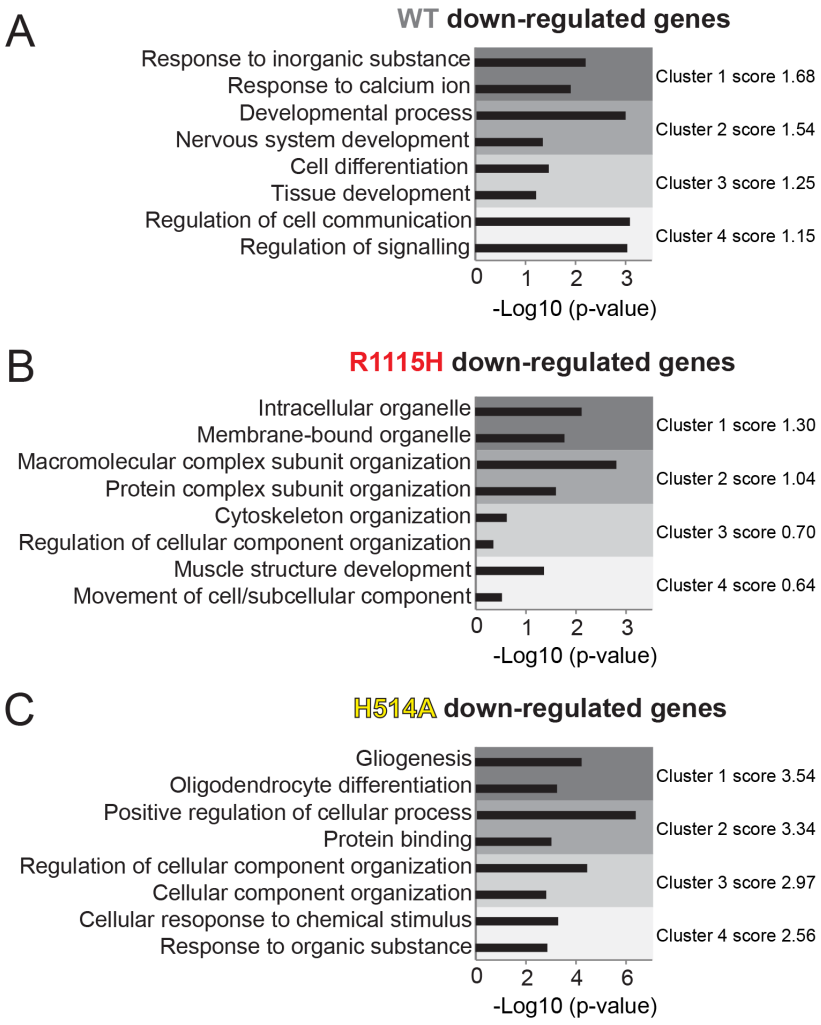

Figure 2.9 Ontology analysis of KDM5C-regulated genes.

Down-regulated genes by KDM5C-WT (A), KDM5C-R1115H (B), and KDM5C-H514A (C) were subjected to GO analysis using DAVID (Functional Annotation Bioinformatics Microarray Analysis). Representative two GO terms each from the top four most enriched annotation clusters were presented with p-values and cluster enrichment score.

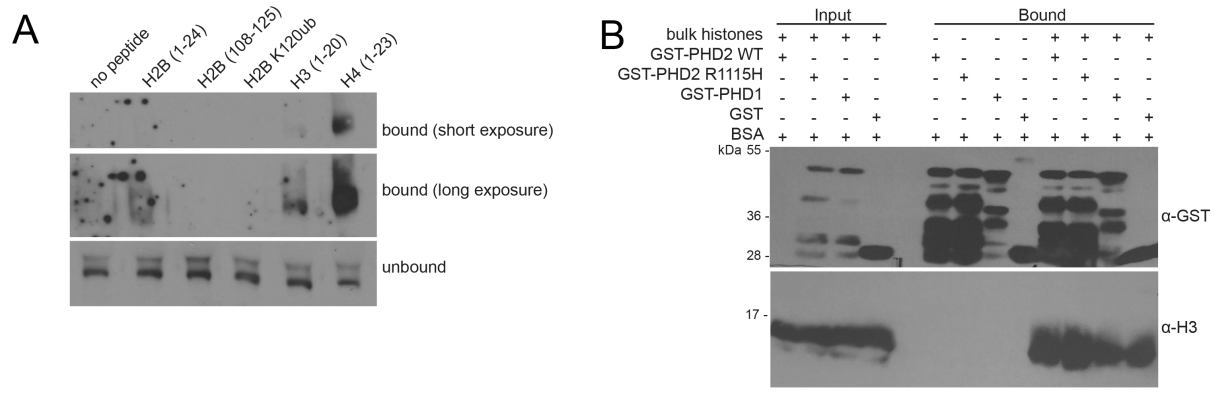

Figure 2.10 KDM5C PHD2 histone peptide binding assays.

(A) Top five candidate histone peptides from microarray assay, tested in *in vitro* binding assay with GST-KDM5C-PHD2-WT. (B) Bulk histones tested in *in vitro* binding assay.

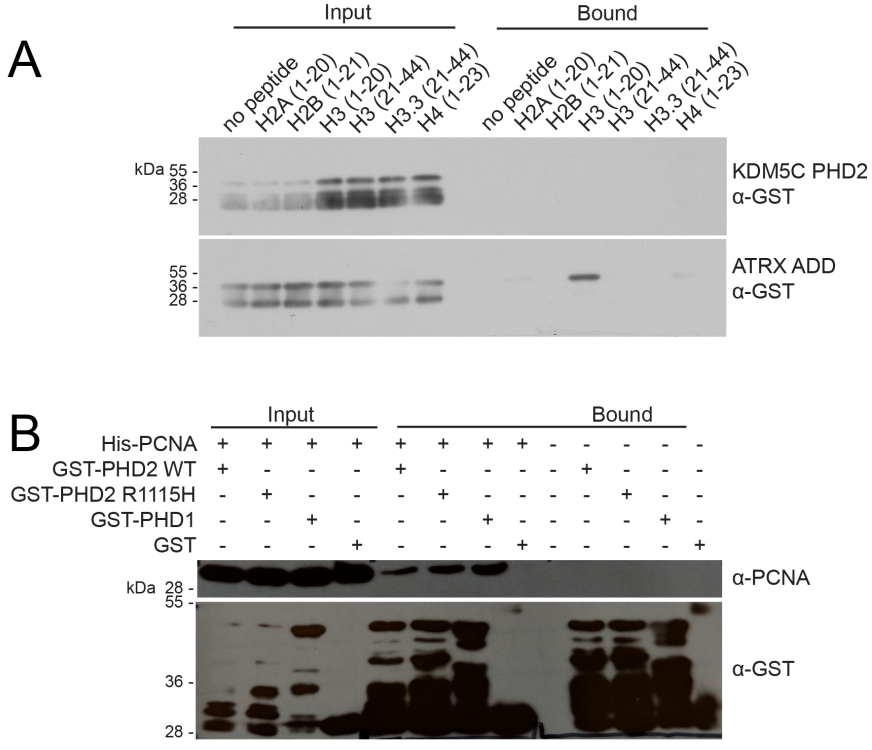

Figure 2.11 KDM5C PHD2 binding assays.

(A) Unmodified histone tail peptides tested *in vitro* binding assay with GST-KDM5C-PHD2-WT. (B) PCNA *in vitro* binding assay.

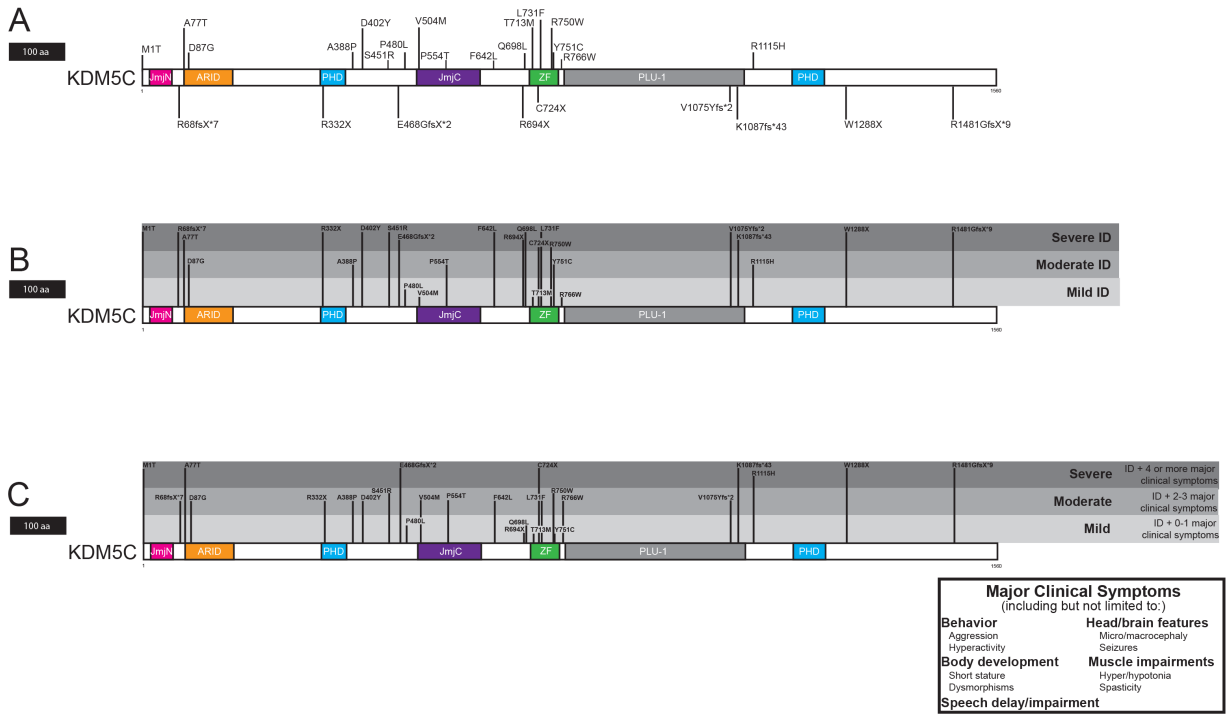

Figure 2.12 Location of KDM5C mutations does not predict disease severity.

(A) Location of 26 reported mutations along the KDM5C protein, with missense mutations above and nonsense and frameshift mutations below. No correlation observed between mutation location and intellectual disability (ID) severity (B) or overall phenotype severity (C). 100 amino acids (aa) bar for scale. JmjN, jumonji N-terminal; ARID, AT-rich interaction domain; PHD, plant homeodomain finger; JmjC, jumonji C-terminal; ZF, zinc finger; PLU-1, PLU1-like domain.

Tables

Table 2.1 *KDM5C* p.Arg1115His is predicted to be damaging.

Computational Predictions of *KDM5C* p.R1115H Pathogenicity			
Program	**Method**	**Score**	**Prediction**
CADD	phred	29.4	Damaging
	raw	6.359	
DANN	rankscore	0.984	Damaging
	score	0.999	
MUpro	SVM	-0.377	Decrease protein stability
Mutation Taster	Score	29	Polymorphism
PolyPhen2	HumDiv	0.941	Possibly damaging
	HumVar	0.535	
PROVEAN		-3.362	Deleterious
SIFT		0.000	Damaging

Table 2.2 Status of X-chromosome inactivation in carrier females.

	UM1 I-1 (grandmother)	UM1 II-2 (mother)	UM1 III-3 (proband)	Ounap et al., 2012
X inactivation pattern	74:26	95:5	NA	100:0
Sex	Female	Female	Male	Female
KDM5C variant	p.Arg1115His (c.3344G > A)	p.Arg1115His (c.3344G > A)	p.Arg1115His (c.3344G > A)	p.Met1Thr (c.2T > C)

Chapter 3 — Amelioration of Brain Histone Methylopathies By Balancing a Writer-Eraser Duo KMT2A-KDM5C

Introduction

Dysregulation of histone methylation has emerged as a major contributor of neurodevelopmental disorders (NDDs) such as autism spectrum disorder and intellectual disability (De Rubeis et al., 2014b; Faundes et al., 2018; Iossifov et al., 2014). Histone methylation can be placed on a subset of lysine and arginine amino acids by histone methyltransferases (writer enzymes) and serves as a signaling platform for a variety of nuclear events including transcription (Kouzarides, 2007). Reader proteins specifically recognize methylated histones, thereby converting methylation signals into higher-order chromatin structures (Taverna et al., 2007). Histone methylation can be removed by a set of histone demethylases (eraser enzymes) (Allis et al., 2007). All three classes of methyl-histone regulators are heavily mutated in NDDs, indicating critical, yet poorly-understood, roles of histone methylation dynamics in brain development and function (Iwase et al., 2017; Iwase and Shi, 2011; Ronan et al., 2013).

Histone H3 lysine 4 methylation (H3K4me) is one of the most well-characterized histone modifications. H3K4me is primarily found at transcriptionally active areas of the genome. The three states, mono-, di-, and tri-methylation (H3K4me1-3), uniquely mark gene regulatory elements and play pivotal roles in distinct steps of transcription. While H3K4me3/2 are enriched at transcriptionally-engaged promoters, H3K4me1 is a hallmark of transcriptional enhancers (Barski et al., 2007; Heintzman et al., 2007). At promoters, H3K4me3 contributes to recruitment

of general transcription machinery TFIID and RNA polymerase II (Lauberth et al., 2013; Vermeulen et al., 2007). H3K4me1 has been shown to tether BAF, an ATP-dependent chromatin remodeling complex, at enhancers (Local et al., 2018).

H3K4me is extensively regulated by seven methyltransferases and six demethylases in mammals (Allis et al., 2007). Consistent with the important roles of H3K4me in transcriptional regulation, genomic distribution of H3K4me appears highly dynamic during brain development (Cheung et al., 2010), in which widespread gene expression changes take place. Developmental H3K4me dynamics appears to be altered in the prefrontal cortices of individuals with autism (Shulha et al., 2012a; Shulha et al., 2012b). However, contributions of each of the 13 enzymes in the dynamic H3K4me landscapes of the developing brain remains largely unknown. Strikingly, genetic alterations in nine of the 13 H3K4me enzymes and at least two H3K4me readers have been associated with human NDDs to date, indicating critical roles of H3K4me balance (Vallianatos and Iwase, 2015) (Figure 3.1A). These human conditions can be collectively referred to as brain H3K4 methylopathies and point to non-redundant yet poorly-understood roles of these genes controlling this single post-translational modification for faithful brain development.

As histone modifications are reversible, one can, in theory, correct an imbalance by modulating the writers or erasers. Chemical inhibitors of histone deacetylases (HDACs) have been successfully used to rescue phenotypes in mouse models of NDDs. HDAC inhibitors were able to ameliorate learning disabilities in mouse models of Rubinstein-Taybi and Kabuki syndromes, which are deficient for CREBBP or KMT2D, writer enzymes for histone acetylation or H3K4me, respectively (Alarcon et al., 2004; Bjornsson et al., 2014). However, none of these chemical compounds has yet been proven applicable to human NDDs. Moreover, the HDAC inhibitors such as SAHA and AR-42 used in these studies interfere with multiple HDACs (Park

et al., 2015), which could potentially result in widespread side effects. Given the non-redundant roles of the H3K4me enzymes, a more specific perturbation is desirable.

In order to achieve specific modulation of H3K4me rather than inhibiting multiple histone modifiers in a given NDD, an important first step is to delineate functional relationships between the H3K4 enzymes. In the present work, we focus on a pair of NDD-associated writer/eraser enzymes: KMT2A and KDM5C. Haploinsufficiency of *KMT2A* underlies Weidemann-Steiner Syndrome (WDSTS), characterized by developmental delay, intellectual disability, characteristic facial features, short stature, and hypotonia (Jones et al., 2012; Strom et al., 2014). Loss of KDM5C function defines Mental Retardation, X-linked, syndromic, Claes Jensen type (MRXSCJ), in which individuals display an intellectual disability syndrome with aggression, short stature, and occasional autism comorbidity (Adegbola et al., 2008; Claes et al., 2000; Jensen et al., 2005b; Vallianatos et al., 2018). Mouse models have provided experimental support for causative impacts of KMT2A and KDM5C deficiencies in impaired cognitive development. Heterozygous *Kmt2a* knockout (KO) mice show compromised fear learning (Gupta et al., 2010), and excitatory-neuron-specific *Kmt2a* deletion similarly led to impaired learning, memory, and anxiety behaviors, as well as altered H3K4me3 distributions and transcriptomes (Jakovcevski et al., 2015; Kerimoglu et al., 2017). In these studies, however, the social behavior and relevant cellular consequences of *Kmt2a* loss were not examined. *Kdm5c*-knockout (KO) mice mimic many MRXSCJ features, including small body size, aggressive behavior, and reduced social activity and learning (Iwase et al., 2016; Scandaglia et al., 2017). *Kdm5c*-KO neurons in the basolateral amygdala exhibit malformation of dendritic arbors and spines along with misregulation of neurodevelopmental genes. However, the functional relationships between KMT2A and KDM5C, e.g. how deficiencies in opposing enzymatic

activities can lead to same learning deficits, remain completely unknown. Additionally, despite the strong association with NDDs, successful modulation of histone methylation to restore normal brain physiology has not been reported in these or any other animal models of histone methylopathies.

In the present work, we tested whether modulating either single H3K4me writer or eraser can ameliorate the neurodevelopmental symptoms observed in the WDSTS and MRXSCJ mouse models. We generated *Kmt2a*-, *Kdm5c*-double mutant (DM) mice, and performed systematic comparisons between wild-type (WT), single mutants, and DM mice. The results detailed below revealed common yet mutually-suppressive traits in the two disease models, thereby providing a binary therapeutic strategy for the two conditions.

Results

KMT2A and KDM5C co-exist broadly in the brain

We first examined expression patterns of KMT2A and KDM5C using publicly-available resources, and found the two genes are broadly expressed throughout brain regions of adult mice and humans (Figure 3.2) (Hawrylycz et al., 2012; Johnson et al., 2009; Lein et al., 2007; Pletikos et al., 2014; Zhang et al., 2017) (Tasic et al., 2016). *Kmt2a* and *Kdm5c* are expressed at comparable levels in all major excitatory and inhibitory neuron subtypes as well as glia cells in mouse visual cortex (Figure 3.2A), and also throughout mouse brains (Figure 3.2B). Consistently, developing and aging human brains express *KMT2A* and *KDM5C* at high, steady levels (Figure 3.2C). Thus, both writer and eraser are co-expressed across brain cell types, regions, and developmental stages in both human and mouse.

Generation of *Kmt2a-Kdm5c* double-mutant (DM) mice

To test genetic interaction of *Kmt2a* and *Kdm5c in vivo*, we generated *Kmt2a-Kdm5c* double-mutant (DM) mice. Experimental mice were F1 hybrids of the two fully-congenic laboratory mouse strains: 129S1/SvImJ $Kmt2a^{+/-}$ males (Cao et al., 2014) and C57BL/6J $Kdm5c^{+/-}$ females (Iwase et al., 2016) (Figure 3.1B). This cross resulted in the following genotypes of male mice: wildtype (WT); *Kmt2a* heterozygote (*Kmt2a*-HET: $Kmt2a^{+/-}$), *Kdm5c* hemizygous knock-out (*Kdm5c*-KO: $Kdm5c^{-/y}$), and *Kmt2a-Kdm5c* double-mutant (DM: $Kmt2a^{+/-}$, $Kdm5c^{-/y}$), thereby allowing us to perform systematic comparison between the WDSTS model (*Kmt2a*-HET), the MRXSCJ model (*Kdm5c*-KO), and their composite (DM). We focus on males, because MRXSCJ predominantly affects males and *Kdm5c*-heterozygous female mice exhibit only minor cognitive deficits (Scandaglia et al., 2017).

These mice were born at expected Mendelian ratios of 25% per genotype, demonstrating the DM mice were not synthetic lethal (Figure 3.1C). Genotypes were confirmed at RNA and DNA levels (Figure 3.3A-C), and protein level for KDM5C (Figure 3.3D). Brain anatomy showed no gross deformities in any of the genotypes (Figure 3.3E). Body weight, during the course of development and in adult, however, was reduced in the two single mutants as well as in DM mice (Figure 3.1D-E). The weight reduction was slightly more pronounced in DM compared to single mutants ($F(3,82) = 11.76$, $p < 0.001$, One-way ANOVA). Thus, loss of *Kdm5c* and *Kmt2a* heterozygosity both led to growth retardation, which was not corrected but rather slightly exacerbated in DM mice.

Altered H3K4me3 landscapes in WDSTS and MRXSCJ models and rescue effects in DM

H3K4me3 is a reaction product of KMT2A-mediated methylation (Dou et al., 2006), while a substrate for KDM5C-mediated demethylation (Iwase et al., 2007; Tahiliani et al.,

2007b). We sought to determine the impact of KMT2A- and KDM5C-deficiencies and double mutation on the H3K4me3 landscape within the brain. We chose to examine the amygdala tissue, because it plays crucial roles in social behavior and fear memory, which are impaired in *Kdm5c*-KO mice (Iwase et al., 2016). In Western blot analyses, global H3K4me1-3 levels were not altered dramatically in any mutant (Figure 3.4A). We thus performed H3K4me3 chromatin immunoprecipitation coupled with deep sequencing (ChIP-seq) to probe local changes genome-wide. To assess the IP specificity, we spiked-in an array of recombinant nucleosomes carrying 15 common methylations along with DNA barcodes appended to the Widom601 nucleosome positioning sequence (Shah et al., 2018) (see Methods). The two H3K4me3 nucleosomes dominated the Widom601-containing DNA in all IP reactions with negligible signals from other methylation states such as H3K4me1 or H3K4me2 (Figure 3.4B), demonstrating a superb specificity of the ChIP.

To obtain a global picture of H3K4me changes, we examined the H3K4me3 signals between WT and the three mutants throughout the mouse genome partitioned into 1-kilobase (kb) bins (Figure 3.5A). We found an overall similarity in H3K4me3 coverage across *Kmt2a*-HET, *Kdm5c*-KO, and DM on a genome-wide scale, as well as at promoter regions (Figure 3.5A, Figure 3.4C). We then broke down the genome into promoter (± 1 kb from transcription start sites [TSS]), intergenic (between genes), and intragenic (within a gene) regions, and asked if any areas are preferentially dysregulated in any of the mutant animals. In WT, 61% of H3K4me3 fell within promoters, consistent with H3K4me3 as a hallmark of promoters (Heintzman et al., 2007; Lauberth et al., 2013; Vermeulen et al., 2007), while smaller fractions, 18% and 21%, were found in intergenic or intragenic regions, respectively (Figure 3.4D). This H3K4me3 distribution pattern was largely consistent across the other genotypes (Figure 3.4D), except for *Kdm5c*-KO

and DM amygdala which had slightly higher proportions of intragenic (25% for both) and intergenic (30% and 29%, respectively) methylation (Figure 3.4D).

Examining local differentially-methylated regions (DMRs), i.e. either hyper- or hypo-methylated for H3K4me3 compared to WT, we found fewer DMRs in *Kmt2a*-HET (1,940) than in *Kdm5c*-KO (11,990) (Figure 3.5B-G, Figure 3.4E-H). This difference is likely due to the heterozygosity of *Kmt2a* which leaves one functional copy of *Kmt2a,* versus the complete loss of *Kdm5c*. Consistently, complete loss of *Kmt2a* in hippocampal neuronal nuclei was previously shown to reduce H3K4me3 in more than four thousand loci (Kerimoglu et al., 2017). In the *Kmt2a*-HET amygdala, hypermethylated loci were primarily found at intragenic regions (56%), while hypomethylated regions were found mainly at promoters (76%, Figure 3.5C). *Kdm5c*-KO DMRs were biased towards an increase in methylation signals (8,284 hypermethylated vs. 3,706 hypomethylated), consistent with loss of a demethylase. In the *Kdm5c*-KO amygdala, the hypermethylated loci showed a roughly even split between promoters, intragenic, and intergenic regions, while the majority of the *Kdm5c*-KO hypomethylated regions were located at promoters (89%, Figure 3.5F). Hypermethylation in non-promoter regions was also detected as an appearance of additional H3K4me3 peaks in *Kdm5c*-KO amygdala (Figure 3.4D). When we overlapped single mutant DMRs (Figure 3.5H), most DMRs were unique to *Kdm5c*-KO (10,994). Interestingly, one half of the *Kmt2a*-HET DMRs overlapped with *Kdm5c*-DMRs (Figure 3.5H), and most of these DMRs were largely misregulated in the same direction between the two single mutants (Figure 3.5I), despite the opposing activity of this pair of enzymes. Motif analysis identified distinct as well as common transcription factor-binding motifs at *Kmt2a*-HET and *Kdm5c*-KO DMRs (Figure 3.4I-J). Thus, *Kmt2a*- and *Kdm5c*-deficiencies lead to both unique and common alterations in H3K4me3 landscapes.

We next asked if any of these DMRs were corrected in double mutants (DM). We defined "rescued" regions as DMRs identified in single mutants that were no longer categorized as a DMR in DM (therefore, no different from WT). We observed a rescue of roughly half of single mutant DMRs in our DM animals: 42% (821/1,940) of *Kmt2a*-HET DMRs and 54% (6,576/11,990) of *Kdm5c*-KO DMRs were not called as differentially methylated in DM (Figures 3.4D, 3.4G, Figure 3.5E-H). Representative examples of rescued and unrescued DMRs are shown (Figure 3.5J-M).

Most rescued DMRs show smaller yet detectable fold changes of H3K4me3 in DM, indicating that the rescue effect was partial (Figure 3.5N). If KMT2A and KDM5C simply counteract, we should observe that hypermethylated regions in *Kdm5c*-KO are hypomethylated in *Kmt2a*-HET, and normalized in DM. We indeed observed such cases in a small fraction of rescued DMRs (solid bars in Figure 3.5N). Unexpectedly, some regions showed reciprocal H3K4me3 changes between the single mutants in an opposite way as expected; namely, hypomethylation in *Kdm5c*-KO and hypermethylation in *Kmt2a*-HET (open bars in Figure 3.5N). The most prevalent pattern of rescued DMRs was the hypermethylated regions of *Kdm5c*-KO that were still moderately hypermethylated in DMs and unexpectedly in *Kmt2a*-HET as well (striped bars in Figure 3.5N). Thus, simple counteractions between *Kmt2a* and *Kdm5c* are relatively rare events, and rather deficiency of the single enzyme results in a complex change of H3K4me3 homeostasis. Nonetheless, our analyses identified thousands of genomic loci at which KMT2A and KDM5C fully or partially mediate aberrant H3K4me3 levels caused by loss of the opposing enzyme.

Transcriptomic similarity between WDSTS and MRXSCJ models and rescue effects in DM

We previously showed *Kdm5c*-KO mice exhibit aberrant gene expression patterns in the amygdala and frontal cortex (Iwase et al., 2016), and the hippocampus (Scandaglia et al., 2017). Excitatory-neuron specific conditional *Kmt2a*-KO mice were also characterized with altered transcriptomes in the hippocampus and cortex (Jakovcevski et al., 2015; Kerimoglu et al., 2017). However, the global gene expression of *Kmt2a*-HET, which is akin to the WDSTS syndrome genotypes, has not been determined. To compare the impact of *Kmt2a*-haploinsufficiency and *Kdm5c*-KO on the transcriptome, we performed unique molecular identifiers (UMI)-RNA-seq (Jaworski and Routh, 2018) using amygdala tissues of adult mice across the four genotypes. To minimize the impact of PCR-derived duplication on gene expression analysis, we used primers containing UMIs during library amplification, and deduplicated the sequencing reads prior to analysis (see Methods). First, we confirmed the lack or reduction of reads from *Kdm5c* exons 11 and 12 and *Kmt2a* exons 8 and 9 in the corresponding mutants (Figure 3.3A-B). Spike-in RNA controls confirmed the broad dynamic range of differential gene expression analysis (Figure 3.6A). The gene expression changes observed in the *Kdm5c*-KO amygdala were similar between the present dataset and our previous dataset obtained from a different cohort of mice (Iwase et al., 2016), demonstrating the reproducibility of the UMI-RNA-seq approach (Figure 3.6B).

We identified a similar number of differentially-expressed (DE) genes ($p < 0.01$) in *Kmt2a*-HET (136 genes) and *Kdm5c*-KO (127 genes) compared to WT amygdala, while DM yielded 203 DE genes (Figure 3.7A). In general, KMT2A acts as a transcriptional coactivator by placing H3K4me (Cao et al., 2014; Dou et al., 2006; Zhang et al., 2016) and KDM5C primarily suppresses transcription by removing this mark (Iwase et al., 2007), yet roles for KDM5C as a positive regulator of transcription have also been reported (Outchkourov et al., 2013; S et al., 2017). Reminiscent of some H3K4me changes that were similar between the single mutants

(Figure 3.5I and 3.5N), examination of fold changes of all DE genes pointed to similar transcriptome alterations in all three mutants compared to WT (Figure 3.7B). Furthermore, a substantial number of DE genes overlap among the three mutants and many of them showed changes in the same direction between single mutants (Figure 3.7C, Figure 3.6C-D), while no genes were reciprocally misregulated (Figure 3.7D). Consistently, the single-mutant DE genes were largely misregulated in the same direction as the other single mutant (Figure 3.6E-F). With respect to the biological implications of the gene misregulation, we did not find any conspicuous alterations of neuronal activity-dependent genes, cell-type specific transcripts, and developmentally-regulated genes in any of the mutant DE genes (Figure 3.8).

Next, we sought to test if normal expression of any individual genes was restored in DM. To this end, we counted single-mutant DE genes that had higher *p*-values than a relaxed significance threshold ($p > 0.1$) in DM vs. WT comparison; an indicator of normal expression. We found that 33% (42/127) of *Kdm5c*-KO-DE genes and 56% (76/136) *Kmt2a*-HET-DE genes were expressed normally in DM (highlight in Figure 3.7E). The rescue effects were visible when we analyzed all single-mutant DE genes as a group (Figure 3.6D). To better understand how transcriptomic similarity and rescue effect can occur simultaneously, we plotted expression fold changes of the 118 rescued genes (Figure 3.7F). We observed that rescued genes were differentially dysregulated in single mutants, e.g. upregulated in *Kdm5c*-KO but unchanged in *Kmt2a*-HET (Figure 3.7F). Thus, these results indicate that the largely-separate sets of genes contribute to the overall transcriptome similarity and the rescue effect in DM.

Gene-annotation enrichment analysis of these 118 rescued genes did not yield statistically-significant enrichment of any functional pathways, however, we were able to separate rescued genes into specific biological pathways that could potentially be restored in DM. Notably, genes that have established roles in central nervous system development and are

genetically associated with neurodevelopmental disorders were among these restored genes in DM. These genes include *Gnao1* (Kulkarni et al., 2016; Nakamura et al., 2013), *Bcl11b* (Lessel et al., 2018), *Arnt2* (Webb et al., 2013), *Mkks* (Katsanis et al., 2000; Schaefer et al., 2011; Slavotinek et al., 2000; Stone et al., 2000), *Arid1a* (Tsurusaki et al., 2012), *Rora* (Guissart et al., 2018), and *Sez6* (Miyazaki et al., 2006).

We then examined the relationship between the H3K4me3 landscape and transcriptome alterations. If H3K4me3 changes drive the gene misregulation in mutants, we should be able to observe a correlation between these two datasets. However, genes with altered promoter-proximal H3K4me3 did not show significant changes in their expression as a group (Figure 3.9A). While H3K4me3 changes are the direct molecular consequences of KMT2A- and KDM5C-deficiency, the steady-state mRNAs we captured in our RNA-seq approach likely involve indirect and adaptive consequences of loss of these enzyme(s), which can lead to an underwhelming correlation between H3K4me3 and transcriptome data. Indeed, we observed a positive correlation between intergenic H3K4me3 levels and spurious transcripts, which are generated at these regions yet likely unstable, therefore, can reflect transcriptional activity more reliably than steady-state mRNA levels (Figure 3.9B). Such spurious intergenic transcripts were previously observed in the *Kdm5c*-KO hippocampus (Scandaglia et al., 2017). We also examined the H3K4me3 coverage at promoter regions of DE genes (Figure 3.9C). Across the different DE gene categories, H3K4me3 levels did not differ between genotypes, with two exceptions: *Kmt2a*-HET down-regulated and *Kdm5c*-KO up-regulated genes showed the expected changes in median H3K4me3 levels (Figure 3.9C). The correlation was also evident between expression of rescued genes and H3K4me3 (Figure 3.9D). Together, these observations indicate that H3K4me3 changes are not sufficient, yet an important contributor, for gene misregulation in single mutants and its correction in DM.

Shared dendritic phenotypes in *Kmt2a*-HET and *Kdm5c*-KO were reversed in DM

Altered dendrite morphology is a hallmark of many human neurodevelopmental disorders (NDDs), as well as animal models of NDDs (Dierssen and Ramakers, 2006; Irwin et al., 2000; Iwase et al., 2016; Penzes et al., 2011; Xu et al., 2014). We previously found that reduced dendritic length and spine density in basolateral amygdala (BLA) neurons of *Kdm5c*-KO adult male mice (Iwase et al., 2016). Assessment of dendritic morphology in *Kmt2a*-HET has not been reported. We performed comparative dendrite morphometry of pyramidal neurons in the BLA using Golgi staining for the four genotypes (Figure 3.10). For *Kdm5c*-KO neurons, we recapitulated our previous findings of reduced dendrite lengths (Figure 3.10B) ($F(3,89) = 2.776$; $p = 0.0459$; WT vs. *Kdm5c*-KO: $p = 0.0341$, one-way ANOVA followed by Tukey multiple comparison tests) and lower spine density (Figure 3.10C) ($F(3,89) = 82.25$; $p < 0.0001$; WT vs. *Kdm5c*-KO: $p = 0.0079$). *Kmt2a*-HET neurons looked remarkably similar to *Kdm5c*-KO (Figure 3.4A), exhibiting trends of reduction in dendrite length, which was not significantly different than WT, however, was also not different than *Kdm5c*-KO (Figure 3.10B) (WT vs. *Kmt2a*-HET: $p = 0.1772$; *Kdm5c*-KO vs. *Kmt2a*-HET $p = 0.8906$). Similarly, spine densities of *Kmt2a*-HET neurons were significantly lower compared to WT and not significantly different than *Kdm5c*-KO (Figure 3.10C) (WT vs. *Kmt2a*-HET: $p = 0.0053$; *Kdm5c*-KO vs. *Kmt2a*-HET $p = 0.9993$). Loss of both *Kmt2a* and *Kdm5c* together had an overall positive effect on neuron morphology (Figure 3.10A). DM dendrite lengths showed trends of restoration (Figure 3.10B), as they were not significantly different than WT (WT vs. DM: $p = 0.5503$), however were also not different than *Kdm5c*-KO (*Kdm5c*-KO vs. DM: $p = 0.5341$). DM exhibited an increase in dendritic spine density that surpassed a rescue effect (Figure 3.10C) (WT vs. DM: $p < 0.0001$; *Kdm5c*-KO vs. DM: $p < 0.0001$, *Kmt2a*-HET vs. DM: $p < 0.0001$). As morphology of dendritic spines

progressively changes during synaptogenesis and development (Arikkath, 2012), we also asked whether developmental subtypes of dendritic spines were altered in any genotype. We did not find dramatic changes in spine morphology among the four genotypes (Figure 3.10D), indicating selective requirement of *Kdm5c* and *Kmt2a* for regulation of spine numbers, but not for morphology. Overall, we conclude that *Kmt2a*-HET and *Kdm5c*-KO share similar dendritic morphology deficits, which are reversed in DM.

Memory alterations in *Kdm5c*-KO were reversed in DM

After observing the restorative molecular and cellular effects in DM mice, we next sought to determine the effect of loss of *Kmt2a* and/or *Kdm5c* on mouse behaviors through a battery of behavioral tests. In accordance with previous findings (Iwase et al., 2016; Scandaglia et al., 2017), *Kdm5c*-KO mice showed significant deficits in associative fear memory, as measured by the contextual fear conditioning (CFC) tests (Figure 3.11A) ($F(3,64) = 2.83$, $p = 0.046$; WT vs. *Kdm5c*-KO: $p = 0.018$). In the novel object recognition tests (NOR), where WT mice showed preference for the new object, *Kdm5c*-KO mice tended to avoid the novel object (Figure 3.11B) ($F(3,64) = 3.20$, $p = 0.030$; WT vs. *Kdm5c*-KO: $p = 0.007$). Homozygous deletion of *Kmt2a* in excitatory hippocampal neurons leads to impaired fear memory in the CFC (Kerimoglu et al., 2017), a hippocampal-dependent memory test (Maren, 2001). In our tests, *Kmt2a*-HET mice showed no deficits compared to WT mice (Figure 3.11A-B) (CFC: $p = 0.789$; NOR; $p = 0.888$), indicating stronger cognitive deficits in the MRXSCJ model compared to WDSTS model mice. Importantly, DM mice also showed no differences from WT mice (Figure 3.11A-B) (CFC: $p = 0.246$; NOR: $p = 0.756$), suggesting that *Kmt2a* heterozygosity can rescue memory deficits of *Kdm5c*-KO mice. These differences in memory tasks were not attributable to differences in

locomotor activity or shock responsiveness, as none of these parameters showed significant differences among the genotypes (Figure 3.1C-D).

Social behaviors are differently dysregulated in *Kmt2a*-HET, *Kdm5c*-KO, and DM mice

In the marble burying test for anxiety and obsessive behaviors (Figure 3.12), we observed significant differences between genotypes ($F(3,30) = 5.017$, $p < 0.0062$). *Kdm5c*-KO mice buried fewer marbles than WT ($p = 0.0052$), yet this difference was not statistically different from *Kmt2a*-HET mice ($p = 0.1716$) which showed no difference from WT ($p = 0.5911$). DM animals likewise showed no difference from WT ($p = 0.1318$), though also were not different than *Kdm5c*-KO ($p = 0.9445$). While this data may indicate a partial rescue of anxiety behaviors in DM, only four DM mice were tested in this paradigm, making it difficult to draw conclusions without more data.

In the three-chambered social interaction test (Figure 3.13A), we observed significant differences between genotypes ($F(3,61) = 4.314$, $p < 0.008$). *Kmt2a*-HET mice showed no differences from WT ($p = 0.082$), in accordance with previous tests in conditional *Kmt2a*-KO mice (Kerimoglu et al., 2017). In contrast, *Kdm5c*-KO ($p = 0.002$), as previously shown (Iwase et al., 2016), as well as DM ($p = 0.011$) mice showed significantly less preference for the stranger mouse compared with WT animals. These data suggest that *Kmt2a* heterozygosity does not rescue deficits of social interaction in the *Kdm5c*-KO.

In tests of social dominance (Figure 3.13B), *Kmt2a*-HET mice won against WTs in 60.9% in of the matches against WT ($p = 0.091$), and *Kdm5c*-KO mice won at least 68.4% of the time ($p = 0.008$). Surprisingly, DM animals lost more than 80% of their bouts against WT ($p = 1.47 \times 10^{-5}$). Although DM mice were slightly smaller compared to single mutants (Figure 3.1D), this is unlikely to drive submissive behaviors, as body mass has been shown to have minimal

impact on social hierarchy unless excess difference (> 30%) is present between animals (Kim et al., 2015; Varholick et al., 2018; Wang et al., 2014), which is not the case in our study (Figure 3.1D) (11% *Kmt2a*-HET vs. WT, 17% *Kdm5c*-KO vs. WT, 25% DM vs. WT). These results demonstrate that a significant increase of social dominance in *Kdm5c*-KO and a similar trend in *Kmt2a*-HET are mediated by opposing enzymes.

In the resident-intruder test, we observed differences in overall aggression between genotypes (Figure 3.13C) ($F(4,61) = 3.015$, $p = 0.037$), and differences across specific types of aggressive behaviors (Figure 3.13D-H, Figure 3.14A-E) ($F(12,61) = 2.15$, $p = 0.015$). Specifically, we found increased darting (Figure 3.13D, Figure 3.14A) in both *Kdm5c*-KO ($p = 0.006$) and *Kmt2a*-HET ($p = 0.032$) mice together with decreased aggression in DM mice, which showed significantly less mounting (Figure 3.13E, Figure 3.14B) (*cf* WT: $p = 0.072$; *cf Kdm5c*-KO: $p = 0.019$; *cf Kmt2a*-HET: $p = 0.004$), and chasing (Figure 3.13F, Figure 3.14C) (*cf* WT: $p = 0.027$; *cf Kdm5c*-KO: $p = 0.010$; *cf Kmt2a*-HET: $p = 0.007$) than all other genotypes. Moreover, we also observed an overall effect of genotype on submissive behaviors of resident mice (Figure 3.13I) ($F(3,61) = 4.071$, $p = 0.011$). For the specific type of submissive behaviors, DM mice exhibited significantly more cowering (Figure 3.13J, Figure 3.14F) compared with all other genotypes (*cf* WT : $p = 0.028$; cf *Kdm5c*-KO: $p = 0.006$; cf *Kmt2a*-HET: $p = 0.005$), and significantly more running away (Figure 3.13K, Figure 3.14G) compared with *Kdm5c*-KO ($p = 0.008$). Importantly, the genotype effect on submissive behaviors inversely correlated with that of aggressive behavior, reinforcing the difference in specific behaviors rather than changes in locomotor activity.

Together, the behavioral studies revealed more pronounced deficits of *Kdm5c*-KO animals compared to *Kmt2a*-HET mice on memory and social interaction, while *Kmt2a*-HET and *Kdm5c*-KO mice shared increased social dominance and aggression. The consequences of double

mutations varied between the tests, with clear rescue effects on cognitive tasks, dominant behavior, and aggression, and no effect on social interactions. Notably, however, no behavioral traits were exacerbated in DM. These results support the idea that the two enzymes mediate some, if not all, deficiencies caused by writer-eraser imbalance at the behavioral level.

Acute dual inhibition of KMT2A and KDM5C shows rescue effects on gene expression

As the DM mice used in this study are constitutive germline mutants, we are unable to determine the therapeutic window of opportunity for the rescue phenotypes observed throughout our study. For this reason, we performed short-term modulation of both *Kmt2a* and *Kdm5c*. We cultured primary mouse cortical neurons, performed shRNA knock-down of *Kdm5c* and *Kmt2a* each individually, and also together, and measured select genes expression via qPCR. We first validated knock-down of each gene *Kdm5c* or *Kmt2a* (Figure 3.15). We noticed that knock-down of one gene does affect the expression levels of the opposing gene, suggesting coregulation. We next tested expression of genes we previously found to be up-regulated in our *Kdm5c*-KO cortical neuron cultures (Iwase et al., 2016). In our system, knock-down of *Kdm5c* alone resulted in increased gene expression of two representative genes, *Grin2d* and *Prkcd*, recapitulating what we previously showed from our *Kdm5c*-KO neurons. Dual inhibition of both *Kdm5c* and *Kmt2a* restored gene expression of each gene to WT levels (Figure 3.15). These data demonstrate that *Kmt2a* mediates some *Kdm5c*-responsive genes in at this early developmental time point. Taken together, our studies identify a functional cooperation between KMT2A and KDM5C in both developing and adult stages.

Discussion

The present work represents the first genetic interactions between chromatin modification writer and eraser enzymes *in vivo*, to our knowledge. Discovery of chromatin-modifying enzymes in the past decades made it clear that virtually no DNA- or histone-modifications are irreversible, and instead are subjected to dynamic regulation by writer and eraser enzymes. The genes encoding these enzymes appear to have undergone duplication events during evolution. Complex organisms carry a greater number of genes that encode enzymes for single chromatin modification. For example, only one enzyme, Set1, is responsible for H3K4 methylation in fission yeast. In fly, three genes, *Trx*, *Trr*, and *Set1* mediate H3K4me installation, and all three genes were duplicated in the mammalian genomes, which resulted in six SET-family H3K4 writers (Eissenberg and Shilatifard, 2010; Rao and Dou, 2015). A plethora of work has demonstrated specialized as well as redundant roles of individual histone-modifying enzymes within a family, in broad biological processes such as cancer and development (Rao and Dou, 2015; Shilatifard, 2012). A fundamental question remained — is there any specific writer-eraser pairing in such highly-duplicated gene families for a single chromatin modification? Mishra *et al*. showed that KDM5A antagonizes KMT2A, KMT2B, and KMT2D to modulate the transient site-specific DNA copy number gains in immortalized human cells (Mishra et al., 2018). Cao et al. found that failed differentiation of mouse embryonic stem cells due to *Kmt2d* deletion can be rescued by *Kdm1a* knockdown (Cao et al., 2018). These pioneering efforts identified functional interplay between the opposing enzymes *in vitro*, however, no *in vivo* study has been reported. Thus, the present study substantially advances our understanding of how methyl-histone writer and eraser enzymes functionally interact during brain development and function.

Brain development is particularly relevant to the H3K4me dynamics, because a cohort of neurodevelopmental disorders have been genetically associated with impaired functions of these

enzymes, as discussed earlier. Our work illuminates the similarities between WDSTS and MRXSCJ model mice in gene expression and neuronal morphological levels, although the two conditions are associated with opposing enzymatic activities. Consistently, many symptoms are common between WDSTS and MRXSCJ, including intellectual disability, short stature, seizures, and aggressive behavior (Claes et al., 2000; Jensen et al., 2005b; Jones et al., 2012; Wiedemann, 1989). Thus, our work underscores a shared pathophysiology of the two conditions. Unlike previous studies using chemical approaches that block multiple chromatin regulators (Alarcon et al., 2004; Bjornsson et al., 2014; Park et al., 2015), we demonstrated that manipulation of a single enzyme, KMT2A or KDM5C, is sufficient to reverse many neurological traits. It may not be surprising that not all traits were reversed in DM mice, such as H3K4me3 at specific loci (Figure 3.5), expression of some genes (Figure 3.7), and social preference (Figure 3.13), because compensatory actions by remaining H3K4me-regulators may potentially mediate these un-rescued traits. Our work opens a new avenue for future studies to delineate the full interplay between the 13 H3K4me-regulatory enzymes throughout brain development and function.

Increased social dominance is a novel behavioral trait we found in both WDSTS and MRXSCJ mouse models. The amygdala is well known to mediate social behaviors (Felix-Ortiz and Tye, 2014; McCann et al., 2018). For example, lesions of BLA result in decreased aggression-like behavior and increased social interactions (Levinson et al., 1980; McGregor and Herbert, 1992), and changes in transcriptional regulation in BLA are observed after social interactions (McCann et al., 2018). Decreased dendritic spine density in *Kmt2a*-HET and *Kdm5c*-KO mice inversely correlates with increased social dominance and aggression (Figures 3.13-14), suggesting that decreased spine density does not represent a loss-of-function in the amygdala, and rather, may reflect a loss of inhibitory control over the amygdala. Thus, determining the connectivity of amygdala with other regions, including prelimbic, infralimbic,

and orbitofrontal cortices (Felix-Ortiz et al., 2016) as well as ventral hippocampus (Felix-Ortiz and Tye, 2014) will be critical for understanding the changes in social behaviors in both WDSTS and MRXSCJ models.

With any therapeutic intervention, careful assessments of side effects will be inevitable. In our work, while a substantial fraction of H3K4me3 DMRs and gene misregulation in single mutants were corrected in DM (Figures 3.5 and 3.7), combinatorial ablation of KMT2A and KDM5C should reduce net regulatory action over H3K4me3, which may lead to adverse consequences. Indeed, our genomics approaches identified H3K4me3 DMRs that are unique to the DM brain, and several genes uniquely altered in DM animals (Figure 3.15). It is still plausible that these gene and H3K4me3 changes in DM can lead to phenotypic outcomes that were not examined in this study. Nevertheless, we were encouraged that none of the neurological traits measured in this study showed exacerbation in DM.

It is important to note that the double mutations introduced in our mice were constitutive, and therefore a lifetime of adaptation to loss of these two major chromatin regulators may occur from early developmental stages. A more realistic therapeutic strategy may be acute inhibition of KDM5C and KMT2A in juvenile or mature brain. Previous work characterizing mouse models with excitatory-neuron specific ablation of *Kdm5c* or *Kmt2a* via *CamKII*-Cre found that conditional *Kmt2a* deletion led to clear learning deficits (Kerimoglu et al., 2017), while cognitive impairments in the conditional *Kdm5c*-KO mice were much milder than those of constitutive *Kdm5c*-KO mice (Scandaglia et al., 2017). These results suggest a developmental origin of phenotypes in *Kdm5c*-KO. Future investigations are needed to address whether the effects of acute inhibition of opposing enzymes in these mouse models can restore such neurodevelopmental deficits.

We began these studies with our initial working model, proposing a functional relationship between KMT2A and KDM5C by direct competition for writing and erasing H3K4me at the same genomic loci (Figure 3.16A). Under this model, we would expect to observe increased H3K4me3 and gene expression upon loss of *KDM5C* in the *Kdm5c*-KO mice, and decrease H3K4me3 and gene expression upon loss of *KMT2A* in the *Kmt2a*-HET mice (Figure 3.16B). Importantly, we would expect these opposite molecular effects to manifest at the same genomic loci. Instead, the data in this study suggest that KMT2A and KDM5C do functionally interact, but in a manner different than expected. We revised our initial model and now hypothesize that KMT2A and KDM5C work on separate loci, and functionally interact to mediate abnormality of the opposing enzyme but not by directly competing (Figure 3.17). We suggest loss of one enzyme then triggers the redistribution of the opposite enzyme to change normal occupancy of that enzyme to a location it normally does not go. Under this new model, losing both enzymes together results in the neutralization effect seen in the rescued phenotypes of DM mice. Future experiments to address this new hypothesis include ChIP-seq of KMT2A and KDM5C across the four genotypes, to see how genomic distribution patterns change upon loss of either or both enzymes. With our revised hypothesis we would not expect to see many overlapping peaks in WT mice, but in each *Kmt2a*-HET or *Kdm5c*-KO single mutant we would expect to see a redistribution of the opposing enzyme.

Materials & Methods

Mouse models

Kdm5c-KO mice were previously described (Iwase et al., 2016). *Kmt2a*-HET mice were generated by crossing previously-described *Kmt2a*-flox (exons 8 and 9) mice with B6.129-

Gt(ROSA)26Sor$^{tm1(cre/ERT2)Tyj}$/J-Cre mice (McMahon et al., 2007). To backcross *Kmt2a*$^{+/-}$ mice onto the desired 129S1/SvImJ strain, we employed the marker assisted accelerated backcrossing through Charles River Labs. *Kmt2a*$^{+/-}$ mice were bred to the N4 generation at minimum, where mice were >90% congenic for 129S1/SvImJ. All experimental mice were generated as F1 generation hybrids from mating between 129S1/SvImJ *Kmt2a*$^{+/-}$ males and C57Bl/6 *Kdm5c*$^{+/-}$ females: WT males (*Kmt2a*$^{+/+}$, *Kdm5c*$^{+/y}$); *Kdm5c*-KO males (*Kmt2a*$^{+/+}$, *Kdm5c*$^{-/y}$); *Kmt2a*-HET males (*Kmt2a*$^{+/-}$, *Kdm5c*$^{+/y}$); and *Kdm5c*-*Kmt2a*-DM males (*Kmt2a*$^{+/-}$, *Kdm5c*$^{-/y}$). Genotypes were confirmed using the following primers: for *Kmt2a*, 5'-GCCAGTCAGTCCGAAAGTAC, 5'-AGGATGTTCAAAGTGCCTGC, 5'-GCTCTAGAACTAGTGGATCCC; for *Kdm5c*, 5'-CAGGTGGCTTACTGTGACATTGATG, 5'-TGGGTTTGAGGGATACTTTAGG, 5'-GGTTCTCAACACTCACATAGTG.

Western blot analysis

Total proteins from adult brain tissues were subjected to Western blot analysis using in-house anti-KDM5C (Iwase et al., 2016), and anti-GAPDH antibodies (G-9, Santa Cruz). For histone proteins, nuclei were enriched from the dounce-homogenized brain tissues using Nuclei EZ prep Kit (Sigma, NUC-101). DNA were digested with micrococcal nuclease (MNase, NEB) for 10 minutes at room temperature and total nuclear proteins were extracted by boiling the samples with the SDS-PAGE sample buffer. The following antibodies were used for Western blot analyses: anti-H3K4me3 (Abcam, ab8580), anti-H3K4me2 (Thermo, #710796), anti-H3K4me1 (Abcam, ab8895), and anti-H3 C-terminus (Millipore, CS204377).

Brain histology

Mice were subjected to transcardial perfusion according to standard procedures. Fixed brains were sliced on a freeze microtome, yielding 30 μm sections that were then fixed, permeabilized, blocked, and stained with DAPI. Slides were imaged on an Olympus SZX16 microscope, with an Olympus U-HGLGPS fluorescence source and Q Imaging Retiga 6000 camera. Images were captured using Q-Capture Pro 7 software. Data were collected in a blind fashion, where samples were coded and genotypes only revealed after data collection was complete.

ChIP-seq

Brains from adult (6-8 months) male mice were microdissected to enrich for the amygdala. N=2 animals were used for WT, and N=3 animals were used for *Kmt2a*-HET, *Kdm5c*-KO, and DM as biological replicates. Nuclei were isolated using Nuclei EZ prep Kit (Sigma, NUC-101), and counted after Trypan blue staining. 20,000 nuclei for each replicate were subjected to MNase digestion as previously described (Brind'Amour et al., 2015). We essentially followed the native ChIP-seq protocol (Brind'Amour et al., 2015) with two modifications. One was to use a kit to generate sequencing libraries in one-tube reactions (NEB, E7103S). Another modification was to spike-in the panel of synthetic nucleosomes carrying major histone methylations (EpiCypher, SKU: 19-1001) (Shah et al., 2018). For ChIP, we used the rabbit monoclonal H3K4me3 antibody (Thermo, clone #RM340).

Libraries were sequenced on the Illumina NextSeq 500 platform, with single-end 75 base-pair sequencing, according to standard procedures. We obtained 20 to 59 million reads per sample. Reads were aligned to the mm10 mouse genome (Gencode) and a custom genome containing the sequences from our standardized, synthetic nucleosomes (EpiCypher) for

normalization (Grzybowski et al., 2015), using Bowtie allowing up to 2 mismatches. Only uniquely-mapped reads were used for analysis. Range of uniquely mapped reads for input samples was 38-44 million reads. All IP replicates had a mean of 9.1 million uniquely mapping reads (range: 7.4 to 13.9 million). The enrichment of mapped synthetic spike-in nucleosomes compared to input was calculated and used as a normalization coefficient for read depth each ChIP-seq replicate (Grzybowski et al., 2015).

Peaks were called using MACS2 software (v 2.1.0.20140616) (Zhang et al., 2008) using input BAM files for normalization, with filters for a q-value < 0.1 and a fold enrichment greater than 1. Differentially-methylated regions (DMRs) were called using the MACS2 bdgdiff command with default parameters and incorporating the synthetic nucleosome normalization into the read depth factor. Bedtools was used to calculate coverage across individual replicates. We also used Bedtools to intersect peaks of interest with mm10 promoters (defined here as ±1 kb from annotated transcription start site [TSS]), intragenic regions (as defined by annotated mm10 gene bodies, but excluding the previously defined promoter region), and intergenic regions (regions that did not overlap with promoters or gene bodies). DMRs from single mutants (2a-HET or 5c-KO) were considered "rescued" in DM animals if that single-mutant peak was *not* called as a DMR in the DM analysis. For the global H3K4me3 analysis, the Bedtools multicov command was used to calculate coverage over 1 kb windows throughout the genome, as well as at each promoter (±1 kb from annotated TSS). HOMER (v4.10) was used to carry out motif enrichment analysis (Heinz et al., 2010). We selected the top 5 motifs, and only motifs from known mammalian ChIP-seq experiments were represented in our data. Normalized bam files were converted to bigwigs for visualization in the UCSC genome browser. Genes near peaks were identified by Bedtools and RefSeq genomic accession number were converted to official gene symbol using bioDBnet (Mudunuri et al., 2009).

The ChIP-seq data have been deposited in NCBI's Gene Expression Omnibus (Edgar et al., 2002). Data are accessible through GEO series accession numbers: SuperSeries GSE127818, SubSeries GSE127817.

RNA-seq

Brains from adult (3 to 6 months) male mice were microdissected to enrich for the amygdala. N=3 animals were used per genotype. Tissue was homogenized in Tri Reagent (Sigma). Samples were subjected to total RNA isolation, and RNA was purified using RNEasy Mini Kit (Qiagen). ERCC spike-in RNA was added at this stage, according to manufacturer's instructions (Life Technologies). Ribosomal RNA was depleted using NEBNext rRNA Depletion kit (New England Biolabs). Libraries were prepared using the Click-seq method, using primers containing unique molecular identifiers (UMIs), as described previously (Jaworski and Routh, 2018). Multiplexed libraries were pooled in approximately equimolar ratios and purified using Agencourt RNAClean XP beads (Beckman Coulter).

Libraries were sequenced on the Illumina HiSeq 4000 platform, with paired-end 150 base pair reads, according to standard procedures. Reads were mapped to the mm10 mouse genome (Gencode) using STAR (v2.5.3a) (Dobin et al., 2013), where only uniquely mapped reads were used for downstream analyses. Duplicates were removed using UMI-tools (v0.5.4) (Smith et al., 2017), and a counts file was generated using FeatureCounts (Subread v1.5.0) (Liao et al., 2014). BAM files were converted to bigwigs using deeptools (v3.1.3) (Ramírez et al., 2014; Ramírez et al., 2016). Differentially expressed (DE) genes were called using DESeq2 (v1.14.1) (Anders and Huber, 2010; Love et al., 2014). According to the previous RNA-seq study of *Kdm5c*-KO mice (Iwase et al., 2016), we used $p < 0.01$ to identify DE genes. Data analyses were performed with RStudio (v1.0.136) or GraphPad Prism (v7.00 or 8.02) for Mac (GrapPad Software, La Jolla

California USA, www.graphpad.com). Fold change heatmaps was created using shinyheatmap on the web (Khomtchouk et al., 2017). Cell type expression data was downloaded from the Barres lab Brain RNA-seq Portal (Zhang et al., 2014). Cell type enriched genes were determined as having > 5 FPKM in cell type A and > 2 FPKM cell A FPKM/each other cell type FPKM. We identified 471 astrocyte (A), 629 neuron (N), 840 micorglia (M), 197 oligodendrocyte precursor (Op), 74 newly formed oligodendrocyte (On), 96 myelinating oligodendrocyte (Om), and 716 endothelial (E) cell enriched genes. Temporal expression data from human male amygdala was downloaded from the BrainSpan Atlas of Developing Human Brain (Miller et al., 2014).

The RNA-seq data have been deposited in NCBI's Gene Expression Omnibus (Edgar et al., 2002). Data are accessible through GEO series accession numbers: SuperSeries GSE127818, SubSeries GSE127722.

Neuronal Golgi staining and morphological analyses

Brains from adult (2-8 months) mice were dissected, and brains were incubated in a modified Golgi-Cox solution for 2 weeks at room temperature. The remaining procedure of Golgi immersion, cryosectioning, staining, and coverslipping was performed as described previously (Shmelkov et al., 2010).

Morphological analyses of dendrites were carried out as described previously (Shmelkov et al., 2010). Four animals were used for each genotype, and pyramidal neurons in the basolateral amygdala per animal were quantified: N=24 neurons for WT, *Kmt2a*-HET and *Kdm5c*-KO and N=27 neurons for DM. Quantification was done using commercially available software, NeuroLucida (v10, Microbrightfield, VT), installed on a Dell PC workstation that controlled Zeiss Axioplan microscope with a CCD camera (1600 x 1200 pixels) and with a motorized X, Y, and Z-focus for high-resolution image acquisition (100X oil immersion) and quantifications. The

morphological analyses included: dendritic lengths, spine counts, and spine subtype morphology. All sample genotypes were blinded to the analysts throughout the course of the analysis.

The criteria for selecting candidate neurons for analysis were based on: (1) visualization of a completely filled soma with no overlap of neighboring soma and completely filled dendrites, (2) the tapering of most distal dendrites; and (3) the visualization of the complete 3-D profile of dendritic trees using the 3-D display of the imaging software.

For quantitative analysis of spine subtypes (thin, stubby, mushroom, filopodia and branched spines), only spines orthogonal to the dendritic shaft were included in this analysis, whereas spines protruding above or beneath the dendritic shaft were not sampled. This principle remained consistent throughout the course of analysis.

After completion, the digital profile of neuron morphology was extrapolated and transported to a multi-panel computer workstation, then quantitated using NeuroExplorer program (Microbrightfield, VT), followed by statistical analysis (one- and two-way ANOVAs, $p < 0.05$).

Behavioral paradigms

Prior to behavioral testing, mice were acclimated to the animal colony room for one week single-housing in standard cages provided with lab diet and water *ad libitum*. A 12-hour light-dark cycle (7:00AM-7:00PM) was utilized with temperature and humidity maintained at 20 ±2 ºC and >30%, respectively. The University of Michigan Committee on the Use and Care of Animals approved all tests performed in this research. Five tests, listed in order of testing, were performed: Novel Object Recognition (5 days), Context Fear Conditioning (2 days), Three-Chambered Social Interaction (2 days), Social Dominance Tube Test (3-4 days), and Resident-intruder (2-3 days). All testing was conducted in the morning by experimenters blind to

genotype. 70% ethanol was used as a cleaning agent in every test between each trial. Data were collected in a blind fashion, where mice were coded and genotypes only revealed after testing was complete.

Novel Object Recognition: Mice were first habituated to testing arenas (40 x 30 x 32.5 cm^3) in three, 10 minute sessions over six consecutive days (Tchessalova and Tronson, 2019; Vogel-Ciernia and Wood, 2014). 24 hours later, mice were allowed to explore on two identical objects (jar or egg, counterbalanced across animals) for two, 10-minute trials spaced three hours apart. All animals were returned to the arena tested 24 hours after the first training session and presented with one training object ("familiar" object: jar or egg) and one "novel" object (egg or jar). Exploration of the objects was defined as nose-point (sniffing) within 2 cm of the object. Behavior was automatically measured by Ethovision XT9 software using a Euresys Picolo U4H.264No/0 camera (Noldus, Cincinnati, OH). Preference was calculated as the time spent exploring novel object/total time exploring both objects. One-sample t-tests against 50% (no preference) were used to establish whether animals remembered the original objects.

Contextual Fear Conditioning: Context fear conditioning was assessed as previously described (Keiser et al., 2017). Mice were placed into a distinct context with white walls (9 ¾ × 12 ¾ × 9 ¾ in) and a 36 steel rod grid floor (1/8 in diameter; ¼ spaced apart) (Med-Associates, St. Albans, VT) and allowed to explore for 3 minutes, followed by a 2-second 0.8 mA shock, after which mice were immediately returned to their home cages in the colony room. 24 hours later, mice were returned to the context and freezing behavior was assessed with NIR camera (VID-CAM-MONO-2A) and VideoFreeze (Med Associates, St Albans, VT). Freezing levels were compared between genotypes using a between-groups analysis (one-way ANOVA) with genotype as the between-subjects factor.

Three-Chambered Social Interaction: Mice were placed into a three-chambered apparatus consisting of one central chamber (24 x 20 x 30 cm^3) and two identical side chambers (24.5 x 20 x 30 cm^3) each with a containment enclosure (8 cm diameter; 18 cm height; grey stainless steel grid 3 mm diameter spaced 7.4 mm apart) and allowed to habituate for 10 minutes. 24 hours later, mice were returned to the apparatus that now included a 2-3 month old stranger male mouse (C57BL/6N) on one side of the box ("stranger"), and a toy mouse approximately same size and color as stranger mouse on other ("toy"). Exploration of either the stranger or toy was defined as nose-point (sniffing) within 2 cm of the enclosure and used as a measure of social interaction (Crawley, 2007). Behavior was automatically scored by Ethovision XT9 software as described above, and social preference was defined as time exploring stranger/total exploration time. Social preference was analyzed using one-sample t-tests for each genotype. A repeated measures analysis was used for each aggression (genotype x aggression measures ANOVA) and submissive behaviors (genotype x submissive) to analyze aggressive behaviors.

Social Dominance Tube Test: 24 hours prior to testing, mice were habituated to the plastic clear cylindrical tube (1.5 in diameter; 50 cm length) for 10 minutes. During test, two mice of different genotypes were placed at opposite ends of the tube and allowed to walk to the middle. The match concluded when the one mouse (the dominant mouse) forced the other mouse (the submissive mouse) to retreat with all four paws outside of the tube (a "win" for the dominant mouse) (Larrieu et al., 2017; Moretti et al., 2005; Zhou et al., 2017). Each mouse underwent a total of three matches against three different opponents for counterbalancing. Videos were recorded by Ethovision XT9 software as described above, and videos were manually scored by trained experimenters blind to genotype. The number of "wins" was reported as a percentage of total number of matches. Data were analyzed using an Exact Binomial Test with 0.5 as the probability of success (win or loss).

Resident-intruder aggression: Resident-intruder tests were used to assess aggression. Tests performed on consecutive days, where the resident mouse was exposed to an unfamiliar intruder mouse for 15 minutes (Guzmán et al., 2013; Miczek et al., 2001). A trial was terminated prematurely if blood was drawn, if an attack lasted continuously for 30 seconds, or if an intruder showed visible signs of injury after an attack. Resident mice were assessed for active aggression (darting, mounting, chasing/following, tail rattling, and boxing/parrying), as well as submissive behaviors (cowering, upright, running away). Intruder mice were assessed for passive defense (freezing, cowering, and digging). Behavior was recorded and videos scored manually by experimenters blind to genotype. Data were analyzed using a between groups analysis (one-way ANOVA) with genotype as the between-subjects factor.

Notes & Acknowledgements

This work was available as a preprint in *BioRxiv* (Vallianatos *et al.*, 2019) and submitted to a journal for consideration at time of writing. The following additions were made: marble burying test, acute inhibition, discussion of initial and revised working models for KMT2A and KDM5C interaction.

I performed all experiments and analyses, with the following exceptions: First, Dr. Young Ah Seo performed global H3K4me3 Western blots. Second, Dr. Shigeki Iwase prepared ChIP libraries. Third, Mr. Robert S. Porter performed H3K4me3 ChIP-seq analyses. Fourth, Ms. Patricia M. Garay analyzed RNA-seq data for activity-dependent genes. Fifth, Dr. Michael C. Wu oversaw dendritic morphometry analyses at Neurodigitech, including specimen histology, image acquisition, and feature analyses. Sixth, Dr. Natalie Tronson oversaw the mouse behavioral tests performed by Ms. Brynne Raines and Dr. Katie Collette. Finally, next-generation sequencing was performed at the following locations: Girihlet, for ChIP-seq; and

Genewiz, for RNA-seq. Drs. Yali Dou and Catherine Keegan provided key experimental recourse and made important intellectual contributions.

We thank Dr. Ken Kwan, Ms. Mandy Lam, and Mr. Owen Funk for their assistance with the Click-seq library preparation protocol and use of their microscope; Mr. Chris Gates for his assistance with RNA-seq analyses; Ms. Linh Vu for her assistance preparing shRNA plasmids and viruses for pairwise knock-down experiments; Ms. Clara Farrehi for her assistance with transcriptome analyses; Mr. Jordan Rich for his assistance with pairwise knock-down experiments and global histone methylation Western blots; and Mr. Demetri Tsirukis for his assistance with brain histology. We also thank Drs. Sally Camper, Kenneth Kwan, Stephen Parker, Stephanie Bielas, Michael-Christopher Keogh, as well as the members of the Iwase and Bielas labs, for helpful discussions and critical review of the data.

Figures

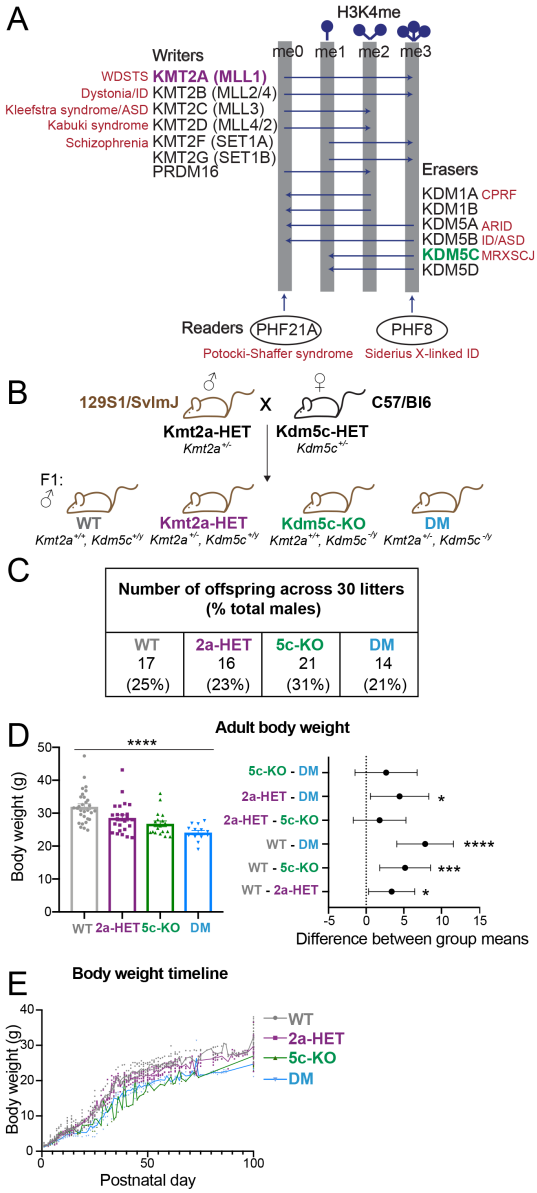

Figure 3.1 The H3K4 methylopathies and generation of the *Kmt2a-Kdm5c* double-mutant (DM) mouse.

(A) H3K4me writers and erasers, depicted by their ability to place or remove H3K4me. Reader proteins recognizing specific H3K4me substrates (arrows) are depicted below. Genes are listed next to their associated neurodevelopmental disorder. WDSTS: Weideman-Steiner Syndrome; ID: intellectual disability; ASD: autism spectrum disorder, CPRF: cleft palate, psychomotor retardation, and distinctive facial features; ARID: autosomal recessive ID; MRXSCJ: mental retardation, X-linked, syndromic, Claes-Jensen type. (B) Mouse breeding scheme crossing congenic 129S1/SvlmJ *Kmt2a*-heterozygous males with congenic C57/Bl6 *Kdm5c*-heterozygous females, resulting in F1 generation mice. Only males were used in this study. (C) Numbers of male offspring across 30 litters, showing Mendelian ratios of expected genotypes. (D) Left panel: Body weight of adult mice > 2 months of age (mean ± SEM, ****$p < 0.0001$ in One-way ANOVA). Right panel: Difference between group means of weight (mean ± 95% confidence intervals, *$p < 0.05$, **$p < 0.01$, ***$p < 0.001$, ****$p < 0.0001$ in Tukey multiple comparison test). (E) Body weight tracked from birth, postnatal day 1 (P1).

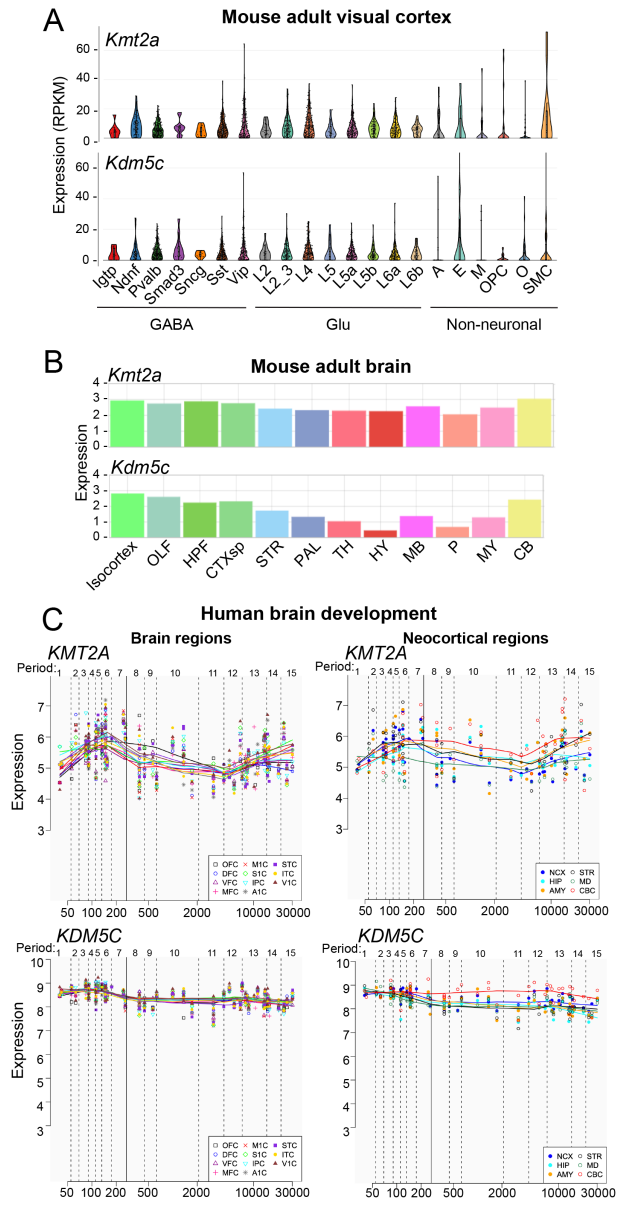

Figure 3.2 Expression of KMT2A and KDM5C.

(A) Expression of *Kmt2a* and *Kdm5c*, from FACS-sorted single cells of mouse visual cortex, shown in reads per kilobase of transcript per million mapped reads (RPKM). Neuronal cells: GABAergic (GABA), Glutamatergic (Glu). Non-neuronal cells: astrocytes (A); endothelial cells (E); microglia (M), oligodendrocyte precursor cells (OPC); oligodendrocytes (O); smooth muscle cells (SMC). Image credit: Broad Institute "Single Cell Portal" transcriptome of adult mouse visual cortex (Tasic et al., 2016). (B) Expression of *Kmt2a* and *Kdm5c* mRNA from adult mouse brain, shown in log2 of raw expression value from *in situ* hybridization. Brain regions: Isocortex, olfactory areas (OLF), hippocampal formation (HPF), cortical subplate (CTXsp), striatum (STR), pallidum (PAL), thalamus (TH), hypothalamus (HY), midbrain (MB), pons (P), medulla (MY), cerebellum (CB). Image credit: Allen Institute, Allen Mouse Brain Atlas (2004) (Lein et al., 2007). (C) Expression of *KMT2A* and *KDM5C* transcripts, from developing and adult human brains, shown in RPKM over time (age in days). Human development and adulthood were split into the following Periods: 1-7 fetal development; 8-9 birth and infancy; 10-11 childhood; 12 adolescence; and 13-15 adulthood. Image credit: Human Brain Transcriptome Atlas (Kang et al., 2011; Pletikos et al., 2014).

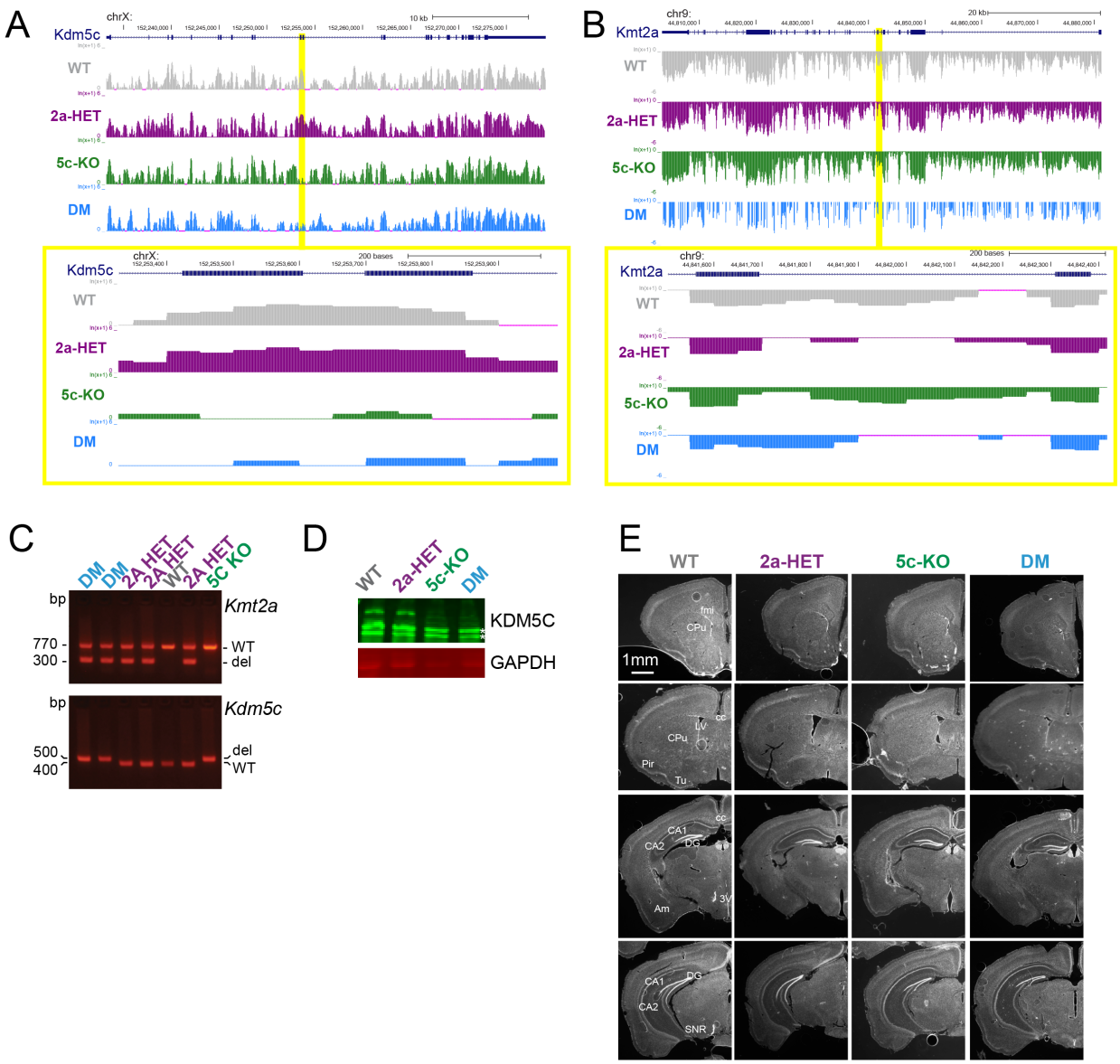

Figure 3.3 Genotype confirmation and gross brain morphology of mutant mice.

(A-B) RNA-seq read coverage of *Kmt2a* (A) and *Kdm5c* (B) genes, and targeted exons (highlight). (C) Genotyping using genomic DNA, confirming presence of *Kmt2a* and/or *Kdm5c* deleted alleles ("del") only in appropriate genotypes. (D) Western blot for KDM5C protein. Stars indicate non-specific bands present in all samples. GAPDH shown for equal loading. (E) Serial brain sections 30 µm thick stained with DAPI to mark nuclei. Sections shown at Bregma regions 1.41, 0.49, -2.15, and -2.91 mm (top to bottom). Regions highlighted: anterior forceps of the corpus callosum (fmi), caudate putamen (CPu), corpus callosum (cc), lateral ventricle (LV), piriform cortex (Pir), olfactory tubercle (Tu), hippocampal fields CA1 and CA2, dentate gyrus (DG), anteromedial nucleus (AM), third ventricle (3V), substantia nigra pars reticularis (SNR). Scale bar: 1mm.

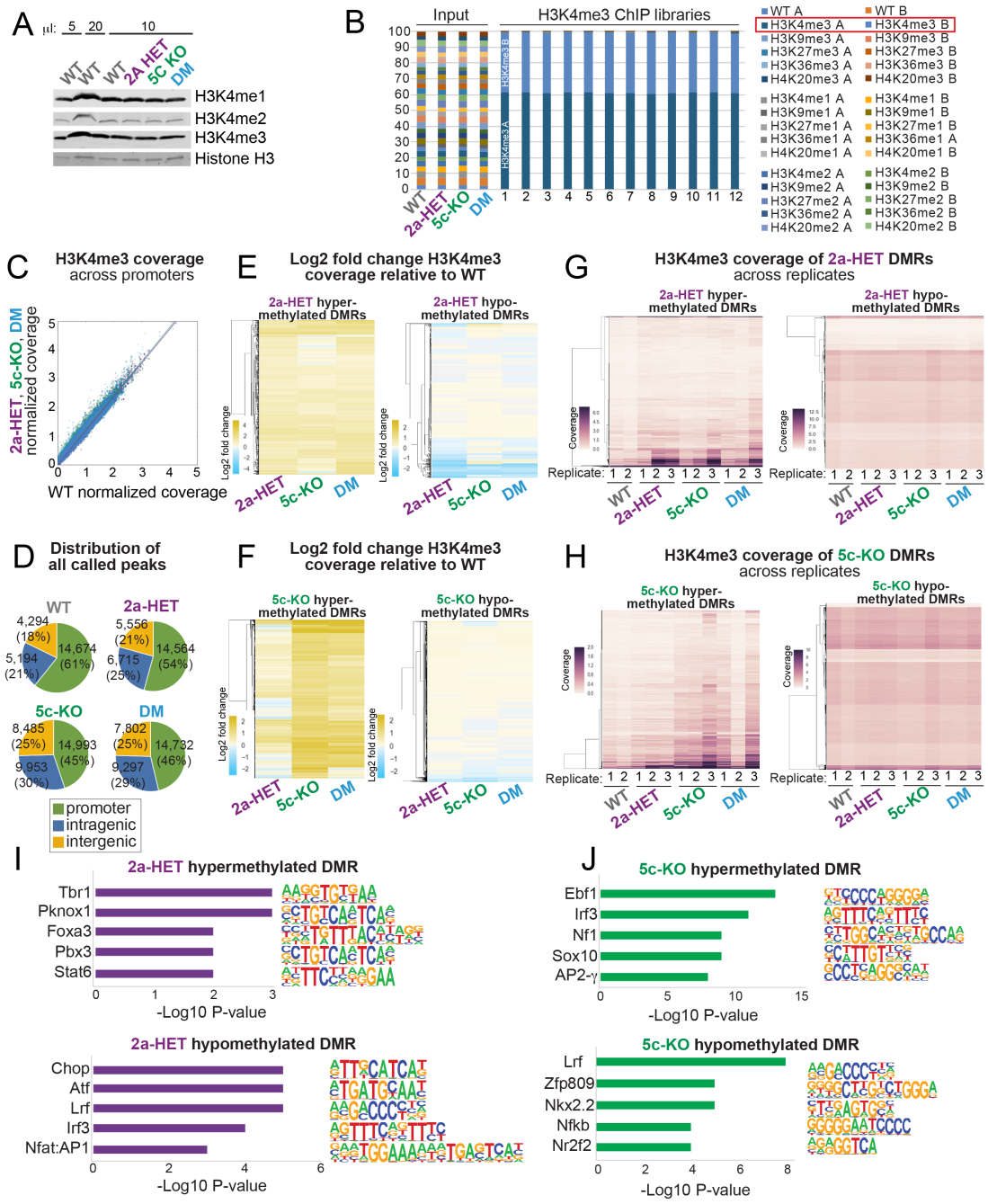

Figure 3.4 H3K4me3 in the amygdala.

(A) Western blot of whole brain lysates. Total histone H3 was detected using an antibody recognizing the C-terminus of H3 and used as a control for equal loading. (B) Validation of H3K4me3 ChIP-seq specificity. Barcode reads originating from spike-in nucleosomes were counted. (C) H3K4me3 coverage in *Kmt2a*-HET, *Kdm5c*-KO, or DM compared to WT at promoters (± 1 kb of transcription start sites). (D) Distribution of all H3K4me3 peaks across the genome, in all genotypes. (E-F) Log2 fold change of H3K4me3 coverage across genotypes relative to WT, at *Kmt2a*-HET DMRs (E) or *Kdm5c*-KO DMRs (F). Scale indicates log2 fold change of depleted (blue) to enriched (yellow) H3K4me3. (G-H) H3K4me3 coverage of individual replicates at *Kmt2a*-HET DMRs (G) or *Kdm5c*-KO DMRs (H) in all genotypes. Scale indicates low (light) to high (dark) H3K4me3 coverage. (I-J) Top five mammalian transcription factor motifs identified in *Kmt2a*-HET (I) and *Kdm5c*-KO (J) DMRs.

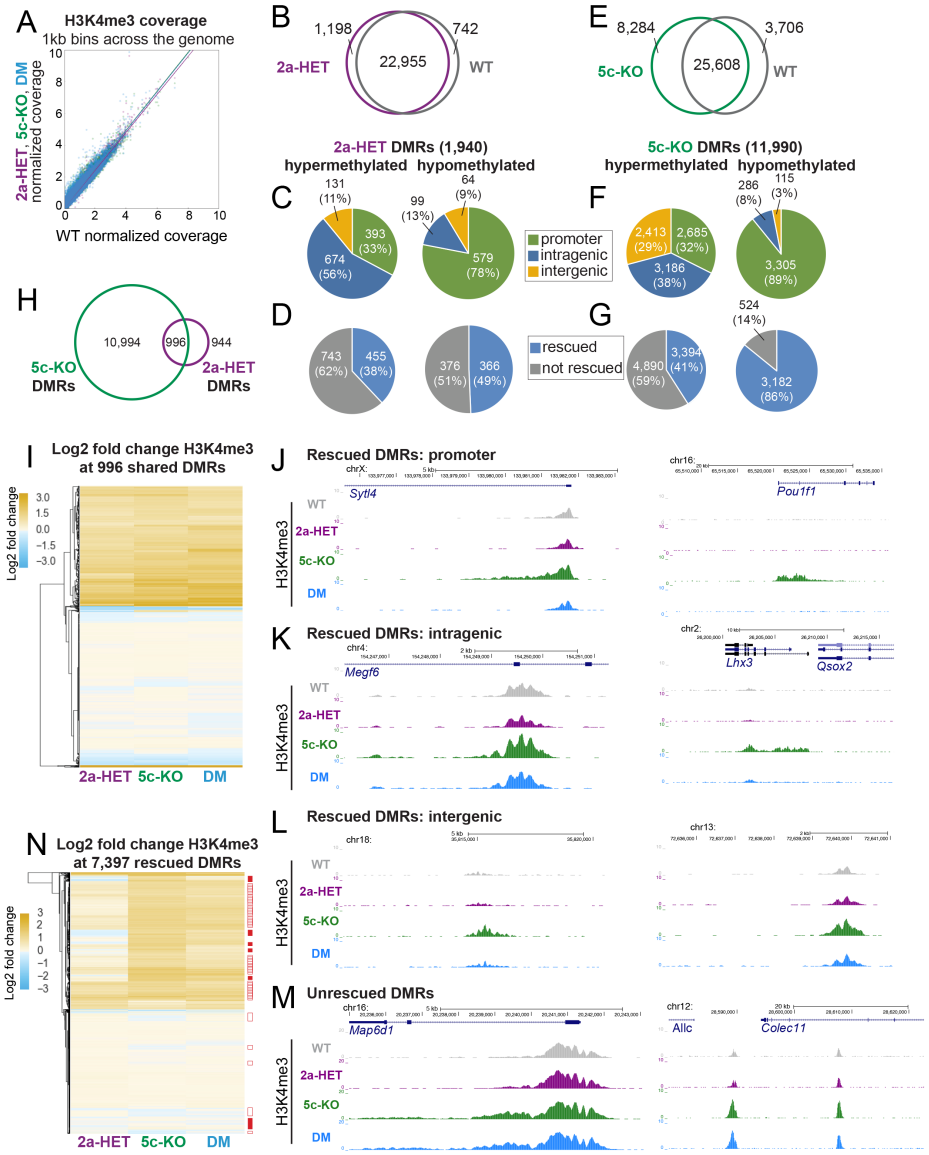

Figure 3.5 Altered H3K4me3 landscapes in the amygdala and rescue effect in DM.

(A) H3K4me3 coverage in 2a-HET, 5c-KO, or DM compared to WT across the genome, that was partitioned into 1 kilobase (kb) bins. (B-D) *Kmt2a*-HET differentially-methylated regions (DMRs), identified as peaks hypermethylated or hypomethylated compared to WT using MACS2 (Zhang et al., 2008) ($q < 0.1$) (B), their location at promoters, within genes (intragenic), or between genes (intergenic) (C), and how many were rescued in DM (D). (E-G) *Kdm5c*-KO DMRs, identified as peaks hypermethylated or depleted compared to WT (E), their location at promoters, within genes (intragenic), or between genes (intergenic) (F), and how many were rescued in DM (G). (H) Overlap between all *Kdm5c*-KO and *Kmt2a*-HET DMRs. (I) Heatmap of H3K4me3 fold change relative to WT, of 996 shared DMRs between *Kmt2a*-HET and *Kdm5c*-KO. Scale indicates log2 fold change of depleted (blue) to enriched (yellow) H3K4me3. (J-M) Peak track view of two representative loci for each of the major genome areas: promoter (J), intragenic (K), and intergenic (L) DMRs rescued in DM, or un-rescued in DM (M). (N) Heatmap of H3K4me3 fold change relative to WT, of 7,397 rescued DMRs. Side bars indicate patterns of rescued regions: solid bars = hypermethylated in 5c-KO, hypomethylated in *Kmt2a*-HET; open bars = hypermethylated in both *Kdm5c*-KO, and *Kmt2a*-HET; dashed bars = hypermethylated in all *Kdm5c*-KO, *Kmt2a*-HET, and DM. Scale indicates log2 fold change of depleted (blue) to enriched (yellow) H3K4me3. We analyzed amygdala tissue from 2 or 3 animals for each genotype.

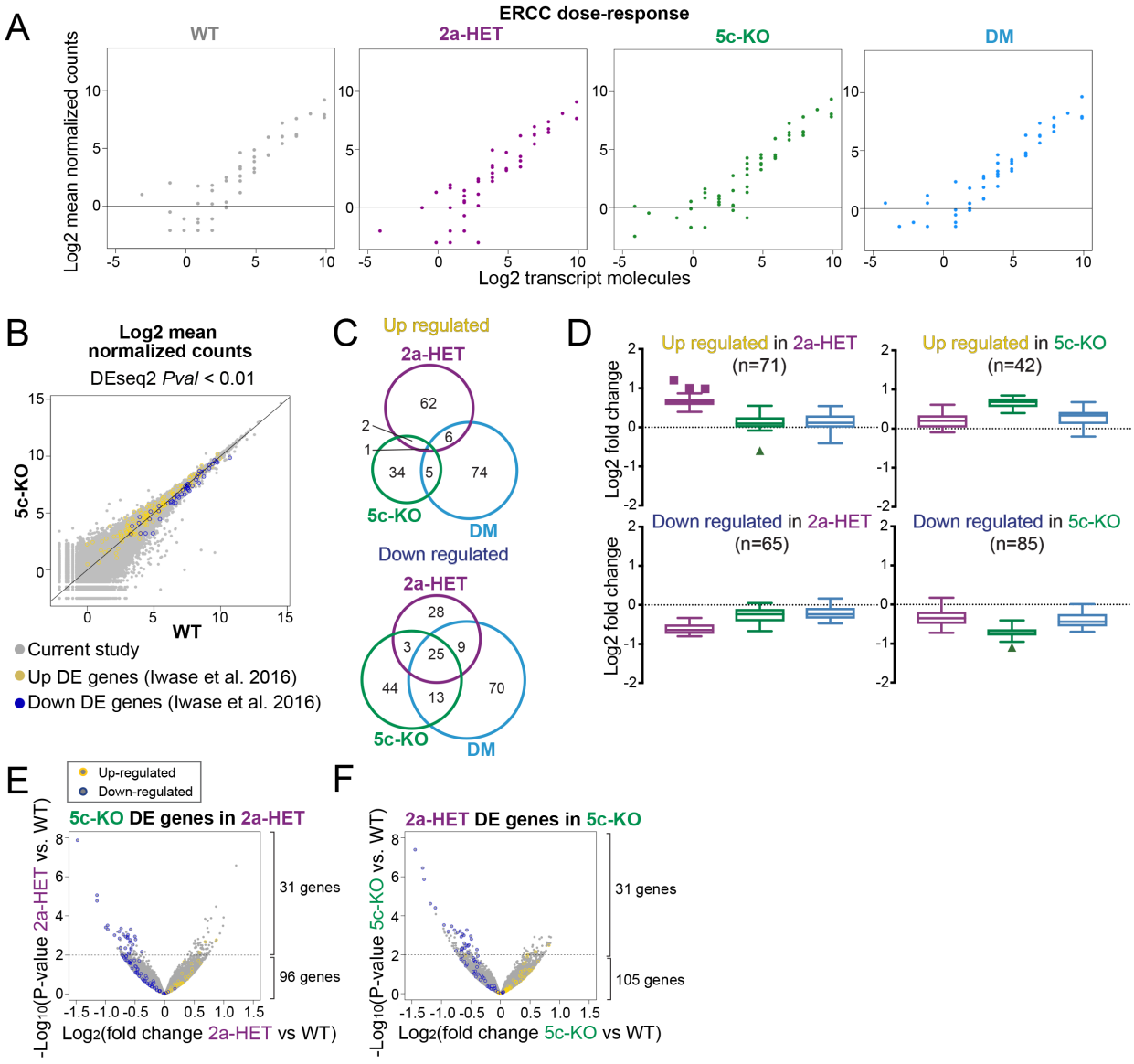

Figure 3.6 Additional analyses of the RNA-seq dataset.

(A) External RNA Controls Consortium (ERCC) spike-in dose-response curves in each genotype, plotting expected vs. observed transcript counts. Each dot represents a spike-in RNA molecule. (B) Comparison of mean normalized counts of *Kdm5c*-KO from present study (grey dots) with our previous RNA-seq approach (Iwase et al., 2016). Previously identified up- (yellow) and down- (blue) regulated genes show consistent patterns in the present study. (C) Intersection of up- and down-regulated DE genes across genotypes. (D) Fold change of DE genes across genotypes. Boxplot features depict: box, interquartile range (IQR); line, median; whiskers, proportion of IQR past low and high quartiles. (E-F) Volcano plots depicting similarity of gene expression patterns in *Kdm5c*-KO and *Kmt2a*-HET DE genes. Genes identified as DE in either single mutant shown as open circles. By and large, genes identified as up (yellow) or down (blue) in one category are expressed in the same direction in the reciprocal genotype. Dashed line depicts $p = 0.01$ threshold for determining DE genes.

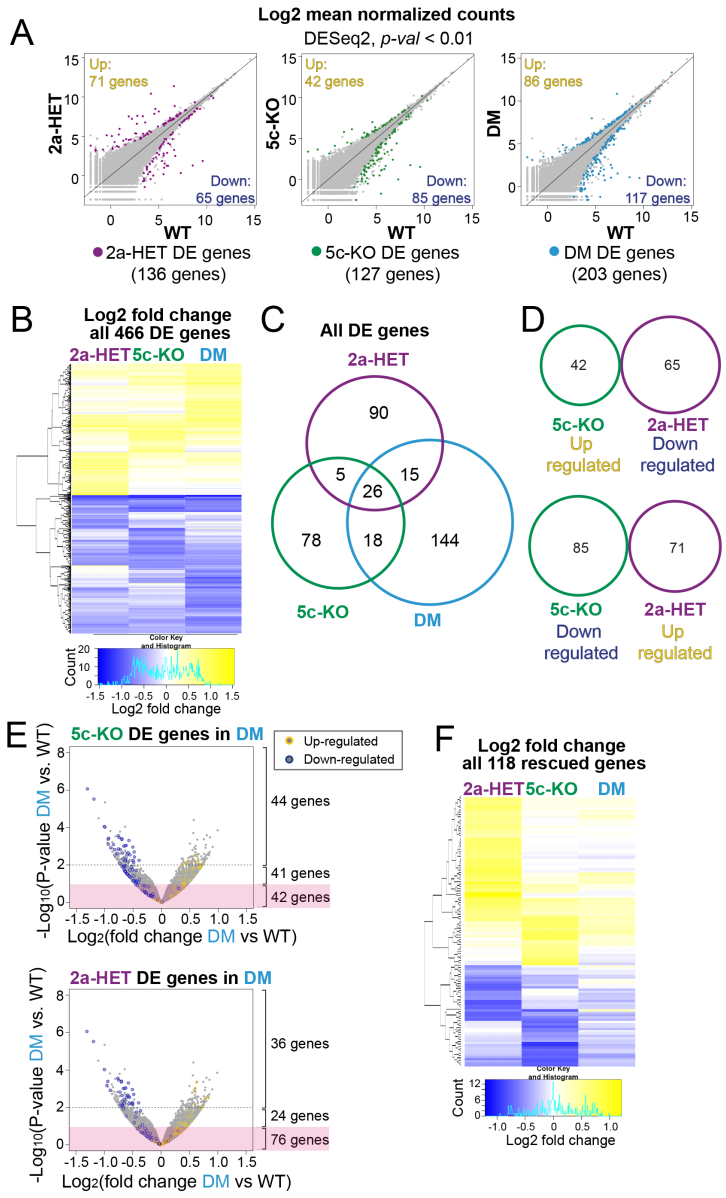

Figure 3.7 Similar transcriptomes between the *Kdm5c*-KO and *Kmt2a*-HET and rescue effect in DM.

(A) Transcriptome comparison across three mutant genotypes relative to WT, represented as log2 mean normalized counts from DESeq2 (Love et al., 2014). Differentially-expressed (DE) genes were determined using a threshold of p-value < 0.01 as previously described (Iwase et al., 2016). (B) Log2 fold change relative to WT, of expression of all 466 DE genes identified (136 *Kmt2a*-HET + 127 *Kdm5c*-KO + 203 DM). Scale indicates log2 fold change of down- (blue) to up- (yellow) regulated expression. Histogram on scale indicates count of genes in each color category. (C) Overlap between DE genes across genotypes. (D) Intersection of DE genes from reciprocal categories in single mutants. (C) Volcano plots depicting rescue effect in DM on *Kdm5c*-KO and *Kmt2a*-HET DE genes. DM gene expression plotted in grey, as log2 fold change and p-value in DM compared to WT. Genes identified as DE in either single mutant shown as open circles. Any of these genes that fell within the $p > 0.1$ cutoff (red shaded box) were considered rescued in DM. Dashed line depicts $p = 0.01$ threshold for determining DE genes. (F) Log2 fold change relative to WT, of expression of all 118 rescued genes. Scale indicates log2 fold change of down- (blue) to up- (yellow) regulated expression. Histogram on scale indicates count of genes in each color category. We analyzed amygdala tissue from 3 animals for each genotype.

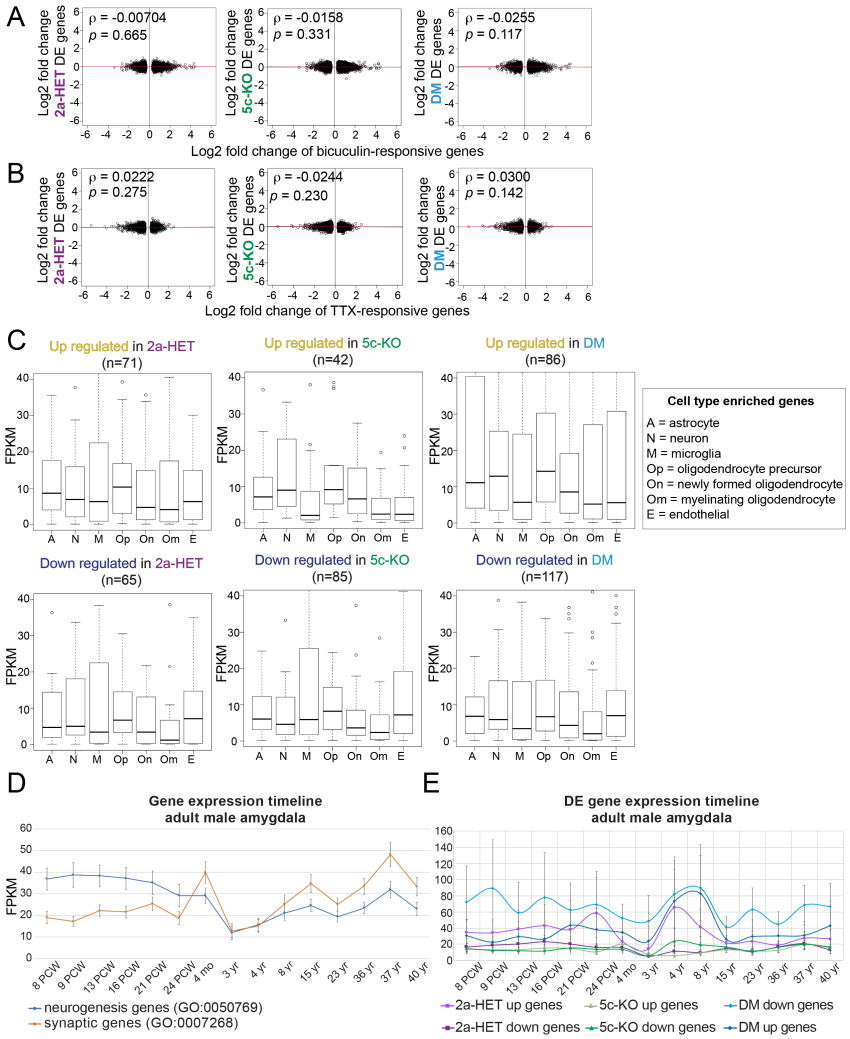

Figure 3.8 Expression of genes that are activity-dependent, cell-type specific, or developmentally regulated, in mutant amygdala.

(A-B) Expression of activity-dependent genes, which we previously identified by nascent RNA sequencing using cortical neurons in response to bicuculine (3,785 genes) (A), or TTX (2,416 genes) (B) (Garay et al., 2019). Spearman Rank-order correlation test for all comparisons showed no linear relationship between fold changes of either set of activity-dependent genes and DE genes in the mutant transcriptomes, indicating normal expression of activity-dependent genes in all three genotypes. (C) DE gene expression across cell types. Genes enriched in seven cell types: astrocytes (A), neurons (N), microglia/macrophages (M), oligodendrocyte precursor cells (Op), newly formed oligodendrocytes (On), myelinating oligodendrocytes (Om), endothelial cells (E). Data were obtained from Zhang et al. (Zhang et al., 2014). None of the DE genes in the mutant amygdala show strong bias to a particular cell type. Boxplot features depict: box, interquartile range (IQR); line, median; whiskers, proportion of IQR past low and high quartiles. (D-E) We examined human adult male amygdala gene expression over time, from embryonic to adult ages. Preconception weeks (PCW), months (mo), years (yr). We examined trajectory of neurogeneisis (GO:0050769) or synaptic (GO:0007268) genes throughout normal development (D). As expected, synaptic genes showed upward shift, while neurogenesis genes exhibited downward shift in their expression during the development. When we plotted the expression of our DE genes across genotypes throughout normal development, we did not find noticeable trends, except that DM down-regulated genes were more highly expressed compared to DE genes in other genotypes (E). Data credit: Allen Institute, BrainSpan Atlas of the Developing Human Brain (2010) (Miller et al., 2014).

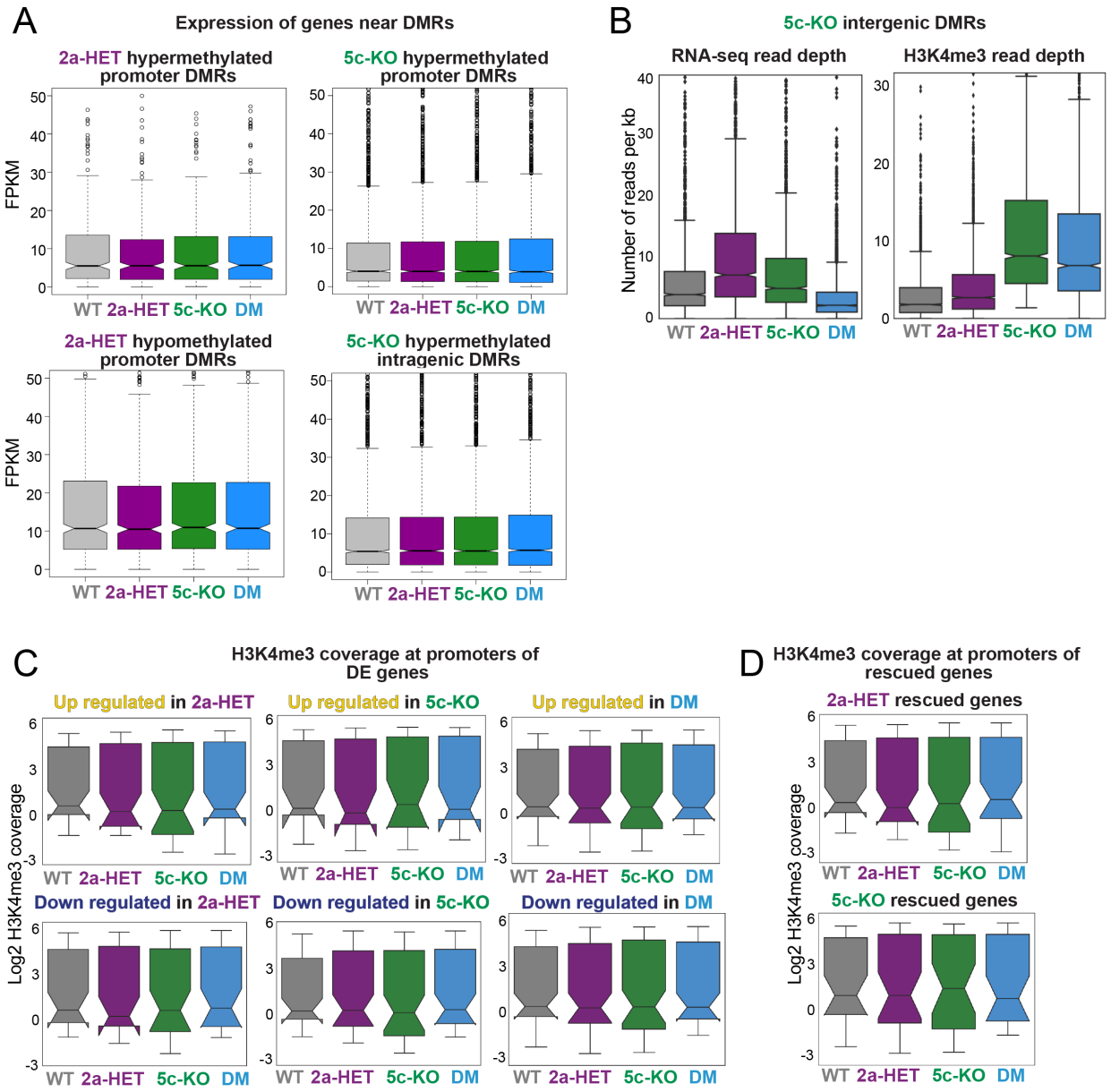

Figure 3.9 Integrative analysis of ChIP-seq and RNA-seq.

(A) Expression of genes associated with promoter- or intragenic-DMRs. (B) RNA-seq read depth and H3K4me3 ChIP-seq read depth at 5c-KO intergenic DMRs, across genotypes. (C) H3K4me3 coverage at promoter regions of differentially expressed (DE) genes. (D) H3K4me3 coverage at promoter regions of rescued genes. Boxplot features depict: box, interquartile range (IQR); line, median; notch, confidence interval for median; whiskers, proportion of IQR past low and high quartiles.

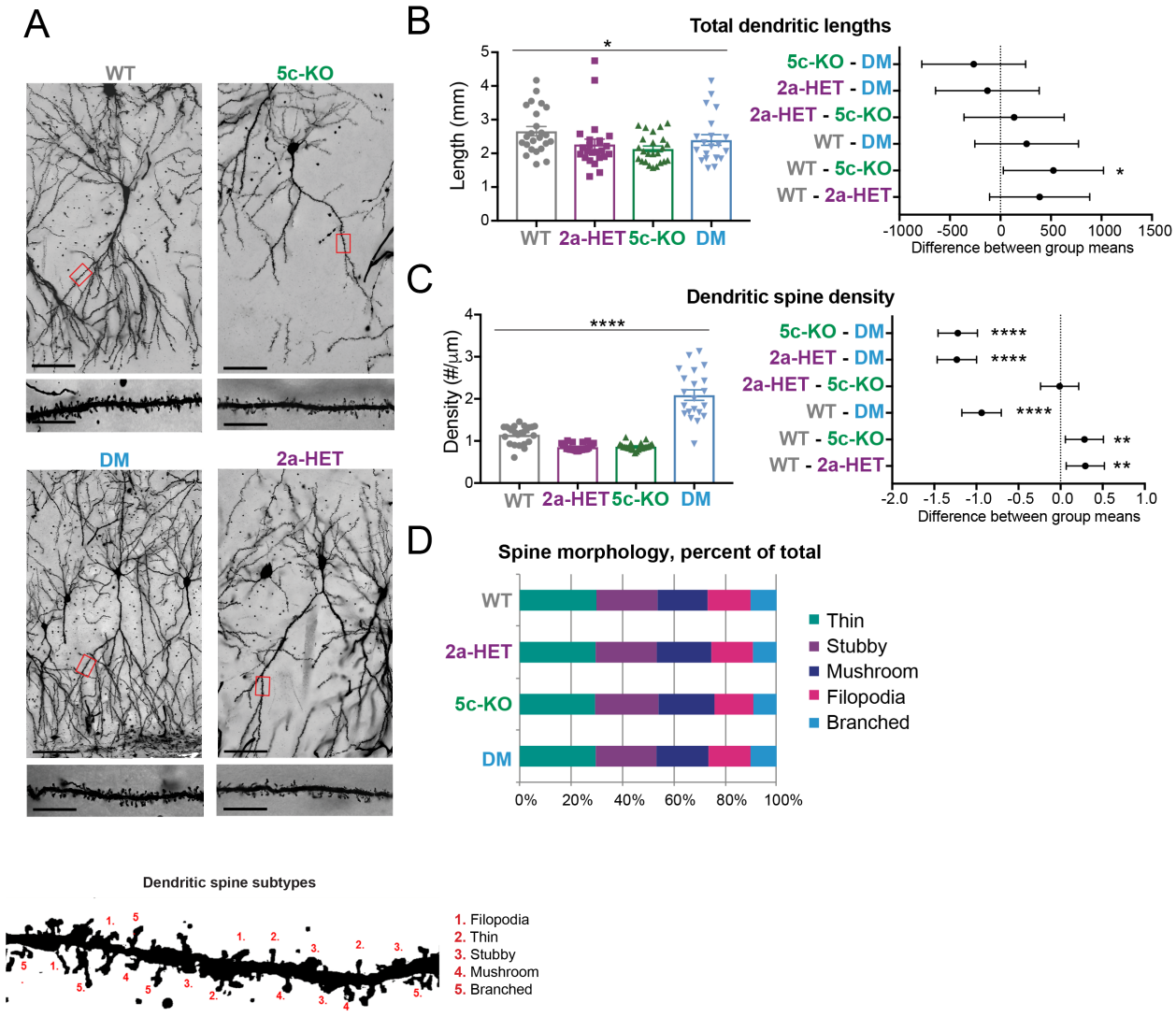

Figure 3. 3.10 Altered dendrite morphology of *Kdm5c*-KO and *Kmt2a*-HET was reversed in DM animals.

(A) Representative images of basolateral amygdala (BLA) pyramidal neurons across all genotypes, depicting overall neuron morphology including dendrite lengths and dendritic spines. Scale bars represent: 100 μm (above, whole neuron image), 10μm (below, spine image). (B and C) Left panel: Total dendrite lengths (B) or spine density (C) Right panel: Difference between group means (mean ± 95% confidence intervals, *$p < 0.05$, **$p < 0.01$, ****$p < 0.0001$ in Tukey multiple comparison test). (D) Quantification of spine morphology subtypes represented as percent of total spines counted. Example of dendrite spine subtypes provided. At least 20 neurons from 4 animals per genotype were quantified.

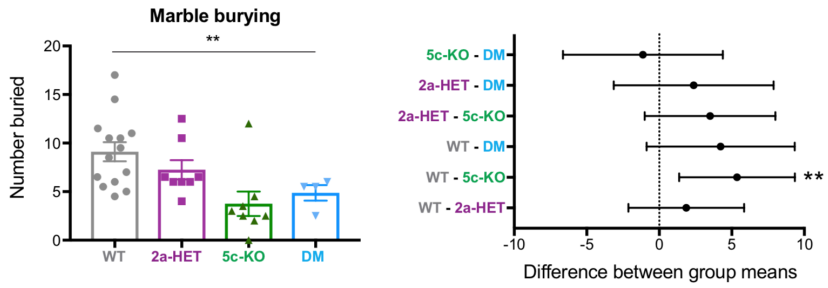

Figure 3.11 Marble burying test.

Marble burying test. Left panel: Number of marbles buried (mean ± SEM, $^{**}p < 0.01$ in One-way ANOVA). Right panel: Difference between group means of number buried (mean ± 95% confidence intervals, $^{**}p < 0.01$ in Tukey's multiple comparison test).

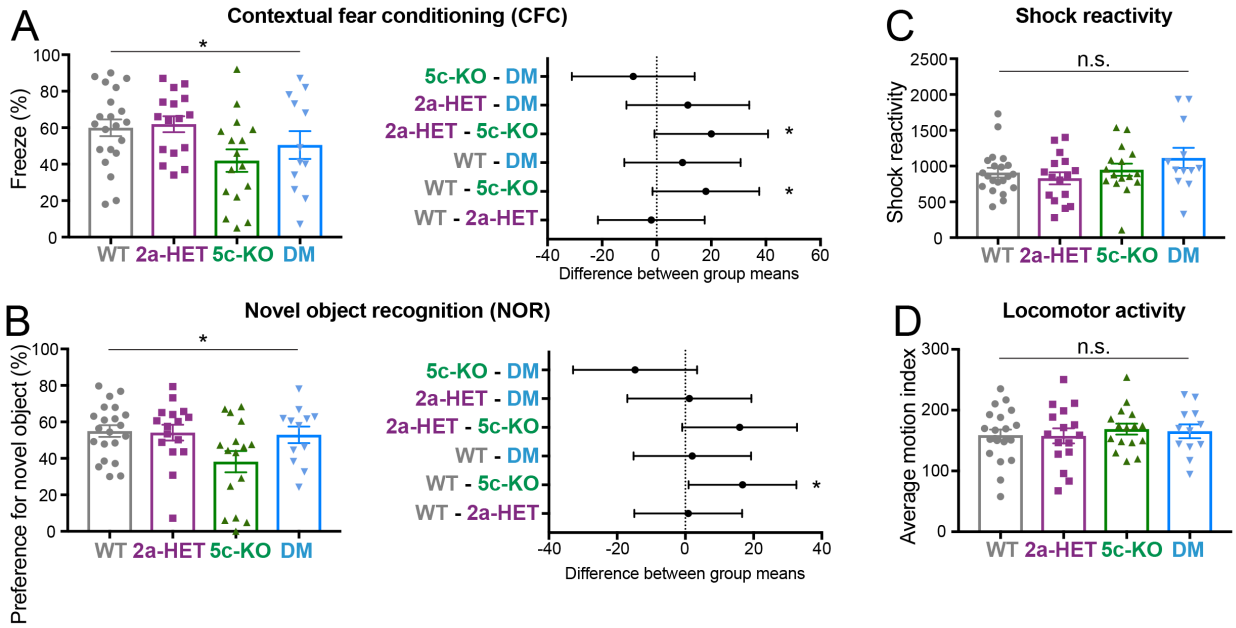

Figure 3.12 Deficit of memory-related behavior in *Kdm5c*-KO and its rescue in DM.

(A) Contextual fear conditioning test. Left panel: Freezing levels after shock on test day (mean ± SEM, $^{*}p < 0.05$ in One-way ANOVA). Right panel: Difference between group means of freezing (mean ± 95% confidence intervals, $^{*}p < 0.05$ in Least Significant Difference (LSD) test). (B) Novel object recognition test. Left panel: Preference for novel versus familiar object (mean ± SEM, $^{*}p < 0.05$ in One-way ANOVA). Right panel: Difference between group means of freeze response (mean ± 95% confidence intervals, $^{*}p < 0.05$ in Least Significant Difference (LSD) test). (C) Response to mild foot-shock (mean ± 95% confidence intervals, no statistical significance [n.s.], One-way ANOVA). (D) Locomotor activity (mean ± 95% confidence intervals, no statistical significance [n.s.], One-way ANOVA). N=21 WT, N=16 *Kmt2a*-HET, N=16 *Kdm5c*-KO, and N=12 DM animals were used for all studies.

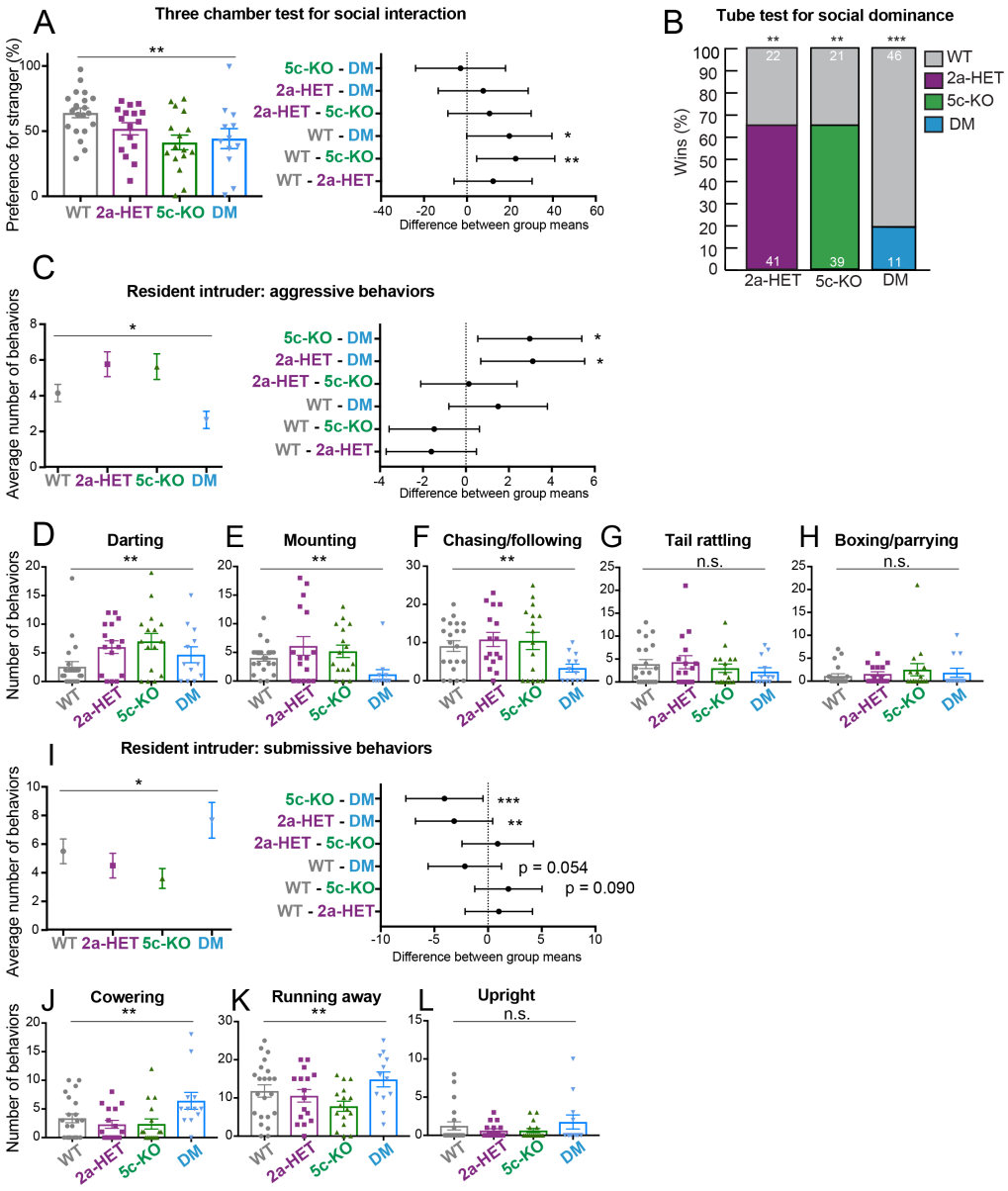

Figure 3.13 Differential impacts of double mutation in social behavior.

(A) Three chamber test for social interaction. Left panel: preference for stranger versus toy mouse (mean ± SEM, $^{**}p < 0.01$ in One-way ANOVA). Right panel: Difference between group means of preference (mean ± 95% confidence intervals, $^{*}p < 0.05$, $^{**}p < 0.01$ in Least Significant Difference (LSD) test). (B) Tube test for social dominance. Proportion of wins in matches of each mutant versus WT. Numbers on colored bars represent total number of wins for WT (grey, above) or each mutant (below) in every matchup. $^{**}p < 0.01$, $^{***}p < 0.001$, Exact binomial test. (C-L) Resident intruder test. (C) Left panel: average number of all aggressive behaviors (mean ± SEM, $^{*}p < 0.05$ in One-way ANOVA). Right panel: Difference between group means of aggressive behaviors (mean ± 95% confidence intervals, $^{*}p < 0.05$ in Least Significant Difference (LSD) test). (D-H) Individual aggressive behaviors (mean ± SEM, $^{**}p < 0.01$ in One-way ANOVA). N.s. depicts no statistical difference. (I) Left panel: average number of all submissive behaviors (mean ± SEM, $^{*}p < 0.05$ in One-way ANOVA). Right panel: Difference between group means of submissive behaviors (mean ± 95% confidence intervals, $^{**}p < 0.01$, $^{***}p < 0.001$ in Least Significant Difference (LSD) test). (J-L) Individual submissive behaviors (mean ± SEM, $^{**}p < 0.01$ in One-way ANOVA). N.s. depicts no statistical difference. N=21 WT, N=16 *Kmt2a*-HET, N=16 *Kdm5c*-KO, and N=12 DM animals were used for all studies.

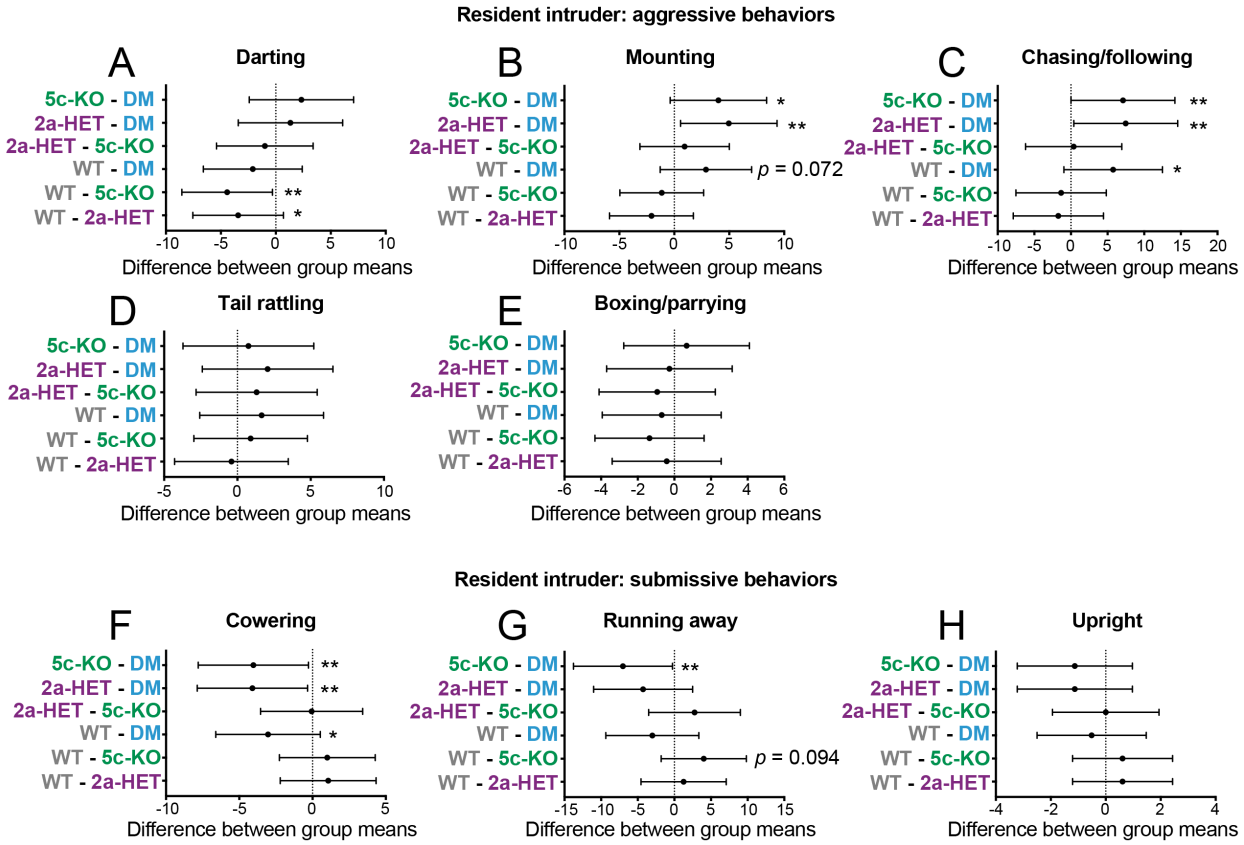

Figure 3.14 Individual behaviors during resident-intruder test.

Differences between group means all aggressive (A-E) and submissive (F-H) behaviors (mean ± 95% confidence intervals, *$p < 0.05$, **$p < 0.01$ in Least Significant Difference (LSD) test).

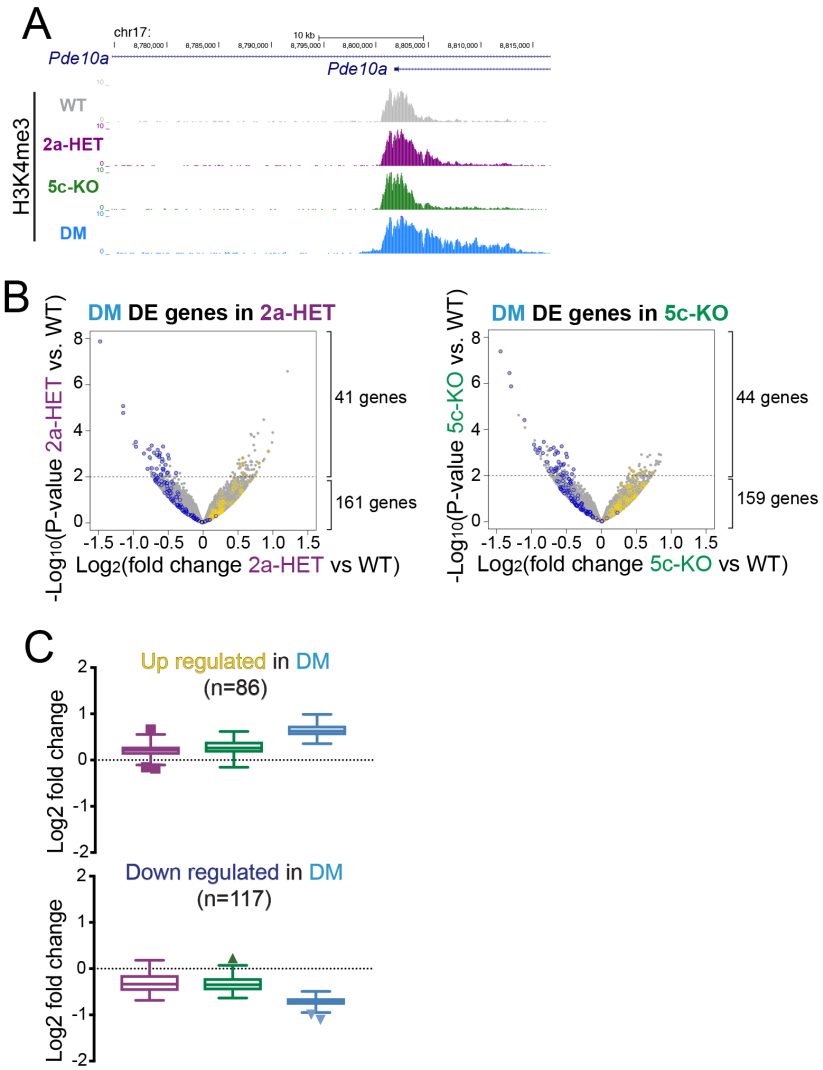

Figure 3.15 Molecular alterations unique to DM mice.

(A) Representative genome browser view of extended H3K4me3 boundary observed at some DM DMRs. (B) Volcano plots depicting larger gene misregulation effects in the DM transcriptome. Transcriptome of *Kmt2a*-HET or *Kdm5c*-KO plotted as grey dots. Genes identified as DE in DM shown as colored open circles. A majority of these genes fell below the line of significance in either single mutant, indicating DM leads to the misregulation of genes that were previously not DE in either *Kmt2a*-HET or *Kdm5c*-KO. Dashed line depicts $p = 0.01$ threshold for determining DE genes. (C) Fold change of DM DE genes across genotypes. DM up- and down-regulated genes were expressed in the same direction in each single mutant, though DM leads to a more pronounced up- or down-regulation effect. Boxplot features depict: box, interquartile range (IQR); line, median; whiskers, proportion of IQR past low and high quartiles.

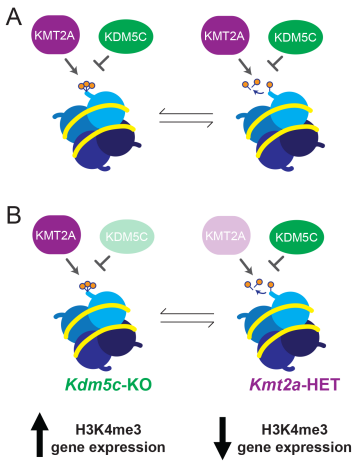

Figure 3.16 Initial working model hypothesizing KMT2A and KDM5C compete at same loci.

At the onset of our studies, we hypothesized that KMT2A and KDM5C functionally interact. (A) Our first working model hypothesizes that writer KMT2A and eraser KDM5C functionally compete at the same genomic loci to balance H3K4me. (B) This model suggests loss *KDM5C* would result in increased H3K4me3 and gene expression, and loss of *KMT2A* would result in decreased H3K4me3 and gene expression, at these shared loci.

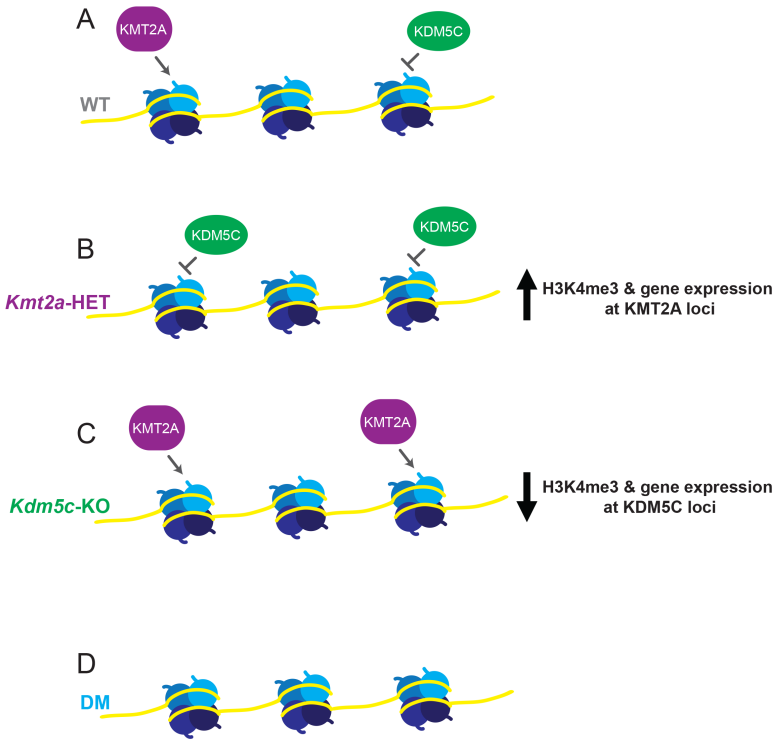

Figure 3.17 Revised working model posits KMT2A and KDM5C work on separate loci.

At the conclusion of our studies, we reveal KMT2A and KDM5C indeed functionally ineract, but in a manner different than our initial model. We now hypothesize that under wildtype (WT) conditions (A), KMT2A and KDM5C act at largely separate genomic loci. Loss of KMT2A (B) or KDM5C (C) triggers the genomic redistribution of the opposite enzyme, changing normal genomic occupancy. It is only by losing both enzymes together (D) that the neutralization effect is achieved, observed in the rescued phenotypes.

Chapter 4 — Sex-Specific Effects of Loss of H3K4me Writer-Eraser Duo KMT2A-KDM5C in Memory and Social Behavior

Introduction

Recent large-scale exome sequencing studies have revealed that mutations in chromatin regulators, including histone methyl proteins, are overrepresented in neurodevelopmental disorders (NDDs) (De Rubeis et al., 2014a; Faundes et al., 2018; Iossifov et al., 2014; Najmabadi et al., 2011; Network and Pathway Analysis Subgroup of Psychiatric Genomics, 2015). Notably, males display four-times higher frequencies of autism spectrum disorder (ASD) than females, yet it is unclear if the source of this difference lies in biological differences and/or our lack of understanding ASD phenotype manifestation in females (Loke et al., 2015; van Bokhoven, 2011). A limited number of animal models for NDDs associated with histone methylation dysregulation are currently available. Moreover, of the models that do exist, few studies look at male and females separately. As a result, we still lack answers to major questions regarding etiology, pathogenesis, and manifestations of NDDs in both sexes.

Histone methylation is one of numerous post-translational modifications of the histone code (Strahl and Allis, 2000), responsible for orchestrating downstream processes including transcriptional regulation (Allis et al., 2007; Kouzarides, 2007). Methylation of the fourth lysine of histone H3 (H3K4me) is a hallmark of actively transcribed genomic loci, where mono-methylation (H3K4me1) marks enhancers, and di- and tri-methylation (H3K4me2/3) mark promoters (Barski et al., 2007; Heintzman et al., 2007). Seven methyltransferase "writers" and six demethylase "erasers" place and remove H3K4me, respectively (Allis et al., 2007), and eight

of these 13 enzymes are mutated in NDDs to date (Vallianatos and Iwase, 2015). We still know very little about how dysregulation of histone methylation leads to deficits in the central nervous system.

The work that follows centers on an H3K4me writer-eraser duo, each mutated in a human NDD: KMT2A and KDM5C. *KMT2A* haploinsufficiency is associated with Weidemann-Steiner Syndrome (WDSTS) in both males and females, characterized by intellectual disability, developmental delay, hairy elbows, and, short stature (Jones et al., 2012; Strom et al., 2014). Mutations in H3K4me3 demethylase gene *KDM5C* are responsible for the NDD mental retardation, X-linked, syndromic, Claes-Jensen type (MRXSCJ). *KDM5C*-MRXSCJ was initially exclusively reported in males, in whom *KDM5C* mutations are transmitted from one of the X chromosomes of carrier mothers. However, recent clinical reports have described at least seven females with cognitive deficits associated with heterozygous *KDM5C* mutations (Ounap et al., 2012; Santos-Reboucas et al., 2011; Simensen et al., 2012). Thus, *KDM5C* mutations may affect not only males but also females. Our lab previously generated *Kdm5c*-knockout (KO) mice, where we showed that male *Kdm5c*-KO animals recapitulate social and cognitive behavioral impairments observed in males with MRXSCJ. We also demonstrated that female *Kdm5c*-heterozugous (HET) mice also display memory deficits (Scandaglia et al., 2017). However, these mice only underwent two memory tests, and were not examined in social contexts at all, which are often perturbed in ASD and we found altered in *Kdm5c*-KO male mice (Iwase et al., 2016; Vallianatos et al., 2019).

The reversible nature of histone modifications suggests that correcting methylation imbalance could be achieved by targeting writers and erasers to fine-tune levels. We previously examined the genetic interactions of an H3K4me writer-eraser duo KMT2A and KDM5C by generating *Kmt2a-Kdm5c* double-mutant (DM) mice, and uncovered new roles for these

chromatin regulators both individually and together in the brain (Vallianatos et al., 2019). We revealed that *Kmt2a-Kdm5c*-DM male mice corrected many of the behavioral deficits of single-mutant male mice. As these first studies only examined male mice, the studies that follow are a continuation of that work examining the genetic interaction of *Kmt2a* and *Kdm5c* in female mice *in vivo*. We reveal functional interactions of KMT2A and KDM5C in females at the behavioral level.

Results

Generation of *Kmt2a-Kdm5c* double-mutant (DM) mice

We crossed 129S1/SvImJ $Kmt2a^{+/-}$ males (Cao et al., 2014) and C57BL/6J $Kdm5c^{+/-}$ females (Iwase et al., 2016) as previously reported (Vallianatos et al., 2019), resulting in the following F1 hybrid female mice: wildtype (WT); *Kmt2a* heterozygote (*Kmt2a*-HET: $Kmt2a^{+/-}$), *Kdm5c* heterozygote (*Kdm5c*-HET: $Kdm5c^{+/-}$), and *Kmt2a-Kdm5c* dual heterozygotes, or double-mutant (DM: $Kmt2a^{+/-}$, $Kdm5c^{+/-}$) (Figure 4.1A). We examined offspring across 30 litters and found that mice were born close to expected Mendelian ratios of 25% (Figure 4.1B), indicating no lethality from loss of either or both alleles.

Examining body weight in adult mice, we found significant differences across genotypes ($F(3,116) = 4.033$, $p = 0.009$) (Figure 4.1C). *Kdm5c*-HET mice were smaller than WT ($p = 0.0115$), consistent with what we have previously reported (Scandaglia et al., 2017). Double-mutant mice were not statistically different than WT ($p = 0.0934$), and yet were also not different from *Kdm5c*-HET ($p = 0.7454$), suggesting a partial rescue effect on weight in DM females. Body weight throughout postnatal development showed a similar intermediate effect of DM compared to WT and *Kdm5c*-HET (Figure 4.1D). Thus, heterozygosity of *Kmt2a* and *Kdm5c* together partially corrected growth retardation in *Kdm5c*-HET females.

KMT2A and KMD5C differentially affect memory types

We performed a battery of mouse behavioral tests in order to determine the effects of loss of *Kmt2a* and *Kdm5c*, individually and in concert, on memory. In the contextual fear conditioning test (CFC) for associative fear memory, we observed a statistical difference between genotypes (Figure 4.2A) ($F(3,77) = 5.082$, $p = 0.0029$, One Way ANOVA). We previously observed impaired freezing in *Kdm5c*-HET mice (Scandaglia et al., 2017), but in this study, the *Kdm5c*-HET mice freeze response was not statistically different from WT ($p = 0.6002$). *Kmt2a*-*Kdm5c*-DM mice, however, exhibited a clear deficit in freezing compared to WT ($p = 0.0123$), indicating dual modulation of both writer and eraser lead to more severe memory deficits compared to either single mutant. Interestingly, we observed differences in shock reactivity across genotypes ($F(3,77) = 7.455$, $p = 0.0002$, One Way ANOVA), with *Kdm5c*-HET mice exhibiting increased reactivity to the foot shock compared to WT ($p = 0.0014$) (Figure 4.2B). These results suggest that sensitivity to shock selectively in our *Kdm5c*-HET female animals could contribute to the greater shock response in these animals (Figure 4.2A). Overall locomotor activity was unchanged in any of the genotypes ($F(3,77) = 0.6686$, $p = 0.5739$, One Way ANOVA) (Figure 4.2C). In contrast to the CFC test, novel object recognition tests (NOR) revealed no statistical difference across the genotypes ($F(3,77) = 1.381$, $p = 0.2548$, One Way ANOVA) (Figure 4.2D). Taken together, these results suggest differential effects for *Kmt2a* and *Kdm5c* interaction in associative memory test CFC compared to recognition memory test NOR.

Social behavior in DM mice

To examine the effect of double mutation on anxiety and obsessive behaviors, we performed the marble burying test and observed no statistical difference between genotypes

($F(3,41) = 0.3982$, $p = 0.7550$) (Figure 4.3A). While this data may indicate a lack of anxiety and obsessive behaviors, it's important to note that only four *Kdm5c*-HET and eight DM mice were tested in this paradigm, making it difficult to draw conclusions without more data.

In the three-chamber social interaction test (Figure 4.3B), we observed significant differences between genotypes ($F(3,77) = 5.802$, $p = 0.0013$, One Way ANOVA). *Kmt2a*-HET mice showed no differences from WT ($p = 0.9956$), aligning with previous tests in conditional *Kmt2a*-KO mice (Kerimoglu et al., 2017). *Kdm5c*-HET mice displayed significantly reduced preference for the stranger mouse compared to WT ($p = 0.0068$) (Figure 4.3B). In sharp contrast, DM mice exhibited a clear reversal of this phenotype, behaving similarly to WT ($p = 0.2653$) (Figure 4.3B). These data suggest that *Kmt2a* heterozygosity can rescue deficits of social interaction in *Kdm5c*-HET female mice.

In tests of social dominance (Figure 4.3C), both *Kmt2a*-HET and Kdm5c-KO mice displayed a 50% win/loss rate ($p = 0.6278$, $p = 1$, respectively), indicative of no aggressive or dominant phenotypes. DM females lost 80% of their bouts against WT ($p = 3.377 \times 10^{-5}$). These results demonstrate that KMT2A and KDM5C cooperate to mediate social dominance behaviors in females.

In sum, our behavioral studies revealed no effects of *Kmt2a*-HET on any memory or social test, yet more pronounced deficits in *Kdm5c*-HET females in some but not all tests. The consequences of double mutations varied between the tests, with no effect on memory, a clear rescue effect on social interaction, and a new effect in social dominance in DM mice. These results support the idea that the two enzymes specifically mediate some deficiencies caused by writer-eraser imbalance in social circuitries.

Discussion

The lack of female animal models for neurodevelopmental disorders has severely hindered our understanding of how NDDs manifest in male versus female brains. Our work demonstrates that separate male and female studies in models of histone methylopathies or other NDDs are needed to fully understand the underlying phenotypes which may differ between the sexes, which may in turn guide diagnoses and treatment of these potentially different NDD manifestations.

Generation of *Kmt2a*-*Kdm5c*-double mutant animals allowed us to perform systematic comparison between the WDSTS model (*Kmt2a*-HET), female *Kdm5c*-MRXSCJ (*Kdm5c*-HET), as well as their composite (DM). We previously showed that effects of memory impairment are *Kdm5c* dose-dependent, noting that female phenotypes were more mild than male phenotypes, suggesting behavioral impairments in female *Kdm5c*-heterozygous (HET) mice were corrected by presence of wildtype (WT) allele (Scandaglia et al., 2017).

The increased response of *Kdm5c*-HET females to shock reveals a potential explanation for the discordance between our previous and current data for the CFC test in female mice. Increase shock sensitivity may elicit quicker shock response, inflating the measured fear response in the CFC test. The marble burying test also showed no difference between genotypes, yet with the low number of animals for *Kdm5c*-HET and DM females (N=4 and 8, respectively) these results need to be repeated before making any conclusions about effects on female anxiety and obsessive behaviors. Although *Kdm5c*-HET mice were slightly smaller compared to single mutants (Figure 4.1C), this was not sufficient to drive submissive behavior in the social dominance tube test (Figure 4.3C). This is in accordance with previous literature, showing as body mass has minimal impact on social hierarchy unless excess difference (> 30%) is present between animals (Kim et al., 2015; Varholick et al., 2018; Wang et al., 2014).

Materials & Methods

Mouse models

Kdm5c-KO mice were previously described (Iwase et al., 2016). *Kmt2a*-HET mice were generated by crossing previously-described *Kmt2a*-flox (exons 8 and 9) mice with B6.129-Gt(ROSA)26Sor$^{tm1(cre/ERT2)Tyj}$/J-Cre mice (McMahon et al., 2007). To backcross *Kmt2a*$^{+/-}$ mice onto the desired 129S1/SvImJ strain, we employed the marker assisted accelerated backcrossing through Charles River Labs. *Kmt2a*$^{+/-}$ mice were bred to the N4 generation at minimum, where mice were >90% congenic for 129S1/SvImJ. All experimental mice were generated as F1 generation hybrids from mating between 129S1/SvImJ *Kmt2a*$^{+/-}$ males and C57Bl/6 *Kdm5c*$^{+/-}$ females: WT females (*Kmt2a*$^{+/+}$, *Kdm5c*$^{+/+}$); *Kdm5c*-HET females (*Kmt2a*$^{+/+}$, *Kdm5c*$^{+/-}$); *Kmt2a*-HET females (*Kmt2a*$^{+/-}$, *Kdm5c*$^{+/+}$); and *Kdm5c*-*Kmt2a*-DM females (*Kmt2a*$^{+/-}$, *Kdm5c*$^{+/-}$). Genotypes were confirmed using the following primers: for *Kmt2a*, 5'-GCCAGTCAGTCCGAAAGTAC, 5'-AGGATGTTCAAAGTGCCTGC, 5'-GCTCTAGAACTAGTGGATCCC; for *Kdm5c*, 5'-CAGGTGGCTTACTGTGACATTGATG, 5'-TGGGTTTGAGGGATACTTTAGG, 5'-GGTTCTCAACACTCACATAGTG.

Behavioral paradigms

Prior to behavioral testing, mice were acclimated to the animal colony room for one week single-housing in standard cages provided with lab diet and water *ad libitum*. A 12-hour light-dark cycle (7:00AM-7:00PM) was utilized with temperature and humidity maintained at 20 ±2 ºC and >30%, respectively. The University of Michigan Committee on the Use and Care of Animals approved all tests performed in this research. Four tests, listed in order of testing, were performed: Novel Object Recognition (5 days), Context Fear Conditioning (2 days), Three-

Chambered Social Interaction (2 days), and Social Dominance Tube Test (3-4 days). All testing was conducted in the morning by experimenters blind to genotype. 70% ethanol was used as a cleaning agent in every test between each trial. Data were collected in a blind fashion, where mice were coded and genotypes only revealed after testing was complete.

Novel Object Recognition: Mice were first habituated to testing arenas (40 x 30 x 32.5 cm^3) in three, 10 minute sessions over six consecutive days (Tchessalova and Tronson, 2019; Vogel-Ciernia and Wood, 2014). 24 hours later, mice were allowed to explore on two identical objects (jar or egg, counterbalanced across animals) for two, 10-minute trials spaced three hours apart. All animals were returned to the arena tested 24 hours after the first training session and presented with one training object ("familiar" object: jar or egg) and one "novel" object (egg or jar). Exploration of the objects was defined as nose-point (sniffing) within 2 cm of the object. Behavior was automatically measured by Ethovision XT9 software using a Euresys Picolo U4H.264No/0 camera (Noldus, Cincinnati, OH). Preference was calculated as the time spent exploring novel object/total time exploring both objects. One-sample t-tests against 50% (no preference) were used to establish whether animals remembered the original objects.

Contextual Fear Conditioning: Context fear conditioning was assessed as previously described (Keiser et al., 2017). Mice were placed into a distinct context with white walls (9 ¾ × 12 ¾ × 9 ¾ in) and a 36 steel rod grid floor (1/8 in diameter; ¼ spaced apart) (Med-Associates, St. Albans, VT) and allowed to explore for 3 minutes, followed by a 2-second 0.8 mA shock, after which mice were immediately returned to their home cages in the colony room. 24 hours later, mice were returned to the context and freezing behavior was assessed with NIR camera (VID-CAM-MONO-2A) and VideoFreeze (MedAssociates, St Albans, VT). Freezing levels were compared between genotypes using a between-groups analysis (one-way ANOVA) with genotype as the between-subjects factor.

Three-Chambered Social Interaction: Mice were placed into a three-chambered apparatus consisting of one central chamber (24 x 20 x 30 cm^3) and two identical side chambers (24.5 x 20 x 30 cm^3) each with a containment enclosure (8 cm diameter; 18 cm height; grey stainless steel grid 3 mm diameter spaced 7.4 mm apart) and allowed to habituate for 10 minutes. 24 hours later, mice were returned to the apparatus that now included a 2-3 month old stranger male mouse (C57BL/6N) on one side of the box ("stranger"), and a toy mouse approximately same size and color as stranger mouse on other ("toy"). Exploration of either the stranger or toy was defined as nose-point (sniffing) within 2 cm of the enclosure and used as a measure of social interaction (Crawley, 2007). Behavior was automatically scored by Ethovision XT9 software as described above, and social preference was defined as time exploring stranger/total exploration time. Social preference was analyzed using one-sample t-tests for each genotype. A repeated measures analysis was used for each aggression (genotype x aggression measures ANOVA) and submissive behaviors (genotype x submissive) to analyze aggressive behaviors.

Social Dominance Tube Test: 24 hours prior to testing, mice were habituated to the plastic clear cylindrical tube (1.5 in diameter; 50 cm length) for 10 minutes. During test, two mice of different genotypes were placed at opposite ends of the tube and allowed to walk to the middle. The match concluded when the one mouse (the dominant mouse) forced the other mouse (the submissive mouse) to retreat with all four paws outside of the tube (a "win" for the dominant mouse) (Larrieu et al., 2017; Moretti et al., 2005; Zhou et al., 2017). Each mouse underwent a total of three matches against three different opponents for counterbalancing. Videos were recorded by Ethovision XT9 software as described above, and videos were manually scored by trained experimenters blind to genotype. The number of "wins" was reported as a percentage of total number of matches. Data were analyzed using an Exact Binomial Test with 0.5 as the probability of success (win or loss).

Notes & Acknowledgements

I performed all experiments and analyses, with the following exceptions: First, Dr. Natalie Tronson oversaw the CFC, NOR, social interaction, and social dominance mouse behavioral tests performed by Ms. Brynne Raines and Dr. Katie Collette. Drs. Yali Dou and Catherine Keegan provided key experimental resourse and made important intellectual contributions.

We thank Drs. Sally Camper, Kenneth Kwan, Stephen Parker, Stephanie Bielas, as well as the members of the Iwase and Bielas labs, for helpful discussions and critical review of the data.

Figures

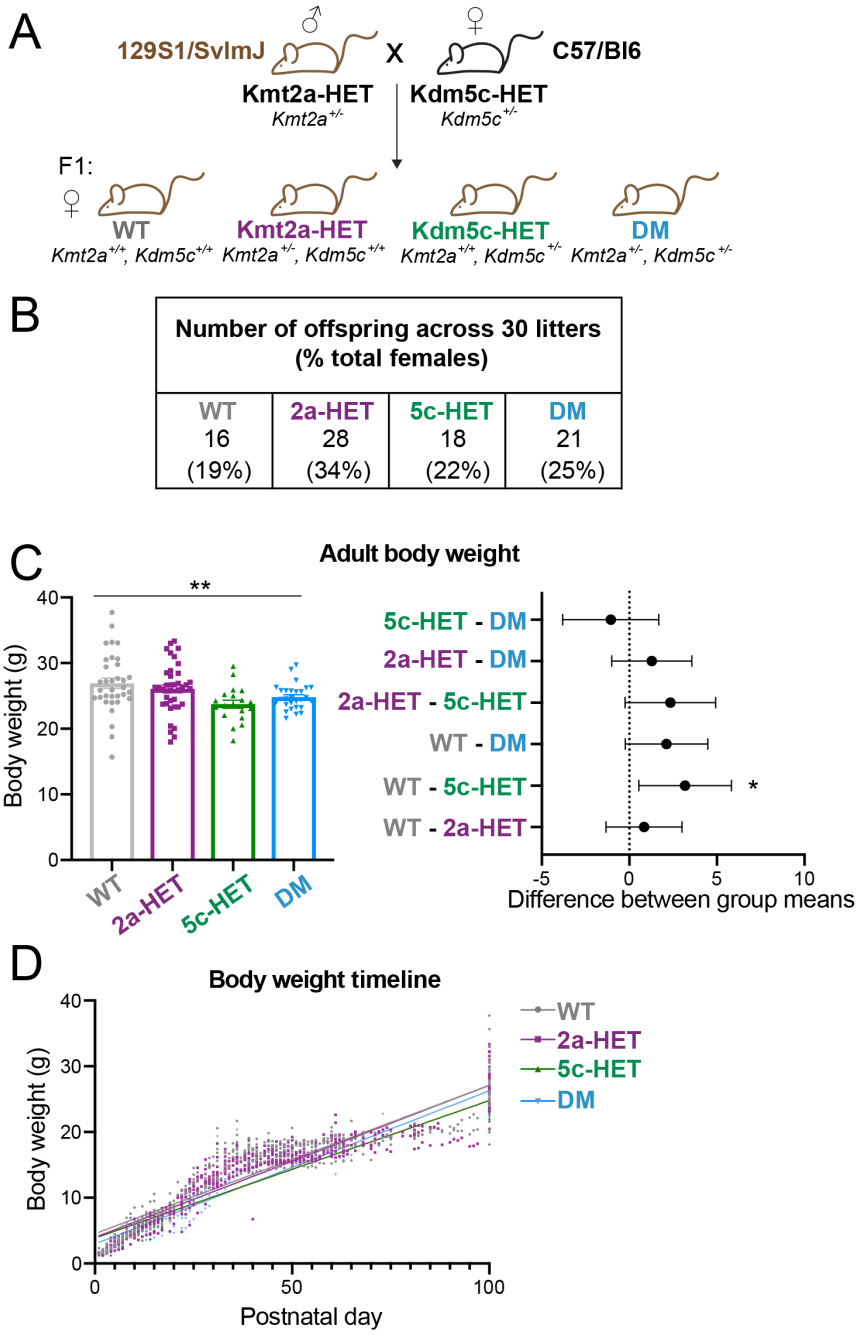

Figure 4.1 Generation of *Kmt2a-Kdm5c* double-mutant (DM) female mice.

(A) Mouse breeding scheme crossing congenic 129S1/SvImJ *Kmt2a*-heterozygous males with congenic C57/BL6 *Kdm5c*-heterozygous females, resulting in F1 generation mice. Only females were used in this study. (B) Numbers of female offspring across 30 litters, showing Mendelian ratios of expected genotypes. (C) Left panel: Body weight of adult mice > 2 months of age (mean ± SEM, $^{**}p < 0.01$ in One-way ANOVA). Right panel: Difference between group means of weight (mean ± 95% confidence intervals, $^{*}p < 0.05$, in Tukey multiple comparison test). (D) Body weight tracked from birth, postnatal day 1 (P1).

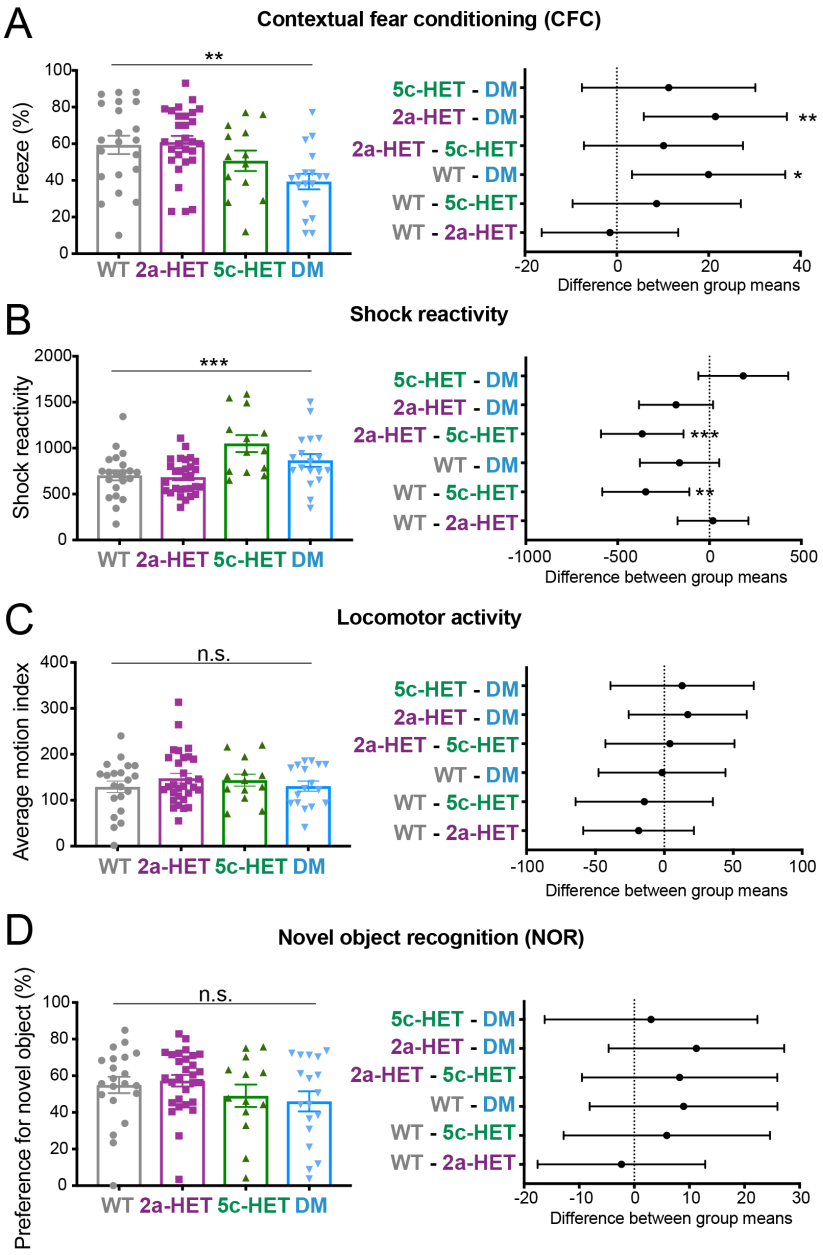

Figure 4.2 Differential impacts of double mutation on memory.

(A) Contextual fear conditioning test. Left panel: Freezing levels after shock on test day (mean ± SEM, $^{**}p < 0.01$ in One-way ANOVA). Right panel: Difference between group means of freezing (mean ± 95% confidence intervals, $^{*}p < 0.05$, $^{**}p < 0.01$ in Tukey multiple comparison test). (B) Left panel: Response to mild foot shock (mean ± SEM, $^{***}p < 0.001$ in One-way ANOVA). Right panel: Difference between group means of response to foot shock (mean ± 95% confidence intervals, $^{*}p < 0.05$, $^{**}p < 0.01$ in Tukey multiple comparison test). (C) Left panel: Locomotor activity (mean ± SEM, no statistical significance [n.s], in One-way ANOVA). Right panel: Difference between group means of locomotor activity (mean ± 95% confidence intervals, Tukey multiple comparison test). (D) Novel object recognition test. Left panel: Preference for novel versus familiar object (mean ± SEM, no statistical significance [n.s.] in One-way ANOVA). Right panel: Difference between group means of freeze response (mean ± 95% confidence intervals, Tukey multiple comparison test). N=21 WT, N=29 *Kmt2a*-HET, N=13 *Kdm5c*-HET, and N=18 DM animals were used for all studies.

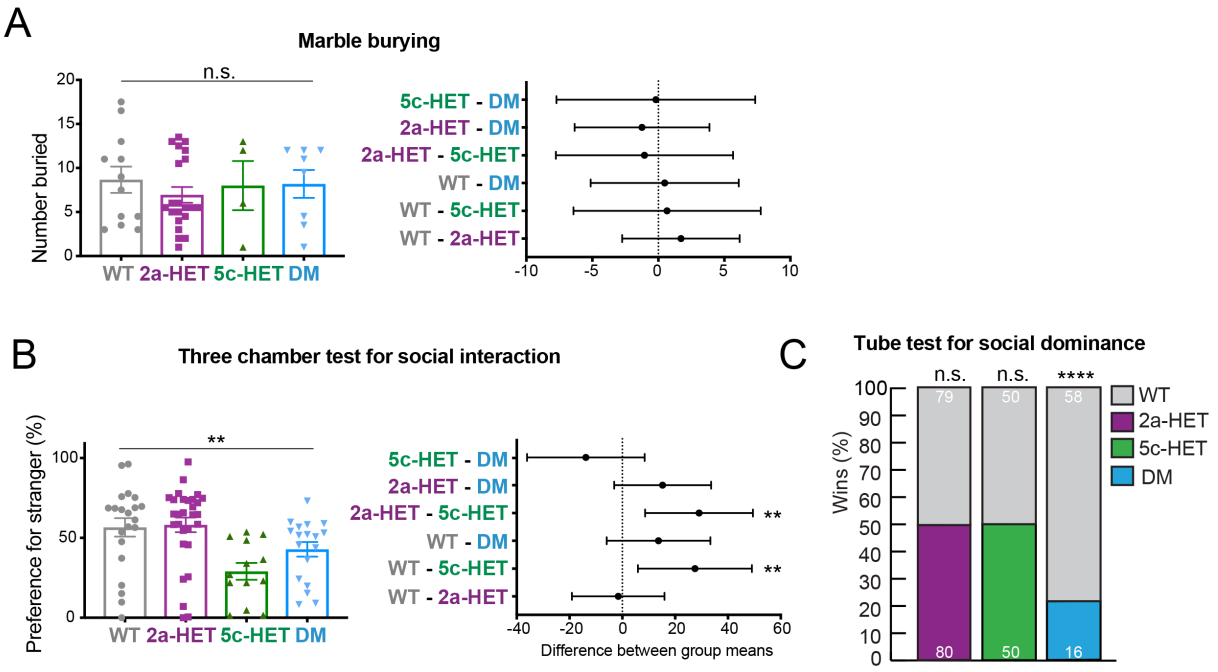

Figure 4.3 Deficit of anxiety and social behaviors in *Kdm5c*-HET and its rescue in DM.

(A) Marble burying test. Left panel: number of marbles buried (mean ± SEM, no significant difference [n.s] in One-way ANOVA). Right panel: Difference between group means of preference (mean ± 95% confidence intervals). N=21 WT, N=12 *Kmt2a*-HET, N=4 *Kdm5c*-HET, and N=8 DM animals were used. (B) Three chamber test for social interaction. Left panel: preference for stranger versus toy mouse (mean ± SEM, $**p < 0.01$ in One-way ANOVA). Right panel: Difference between group means of preference (mean ± 95% confidence intervals, $*p < 0.05$, $**p < 0.01$ in Tukey multiple comparison) test). N=21 WT, N=29 *Kmt2a*-HET, N=13 *Kdm5c*-HET, and N=18 DM animals were used. (C) Tube test for social dominance. Proportion of wins in matches of each mutant versus WT. Numbers on colored bars represent total number of wins for WT (grey, above) or each mutant (below) in every matchup. N.s., not significant; $****p < 0.0001$; Exact binomial test. N=21 WT, N=29 *Kmt2a*-HET, N=13 *Kdm5c*-HET, and N=18 DM animals were used.

Chapter 5 — Conclusions and Future Directions

Chromatin remodeling is an essential process that requires the precise coordination of chromatin-regulating proteins to ensure proper gene expression in a temporal and cell-specific manner. Human genetics studies continue to identify chromatin regulators, including histone methyl regulators, as major contributors to neurodevelopmental disorders (NDDs), highlighting key roles for these proteins in the central nervous system. Understanding the etiology of NDDs, including the molecular consequences of new mutations, will provide an important foundation for developing therapeutics for individuals with these lifelong disorders.

Methylation of histone H3 at the fourth lysine (H3K4me) is a marker of promoters and enhancers of actively transcribed genomic loci. Two families of proteins regulate H3K4me and therefore influence gene expression: methyltransferases are the "writers" that place methyl marks and promote gene expression, and demethylases are the "erasers" that take them off and repress genes. Mutations in nine of the 13 H3K4me regulators have been identified in NDDs to date, including intellectual disability, autism, and schizophrenia. These disorders lead to lifelong cognitive, emotional, and social disability, which entail a significant personal and health care burden worldwide.

Single gene mutations are sufficient to manifest in disease states despite extensive enzymatic redundancy for H3K4me, suggesting specialized genomic roles for each enzyme. Indeed, the common neurological phenotypes from loss-of-function mutations in H3K4me regulators suggests acquisition of roles critical to central nervous system development, and/or a sensitivity of the brain to perturbations in H3K4me regulation. What is the plasticity of

chromatin in fate-determined cells in the brain? How do these 13 H3K4me enzymes work individually and together to balance methylation states? What is the relationship between opposing writers and erasers? Can we exploit the opposing actions of writer-eraser pairs to ameliorate NDD phenotypes?

My thesis research investigated H3K4me balance in neurodevelopment at molecular, cellular, and behavioral levels, in normal and pathologic brain development. The goal of this work was to probe the contributions of H3K4me-regulating enzymes in the brain, both individually and in concert. The nature of this work united the fields of genetics, neuroscience, and medicine, and as such I utilized multidisciplinary approaches. Combining techniques in biochemistry, computational genomics, molecular genetics, mouse genetics and behavior, neurobiology, and pharmacogenetics allowed me to gain a fuller picture of the actions of these enzymes in the central nervous system.

The work in this dissertation centered around H3K4me writer KMT2A and eraser KDM5C and uncovered new molecular roles for this pair in the mammalian brain.

Chapter 2 introduced a novel human mutation in *KDM5C* in a young male with intellectual disability, autism, short stature, and impairments in adaptive behaviors. His was the most distally-located missense mutation reported in the literature to date, residing in the C-terminal end of the protein which has been shown to be dispensable for demethylase function (Vinogradova et al., 2016). Indeed, we showed that the R1115H mutation does not dramatically alter demethylase activity of the protein, unlike a majority of loss-of-function *KDM5C* mutations characterized (Brookes et al., 2015a; Iwase et al., 2007; Rujirabanjerd et al., 2010; Tahiliani et al., 2007a). Instead, we observed differences in transcriptional regulation of KDM5C-R1115H compared to KDM5C-WT when both were overexpressed in cortical neuron cultures. The deficiency of R1115H in repressing genes down-regulated in KDM5C-WT indicated a loss-of-

function effect. The distinct patterns of up- and down-regulated genes from R1115H over-expression revealed possible neofunctionalization of the mutant protein.

One limitation from the RNA-seq study was the overexpression system used in this experiment. We detected human *KDM5C* cDNAs at more than 17 times the levels of endogenous *Kdm5c*. KDM5C is known to bind to chromatin and function as a transcriptional repressor (Iwase et al., 2007; Tahiliani et al., 2007a). Therefore, it is not difficult to imagine that such massive overexpression could reduce global transcription. Another important consideration is that none of the differentially expressed (DE) genes identified in this assay fell below any standard false discovery rate threshold (FDR < 0.01-0.1) for multiple comparisons. This opens the possibility of more type I "false positive" errors, or in this case more genes identified as DE than is the case. This could be addressed through repeat studies to increase the sample number in each condition, and/or validating called DE genes in an identical replicate experiment via qPCR or RNA-seq. Nevertheless, the focus of the work was not on the individual DE genes themselves, but rather the overall transcriptome upon KDM5C-WT or mutant overexpression.

The work in Chapter 2 provides evidence supporting pathogenicity of KDM5C R1115H for the proband's phenotypes. However, exome sequencing revealed an additional patient variant in the *CIC* (*Capicua Transcriptional Repressor*) gene, which was not characterized in this study but cannot be ruled out as a candidate contributor to the phenotype. Human mutations in *CIC* have recently been reported in an intellectual disability syndrome (Lu et al., 2017), and CIC has been shown to play important roles in learning, memory, as well as neuron maturation (Lu et al., 2017). This does not discount any of the data functionally characterizing the R1115H mutation. Rather, it reveals that the patient phenotype may be complicated by effects from the *CIC* mutation.

Data from Chapters 3 and 4 provide molecular, cellular, and/or behavioral characterizations of two mouse models of H3K4me NDDs: the *Kmt2a*-HET and *Kdm5c*-KO/HET mice, each models of KMT2A-associated Weidemann Steiner Syndrome (WDSTS) and KDM5C-associated mental retardation, X-linked, syndromic, Claes Jensen type (MRXSCJ), respectively. We also explored the potential for writer-eraser interaction, by generating *Kmt2a-Kdm5c*-double-mutant animals. We profiled H3K4me3 global landscapes, transcriptomes, neuron morphology in male mice, and behavior in both males and females. In males, single-mutant animals were surprisingly more similar to each other than they were different in nearly all assays, indicating that despite opposite enzymatic activities there is a common phenotypic outcome. Indeed, many symptoms are common between *KMT2A*-WDSTS and *KDM5C*-MRXSCJ, including intellectual disability, short stature, seizures, and aggressive behaviors (Claes et al., 2000; Jensen et al., 2005b; Jones et al., 2012; Wiedemann, 1989). Double-mutant male animals showed clear reversal of dendritic phenotypes and several behaviors, showing manipulation of a single enzyme is sufficient to rescue many neurological traits.

A technical limitation to Chapter 3 and 4 studies lies in our approach using these germline-mutant mice, namely that examining phenotypes in adult animals with constitutive deletions guarantees the observation of direct, indirect, and adaptive effects. We performed small-scale acute inhibition in cortical neuron culture, and future studies can expand upon this shortened time scale to better inform chromatin plasticity and writer-eraser dynamics. One limitation particular to Chapter 4 female-centered studies was lack of screening for estrus cycle prior to behavioral tests (Caligioni, 2009). This is particularly key for behavioral work, as estrus cycle has been shown to have an effect on WT mice in fear extinction (Milad et al., 2009).

This work has expanded our understanding of the molecular mechanisms of KMT2A and KDM5C in the brain, and provides many avenues for future research.

Chapter 2 details a patient-associated mutation in KDM5C with intact enzymatic activity, yet altered gene-regulatory function, suggesting the mutation may interfere with KDM5C function in an activity-independent manner. Many chromatin regulators are known to work in complex with several other proteins (Hsu et al., 2018; Lee et al., 2005; Qu et al., 2018). Future work is needed to characterize potential KDM5C binding partners. One study identified RACK7 (*Receptor for Activated C Kinase*, also known as *Zinc Finger NYMD-Type Containing 8 ZMYMD8*) as an interacting partner with KDM5C working to suppress enhancer activity (Shen et al., 2016). It is unknown whether this complex functions in the brain, or throughout development, or whether any MRXSCJ mutations could ablate this interaction. The C-terminal end of KDM5C has been shown to be dispensable for enzymatic activity. It harbors a PHD domain with unclear function, and potentially hosts sites of other protein-protein interactions. Repressive but non-enzymatic roles for a histone demethylase were recently characterized for yeast eraser Epe1 (Raiymbek et al., 2019). It would be interesting to test whether KDM5C and other demethylases function similarly. Could chromatin states themselves function as signaling complexes? Do enzymes only function in eu- or heterochromatic contexts?

I revealed that the correct location of the PCNA PIP-box consensus sequence lies within the PHD2 domain of KDM5C. My binding assays revealed that, at least *in vitro*, KDM5C PHD2 as well as PHD1, despite lack of PIP-box, could both bind PCNA. Future studies are needed to confirm this interaction *in vivo* and with the full-length proteins, as well as to map the binding sites on each protein. This association of KDM5C with replication machinery suggests KDM5C may work to demethylate chromatin on parental and/or daughter strands during DNA replication. Perhaps this coupling of a demethylase to replication forks is critical to maintaining epigenetic memory of histone modifications on daughter DNA strands. If this is the case, perhaps perturbation would affect dividing cells in the early developing brain, rendering them incapable

of maintaining proper methylation patters before fate commitment, at which point the chromatin landscape is less plastic. It is unclear how the PCNA-KDM5C interaction would be a biologically meaningful interaction in post-mitotic neurons.

While few KDM5C female mutations have been reported in the literature, I have anecdotal evidence that the number of females affected may be higher than we believe. I've been involved in a newly-formed Facebook group for KDM5C families, where 21 families have joined to share the information about their affected children. Seven, or one third, of these children are females, and the severity of their phenotypes tend to be more mild learning difficulties and behavioral abnormalities compared to the males. What mechanisms underlie susceptibilities of females? How does histone methylation regulation contribute to sex differences? My initial work characterizing behaviors of *Kdm5c*-HET mice revealed that impairment in social interaction can be reversed when *Kmt2a* is haploinsufficient. Future molecular and cellular characterizations are needed to better understand these female NDDs, and the cooperation effect of KMT2A and KDM5C in female central nervous system.

Several studies support the amygdala as the seat of fear conditioning, important for acquisition, storage, and expression of conditioned fear memory (Jimenez and Maren, 2009; Maren, 2001) . Comprised of several nuclei substructures, the basolateral amygdala (BLA) is thought to integrate sensory information for fear memory tracing. Interestingly, we observed similar dendritic length and spine deficits in the BLA of male *Kmt2a*-HET and *Kdm5c*-KO mice, but different phenotypes on fear memory in the CFC test between these two genotypes. BLA neuron morphology may contribute to *Kdm5c*-KO male fear memory response, but other factors may underlie the intact fear memory in *Kmt2a*-HET animals. BLA neurons project to other amygdalar nuclei such as the central nucleus (CeA), which in turn projects to other brain regions to ultimately mediate fear response (Paré et al., 2004). It is possible that in *Kmt2a*-HET animals

there are compensatory effects within this circuit that negate the BLA morphology deficits and support normal function in the CFC test. Future studies could look at connectivity to prelimbic, infralimbic, and orbitofrontal cortices (Felix-Ortiz et al., 2016) as well as ventral hippocampus (Felix-Ortiz and Tye, 2014). Similarly, studies of network activation by immediate early gene *c-Fos* could delineate effects on brain circuits. Future studies can examine the prefrontal cortex-amygdalar axis. The frontal cortex has recently been implicated to interact with the amygdala in extinction of fear memory. I also observed differential sensitivity to loss of *Kdm5c* in frontal cortex versus amygdala (Iwase et al., 2016).

Our findings with the *Kmt2a-Kdm5c* double-mutant mice are the first *in vivo* studies, along with a few recent *in vitro* studies, to indicate that pairwise relationships between histone methyl writers and erasers may exist. We lay the groundwork for future studies to similarly test interactions between the full range of H3K4me enzymes to determine writer-eraser cooperation at the molecular, cellular, or behavioral level.

Bibliography

Abidi, F.E., Holloway, L., Moore, C.A., Weaver, D.D., Simensen, R.J., Stevenson, R.E., Rogers, R.C., and Schwartz, C.E. (2008). Mutations in JARID1C are associated with X-linked mental retardation, short stature and hyperreflexia. Journal of medical genetics *45*, 787-793.

Abidi, F.E., Miano, M.G., Murray, J.C., and Schwartz, C.E. (2007). A novel mutation in the PHF8 gene is associated with X-linked mental retardation with cleft lip/cleft palate. Clinical Genetics *72*, 19-22.

Adegbola, A., Gao, H., Sommer, S., and Browning, M. (2008). A novel mutation in JARID1C/SMCX in a patient with autism spectrum disorder (ASD). Am J Med Genet A *146A*, 505-511.

Agarwal, S., Macfarlan, T.S., Sartor, M.A., and Iwase, S. (2015). Sequencing of first-strand cDNA library reveals full-length transcriptomes. Nature communications *6*, 6002.

Aguilar-Valles, A., Vaissiere, T., Griggs, E.M., Mikaelsson, M.A., Takacs, I.F., Young, E.J., Rumbaugh, G., and Miller, C.A. (2014). Methamphetamine-associated memory is regulated by a writer and an eraser of permissive histone methylation. Biol Psychiatry *76*, 57-65.

Agulnik, A.I., Mitchell, M.J., Lerner, J.L., Woods, D.R., and Bishop, C.E. (1994). A Mouse Y-Chromosome Gene Encoded by a Region Essential for Spermatogenesis and Expression of Male-Specific Minor Histocompatibility Antigens. Human Molecular Genetics *3*, 873-878.

Alabert, C., Bukowski-Wills, J.C., Lee, S.B., Kustatscher, G., Nakamura, K., de Lima Alves, F., Menard, P., Mejlvang, J., Rappsilber, J., and Groth, A. (2014). Nascent chromatin capture proteomics determines chromatin dynamics during DNA replication and identifies unknown fork components. Nat Cell Biol *16*, 281-293.

Alarcon, J.M., Malleret, G., Touzani, K., Vronskaya, S., Ishii, S., Kandel, E.R., and Barco, A. (2004). Chromatin acetylation, memory, and LTP are impaired in CBP+/- mice: a model for the cognitive deficit in Rubinstein-Taybi syndrome and its amelioration. Neuron *42*, 947-959.

Allen, R.C., Zoghbi, H.Y., Moseley, A.B., Rosenblatt, H.M., and Belmont, J.W. (1992). Methylation of HpaII and HhaI sites near the polymorphic CAG repeat in the human androgen-receptor gene correlates with X chromosome inactivation. Am J Hum Genet *51*, 1229-1239.

Allis, C.D., Berger, S.L., Cote, J., Dent, S., Jenuwien, T., Kouzarides, T., Pillus, L., Reinberg, D., Shi, Y., Shiekhattar, R.*, et al.* (2007). New nomenclature for chromatin-modifying enzymes. Cell *131*, 633-636.

American Psychiatric Association., American Psychiatric Association. Task Force on DSM-IV., and American Psychiatric Association. Task Force on Nomenclature and Statistics. (1994).

Diagnostic and statistical manual of mental disorders : DSM-IV, 4th edn (Washington, DC: American Psychiatric Association).

Anders, S., and Huber, W. (2010). Differential expression analysis for sequence count data. Genome biology *11*, R106.

Andres, M.E., Burger, C., Peral-Rubio, M.J., Battaglioli, E., Anderson, M.E., Grimes, J., Dallman, J., Ballas, N., and Mandel, G. (1999). CoREST: a functional corepressor required for regulation of neural-specific gene expression. Proc Natl Acad Sci U S A *96*, 9873-9878.

Ardehali, M.B., Mei, A., Zobeck, K.L., Caron, M., Lis, J.T., and Kusch, T. (2011). Drosophila Set1 is the major histone H3 lysine 4 trimethyltransferase with role in transcription. EMBO J *30*, 2817-2828.

Arikkath, J. (2012). Molecular mechanisms of dendrite morphogenesis. Front Cell Neurosci *6*, 61.

Asensio-Juan, E., Gallego, C., and Martinez-Balbas, M.A. (2012). The histone demethylase PHF8 is essential for cytoskeleton dynamics. Nucleic Acids Research *40*, 9429-9440.

Athanasakis, E., Licastro, D., Faletra, F., Fabretto, A., Dipresa, S., Vozzi, D., Morgan, A., d'Adamo, A.P., Pecile, V., Biarnes, X.*, et al.* (2014). Next Generation Sequencing in Nonsyndromic Intellectual Disability: From a Negative Molecular Karyotype to a Possible Causative Mutation Detection. American Journal of Medical Genetics Part A *164*, 170-176.

Augui, S., Nora, E.P., and Heard, E. (2011). Regulation of X-chromosome inactivation by the X-inactivation centre. Nat Rev Genet *12*, 429-442.

Ballas, N., Battaglioli, E., Atouf, F., Andres, M.E., Chenoweth, J., Anderson, M.E., Burger, C., Moniwa, M., Davie, J.R., Bowers, W.J.*, et al.* (2001). Regulation of neuronal traits by a novel transcriptional complex. Neuron *31*, 353-365.

Banka, S., Howard, E., Bunstone, S., Chandler, K.E., Kerr, B., Lachlan, K., McKee, S., Mehta, S.G., Tavares, A.L., Tolmie, J.*, et al.* (2013). MLL2 mosaic mutations and intragenic deletion-duplications in patients with Kabuki syndrome. Clin Genet *83*, 467-471.

Banka, S., Veeramachaneni, R., Reardon, W., Howard, E., Bunstone, S., Ragge, N., Parker, M.J., Crow, Y.J., Kerr, B., Kingston, H.*, et al.* (2012). How genetically heterogeneous is Kabuki syndrome?: MLL2 testing in 116 patients, review and analyses of mutation and phenotypic spectrum. Eur J Hum Genet *20*, 381-388.

Barski, A., Cuddapah, S., Cui, K., Roh, T.Y., Schones, D.E., Wang, Z., Wei, G., Chepelev, I., and Zhao, K. (2007). High-resolution profiling of histone methylations in the human genome. Cell *129*, 823-837.

Bell, C.G., Wilson, G.A., and Beck, S. (2014). Human-specific CpG 'beacons' identify human-specific prefrontal cortex H3K4me3 chromatin peaks. Epigenomics *6*, 21-31.

Bjornsson, H.T., Benjamin, J.S., Zhang, L., Weissman, J., Gerber, E.E., Chen, Y.C., Vaurio, R.G., Potter, M.C., Hansen, K.D., and Dietz, H.C. (2014). Histone deacetylase inhibition rescues

structural and functional brain deficits in a mouse model of Kabuki syndrome. Science translational medicine *6*, 256ra135.

Bogershausen, N., and Wollnik, B. (2013). Unmasking Kabuki syndrome. Clinical Genetics *83*, 201-211.

Brind'Amour, J., Liu, S., Hudson, M., Chen, C., Karimi, M.M., and Lorincz, M.C. (2015). An ultra-low-input native ChIP-seq protocol for genome-wide profiling of rare cell populations. Nat Commun *6*, 6033.

Brookes, E., Laurent, B., Ounap, K., Carroll, R., Moeschler, J.B., Field, M., Schwartz, C.E., Gecz, J., and Shi, Y. (2015a). Mutations in the intellectual disability gene KDM5C reduce protein stability and demethylase activity. Hum Mol Genet *24*, 2861-2872.

Brookes, E., Laurent, B., Ounap, K., Carroll, R., Moeschler, J.B., Field, M., Schwartz, C.E., Gecz, J., and Shi, Y. (2015b). Mutations in the intellectual disability gene KDM5C reduce protein stability and demethylase activity. Hum Mol Genet.

Brown, C.J. (1999). Skewed X-chromosome inactivation: cause or consequence? J Natl Cancer Inst *91*, 304-305.

Burns, R., Majczenko, K., Xu, J., Peng, W., Yapici, Z., Dowling, J.J., Li, J.Z., and Burmeister, M. (2014). Homozygous splice mutation in CWF19L1 in a Turkish family with recessive ataxia syndrome. Neurology *83*, 2175-2182.

Caligioni, C.S. (2009). Assessing reproductive status/stages in mice. Current protocols in neuroscience / editorial board, Jacqueline N Crawley [et al] *Appendix 4*, Appendix 4I.

Cao, F., Townsend, E.C., Karatas, H., Xu, J., Li, L., Lee, S., Liu, L., Chen, Y., Ouillette, P., Zhu, J.*, et al.* (2014). Targeting MLL1 H3K4 methyltransferase activity in mixed-lineage leukemia. Mol Cell *53*, 247-261.

Cao, K., Collings, C.K., Morgan, M.A., Marshall, S.A., Rendleman, E.J., Ozark, P.A., Smith, E.R., and Shilatifard, A. (2018). An Mll4/COMPASS-Lsd1 epigenetic axis governs enhancer function and pluripotency transition in embryonic stem cells. Sci Adv *4*, eaap8747.

Catchpole, S., Spencer-Dene, B., Hall, D., Santangelo, S., Rosewell, I., Guenatri, M., Beatson, R., Scibetta, A.G., Burchell, J.M., and Taylor-Papadimitriou, J. (2011). PLU-1/JARID1B/KDM5B is required for embryonic survival and contributes to cell proliferation in the mammary gland and in ER+ breast cancer cells. Int J Oncol *38*, 1267-1277.

Cau, E., and Blader, P. (2009). Notch activity in the nervous system: to switch or not switch? Neural Dev *4*, 36.

Chen, Z., Zang, J., Whetstine, J., Hong, X., Davrazou, F., Kutateladze, T.G., Simpson, M., Mao, Q., Pan, C.H., Dai, S.*, et al.* (2006). Structural insights into histone demethylation by JMJD2 family members. Cell *125*, 691-702.

Cheng, J., Blum, R., Bowman, C., Hu, D., Shilatifard, A., Shen, S., and Dynlacht, B.D. (2014). A role for H3K4 monomethylation in gene repression and partitioning of chromatin readers. Mol Cell *53*, 979-992.

Cheung, I., Shulha, H.P., Jiang, Y., Matevossian, A., Wang, J., Weng, Z., and Akbarian, S. (2010). Developmental regulation and individual differences of neuronal H3K4me3 epigenomes in the prefrontal cortex. Proc Natl Acad Sci U S A *107*, 8824-8829.

Chicas, A., Kapoor, A., Wang, X., Aksoy, O., Evertts, A.G., Zhang, M.Q., Garcia, B.A., Bernstein, E., and Lowe, S.W. (2012). H3K4 demethylation by Jarid1a and Jarid1b contributes to retinoblastoma-mediated gene silencing during cellular senescence. Proc Natl Acad Sci U S A *109*, 8971-8976.

Chiurazzi, P., Schwartz, C.E., Gecz, J., and Neri, G. (2008). XLMR genes: update 2007. European journal of human genetics : EJHG *16*, 422-434.

Cho, Y.W., Hong, T., Hong, S., Guo, H., Yu, H., Kim, D., Guszczynski, T., Dressler, G.R., Copeland, T.D., Kalkum, M.*, et al.* (2007). PTIP associates with MLL3- and MLL4-containing histone H3 lysine 4 methyltransferase complex. J Biol Chem *282*, 20395-20406.

Christensen, J., Agger, K., Cloos, P.A., Pasini, D., Rose, S., Sennels, L., Rappsilber, J., Hansen, K.H., Salcini, A.E., and Helin, K. (2007). RBP2 belongs to a family of demethylases, specific for tri-and dimethylated lysine 4 on histone 3. Cell *128*, 1063-1076.

Cimino, G., Moir, D.T., Canaani, O., Williams, K., Crist, W.M., Katzav, S., Cannizzaro, L., Lange, B., Nowell, P.C., Croce, C.M.*, et al.* (1991). Cloning of All-1, the Locus Involved in Leukemias with the T(4-11)(Q21-Q23),T(9-11)(P22-Q23), and T(11-19)(Q23-P13) Chromosome Translocations. Cancer Research *51*, 6712-6714.

Claes, S., Devriendt, K., Van Goethem, G., Roelen, L., Meireleire, J., Raeymaekers, P., Cassiman, J.J., and Fryns, J.P. (2000). Novel syndromic form of X-linked complicated spastic paraplegia. Am J Med Genet *94*, 1-4.

Clouaire, T., Webb, S., and Bird, A. (2014). Cfp1 is required for gene expression dependent H3K4me3 and H3K9 acetylation in embryonic stem cells. Genome Biol *15*, 451.

Clouaire, T., Webb, S., Skene, P., Illingworth, R., Kerr, A., Andrews, R., Lee, J.H., Skalnik, D., and Bird, A. (2012). Cfp1 integrates both CpG content and gene activity for accurate H3K4me3 deposition in embryonic stem cells. Genes Dev *26*, 1714-1728.

Cornett, E.M., Dickson, B.M., Vaughan, R.M., Krishnan, S., Trievel, R.C., Strahl, B.D., and Rothbart, S.B. (2016). Substrate Specificity Profiling of Histone-Modifying Enzymes by Peptide Microarray. Methods Enzymol *574*, 31-52.

Crawley, J.N. (2007). Mouse behavioral assays relevant to the symptoms of autism. Brain Pathol *17*, 448-459.

De Rubeis, S., He, X., Goldberg, A.P., Poultney, C.S., Samocha, K., Cicek, A.E., Kou, Y., Liu, L., Fromer, M., Walker, S.*, et al.* (2014a). Synaptic, transcriptional and chromatin genes disrupted in autism. Nature *515*, 209-215.

De Rubeis, S., He, X., Goldberg, A.P., Poultney, C.S., Samocha, K., Ercument Cicek, A., Kou, Y., Liu, L., Fromer, M., Walker, S.*, et al.* (2014b). Synaptic, transcriptional and chromatin genes disrupted in autism. Nature *515*, 209-215.

Defeojones, D., Huang, P.S., Jones, R.E., Haskell, K.M., Vuocolo, G.A., Hanobik, M.G., Huber, H.E., and Oliff, A. (1991). Cloning of Cdnas for Cellular Proteins That Bind to the Retinoblastoma Gene-Product. Nature *352*, 251-254.

Denissov, S., Hofemeister, H., Marks, H., Kranz, A., Ciotta, G., Singh, S., Anastassiadis, K., Stunnenberg, H.G., and Stewart, A.F. (2014). Mll2 is required for H3K4 trimethylation on bivalent promoters in embryonic stem cells, whereas Mll1 is redundant. Development *141*, 526-537.

Dey, B.K., Stalker, L., Schnerch, A., Bhatia, M., Taylor-Papidimitriou, J., and Wynder, C. (2008). The histone demethylase KDM5b/JARID1b plays a role in cell fate decisions by blocking terminal differentiation. Mol Cell Biol *28*, 5312-5327.

Dhar, S.S., Lee, S.H., Kan, P.Y., Voigt, P., Ma, L., Shi, X., Reinberg, D., and Lee, M.G. (2012). Trans-tail regulation of MLL4-catalyzed H3K4 methylation by H4R3 symmetric dimethylation is mediated by a tandem PHD of MLL4. Genes Dev *26*, 2749-2762.

Dierssen, M., and Ramakers, G.J. (2006). Dendritic pathology in mental retardation: from molecular genetics to neurobiology. Genes Brain Behav *5 Suppl 2*, 48-60.

DiTacchio, L., Le, H.D., Vollmers, C., Hatori, M., Witcher, M., Secombe, J., and Panda, S. (2011). Histone lysine demethylase JARID1a activates CLOCK-BMAL1 and influences the circadian clock. Science *333*, 1881-1885.

Dobin, A., Davis, C.A., Schlesinger, F., Drenkow, J., Zaleski, C., Jha, S., Batut, P., Chaisson, M., and Gingeras, T.R. (2013). STAR: ultrafast universal RNA-seq aligner. Bioinformatics *29*, 15-21.

Dou, Y.L., Milne, T.A., Ruthenburg, A.J., Lee, S., Lee, J.W., Verdine, G.L., Allis, C.D., and Roeder, R.G. (2006). Regulation of MLL1 H3K4 methyltransferase activity by its core components. Nature Structural & Molecular Biology *13*, 713-719.

Doyle, A. (1990). Establishment of lymphoblastoid cell lines. Methods Mol Biol *5*, 43-47.

Edgar, R., Domrachev, M., and Lash, A.E. (2002). Gene Expression Omnibus: NCBI gene expression and hybridization array data repository. Nucleic Acids Res *30*, 207-210.

Eissenberg, J.C., and Shilatifard, A. (2010). Histone H3 lysine 4 (H3K4) methylation in development and differentiation. Dev Biol *339*, 240-249.

Faundes, V., Newman, W.G., Bernardini, L., Canham, N., Clayton-Smith, J., Dallapiccola, B., Davies, S.J., Demos, M.K., Goldman, A., Gill, H.*, et al.* (2018). Histone Lysine Methylases and

Demethylases in the Landscape of Human Developmental Disorders. Am J Hum Genet *102*, 175-187.

Felix-Ortiz, A.C., Burgos-Robles, A., Bhagat, N.D., Leppla, C.A., and Tye, K.M. (2016). Bidirectional modulation of anxiety-related and social behaviors by amygdala projections to the medial prefrontal cortex. Neuroscience *321*, 197-209.

Felix-Ortiz, A.C., and Tye, K.M. (2014). Amygdala inputs to the ventral hippocampus bidirectionally modulate social behavior. J Neurosci *34*, 586-595.

Feng, W.J., Yonezawa, M., Ye, J., Jenuwein, T., and Grummt, I. (2010). PHF8 activates transcription of rRNA genes through H3K4me3 binding and H3K9me1/2 demethylation. Nature Structural & Molecular Biology *17*, 445-U483.

Fortschegger, K., de Graaf, P., Outchkourov, N.S., van Schaik, F.M., Timmers, H.T., and Shiekhattar, R. (2010). PHF8 targets histone methylation and RNA polymerase II to activate transcription. Mol Cell Biol *30*, 3286-3298.

Garay, P., Chen, A., Tsukahara, T., Kohen, R., Althaus, C., Wallner, M., Giger, R., Sutton, M., and Iwase, S. (2019). RAI1
Regulates Activity-Dependent Nascent Transcription and Synaptic Scaling (Biorxiv).

Garcia-Bassets, I., Kwon, Y.S., Telese, F., Prefontaine, G.G., Hutt, K.R., Cheng, C.S., Ju, B.G., Ohgi, K.A., Wang, J., Escoubet-Lozach, L.*, et al.* (2007). Histone methylation-dependent mechanisms impose ligand dependency for gene activation by nuclear receptors. Cell *128*, 505-518.

Gayen, S., Maclary, E., Murata-Nakamura, Y., Vallianatos, C.N., Garay, P.M., Iwase, S., and Kalantry, S. (2017). Induction of X-chromosome Inactivation by the Histone Demethylase SMCX/KDM5C. BioRxiv.

Goncalves, T.F., Goncalves, A.P., Fintelman Rodrigues, N., dos Santos, J.M., Pimentel, M.M., and Santos-Reboucas, C.B. (2014). KDM5C mutational screening among males with intellectual disability suggestive of X-Linked inheritance and review of the literature. Eur J Med Genet *57*, 138-144.

Greer, E.L., and Shi, Y. (2012). Histone methylation: a dynamic mark in health, disease and inheritance. Nat Rev Genet *13*, 343-357.

Grembecka, J., He, S., Shi, A., Purohit, T., Muntean, A.G., Sorenson, R.J., Showalter, H.D., Murai, M.J., Belcher, A.M., Hartley, T.*, et al.* (2012). Menin-MLL inhibitors reverse oncogenic activity of MLL fusion proteins in leukemia. Nat Chem Biol *8*, 277-284.

Grzybowski, A.T., Chen, Z., and Ruthenburg, A.J. (2015). Calibrating ChIP-Seq with Nucleosomal Internal Standards to Measure Histone Modification Density Genome Wide. Mol Cell *58*, 886-899.

Guissart, C., Latypova, X., Rollier, P., Khan, T.N., Stamberger, H., McWalter, K., Cho, M.T., Kjaergaard, S., Weckhuysen, S., Lesca, G.*, et al.* (2018). Dual Molecular Effects of Dominant

RORA Mutations Cause Two Variants of Syndromic Intellectual Disability with Either Autism or Cerebellar Ataxia. Am J Hum Genet *102*, 744-759.

Gupta, S., Kim, S.Y., Artis, S., Molfese, D.L., Schumacher, A., Sweatt, J.D., Paylor, R.E., and Lubin, F.D. (2010). Histone methylation regulates memory formation. The Journal of neuroscience : the official journal of the Society for Neuroscience *30*, 3589-3599.

Guzmán, Y.F., Tronson, N.C., Jovasevic, V., Sato, K., Guedea, A.L., Mizukami, H., Nishimori, K., and Radulovic, J. (2013). Fear-enhancing effects of septal oxytocin receptors. Nat Neurosci *16*, 1185-1187.

Hakimi, M.A., Bochar, D.A., Chenoweth, J., Lane, W.S., Mandel, G., and Shiekhattar, R. (2002). A core-BRAF35 complex containing histone deacetylase mediates repression of neuronal-specific genes. Proc Natl Acad Sci U S A *99*, 7420-7425.

Hakimi, M.A., Dong, Y., Lane, W.S., Speicher, D.W., and Shiekhattar, R. (2003). A candidate X-linked mental retardation gene is a component of a new family of histone deacetylase-containing complexes. J Biol Chem *278*, 7234-7239.

Hallson, G., Hollebakken, R.E., Li, T., Syrzycka, M., Kim, I., Cotsworth, S., Fitzpatrick, K.A., Sinclair, D.A., and Honda, B.M. (2012). dSet1 is the main H3K4 di- and tri-methyltransferase throughout Drosophila development. Genetics *190*, 91-100.

Hannibal, M.C., Buckingham, K.J., Ng, S.B., Ming, J.E., Beck, A.E., McMillin, M.J., Gildersleeve, H.I., Bigham, A.W., Tabor, H.K., Mefford, H.C.*, et al.* (2011). Spectrum of MLL2 (ALR) mutations in 110 cases of Kabuki syndrome. Am J Med Genet A *155A*, 1511-1516.

Hawrylycz, M.J., Lein, E.S., Guillozet-Bongaarts, A.L., Shen, E.H., Ng, L., Miller, J.A., van de Lagemaat, L.N., Smith, K.A., Ebbert, A., Riley, Z.L.*, et al.* (2012). An anatomically comprehensive atlas of the adult human brain transcriptome. Nature *489*, 391-399.

Hayakawa, T., Ohtani, Y., Hayakawa, N., Shinmyozu, K., Saito, M., Ishikawa, F., and Nakayama, J. (2007). RBP2 is an MRG15 complex component and down-regulates intragenic histone H3 lysine 4 methylation. Genes to Cells *12*, 811-826.

Heintzman, N.D., Hon, G.C., Hawkins, R.D., Kheradpour, P., Stark, A., Harp, L.F., Ye, Z., Lee, L.K., Stuart, R.K., Ching, C.W.*, et al.* (2009). Histone modifications at human enhancers reflect global cell-type-specific gene expression. Nature *459*, 108-112.

Heintzman, N.D., and Ren, B. (2007). The gateway to transcription: identifying, characterizing and understanding promoters in the eukaryotic genome. Cell Mol Life Sci *64*, 386-400.

Heintzman, N.D., Stuart, R.K., Hon, G., Fu, Y., Ching, C.W., Hawkins, R.D., Barrera, L.O., Van Calcar, S., Qu, C., Ching, K.A.*, et al.* (2007). Distinct and predictive chromatin signatures of transcriptional promoters and enhancers in the human genome. Nat Genet *39*, 311-318.

Heinz, S., Benner, C., Spann, N., Bertolino, E., Lin, Y.C., Laslo, P., Cheng, J.X., Murre, C., Singh, H., and Glass, C.K. (2010). Simple combinations of lineage-determining transcription

factors prime cis-regulatory elements required for macrophage and B cell identities. Molecular cell *38*, 576-589.

Helin, K., and Dhanak, D. (2013). Chromatin proteins and modifications as drug targets. Nature *502*, 480-488.

Horton, J.R., Upadhyay, A.K., Qi, H.H., Zhang, X., Shi, Y., and Cheng, X.D. (2010). Enzymatic and structural insights for substrate specificity of a family of jumonji histone lysine demethylases. Nature Structural & Molecular Biology *17*, 38-U52.

Hsu, P.L., Li, H., Lau, H.T., Leonen, C., Dhall, A., Ong, S.E., Chatterjee, C., and Zheng, N. (2018). Crystal Structure of the COMPASS H3K4 Methyltransferase Catalytic Module. Cell *174*, 1106-1116.e1109.

Hu, D.Q., Gao, X., Morgan, M.A., Herz, H.M., Smith, E.R., and Shilatifard, A. (2013). The MLL3/MLL4 Branches of the COMPASS Family Function as Major Histone H3K4 Monomethylases at Enhancers. Molecular and Cellular Biology *33*, 4745-4754.

Huang da, W., Sherman, B.T., and Lempicki, R.A. (2009a). Bioinformatics enrichment tools: paths toward the comprehensive functional analysis of large gene lists. Nucleic Acids Res *37*, 1-13.

Huang da, W., Sherman, B.T., and Lempicki, R.A. (2009b). Systematic and integrative analysis of large gene lists using DAVID bioinformatics resources. Nat Protoc *4*, 44-57.

Iossifov, I., O'Roak, B.J., Sanders, S.J., Ronemus, M., Krumm, N., Levy, D., Stessman, H.A., Witherspoon, K.T., Vives, L., Patterson, K.E*., et al.* (2014). The contribution of de novo coding mutations to autism spectrum disorder. Nature *515*, 216-221.

Irwin, S.A., Galvez, R., and Greenough, W.T. (2000). Dendritic spine structural anomalies in fragile-X mental retardation syndrome. Cereb Cortex *10*, 1038-1044.

Iwase, S., Berube, N.G., Zhou, Z., Kasri, N.N., Battaglioli, E., Scandaglia, M., and Barco, A. (2017). Epigenetic Etiology of Intellectual Disability. The Journal of neuroscience : the official journal of the Society for Neuroscience *37*, 10773-10782.

Iwase, S., Brookes, E., Agarwal, S., Badeaux, A.I., Ito, H., Vallianatos, C.N., Tomassy, G.S., Kasza, T., Lin, G., Thompson, A*., et al.* (2016). A Mouse Model of X-linked Intellectual Disability Associated with Impaired Removal of Histone Methylation. Cell reports.

Iwase, S., Januma, A., Miyamoto, K., Shono, N., Honda, A., Yanagisawa, J., and Baba, T. (2004). Characterization of BHC80 in BRAF-HDAC complex, involved in neuron-specific gene repression. Biochem Biophys Res Commun *322*, 601-608.

Iwase, S., Lan, F., Bayliss, P., de la Torre-Ubieta, L., Huarte, M., Qi, H.H., Whetstine, J.R., Bonni, A., Roberts, T.M., and Shi, Y. (2007). The X-linked mental retardation gene SMCX/JARID1C defines a family of histone H3 lysine 4 demethylases. Cell *128*, 1077-1088.

Iwase, S., and Shi, Y. (2011). Histone and DNA modifications in mental retardation. Progress in drug research Fortschritte der Arzneimittelforschung Progres des recherches pharmaceutiques *67*, 147-173.

Iwase, S., Shono, N., Honda, A., Nakanishi, T., Kashiwabara, S., Takahashi, S., and Baba, T. (2006). A component of BRAF-HDAC complex, BHC80, is required for neonatal survival in mice. FEBS Lett *580*, 3129-3135.

Iwase, S., Xiang, B., Ghosh, S., Ren, T., Lewis, P.W., Cochrane, J.C., Allis, C.D., Picketts, D.J., Patel, D.J., Li, H.*, et al.* (2011). ATRX ADD domain links an atypical histone methylation recognition mechanism to human mental-retardation syndrome. Nat Struct Mol Biol *18*, 769-776.

Jakovcevski, M., Ruan, H., Shen, E.Y., Dincer, A., Javidfar, B., Ma, Q., Peter, C.J., Cheung, I., Mitchell, A.C., Jiang, Y.*, et al.* (2015). Neuronal Kmt2a/Mll1 histone methyltransferase is essential for prefrontal synaptic plasticity and working memory. The Journal of neuroscience : the official journal of the Society for Neuroscience *35*, 5097-5108.

Jaworski, E., and Routh, A. (2018). ClickSeq: Replacing Fragmentation and Enzymatic Ligation with Click-Chemistry to Prevent Sequence Chimeras. Methods Mol Biol *1712*, 71-85.

Jensen, L.R., Amende, M., Gurok, U., Moser, B., Gimmel, V., Tzschach, A., Janecke, A.R., Tariverdian, G., Chelly, J., and Fryns, J.-P. (2005a). Mutations in the JARID1C gene, which is involved in transcriptional regulation and chromatin remodeling, cause X-linked mental retardation. The American Journal of Human Genetics *76*, 227-236.

Jensen, L.R., Amende, M., Gurok, U., Moser, B., Gimmel, V., Tzschach, A., Janecke, A.R., Tariverdian, G., Chelly, J., Fryns, J.P.*, et al.* (2005b). Mutations in the JARID1C gene, which is involved in transcriptional regulation and chromatin remodeling, cause X-linked mental retardation. Am J Hum Genet *76*, 227-236.

Jensen, L.R., Bartenschlager, H., Rujirabanjerd, S., Tzschach, A., Numann, A., Janecke, A.R., Sporle, R., Stricker, S., Raynaud, M., Nelson, J.*, et al.* (2010). A distinctive gene expression fingerprint in mentally retarded male patients reflects disease-causing defects in the histone demethylase KDM5C. Pathogenetics *3*, 2.

Jimenez, S.A., and Maren, S. (2009). Nuclear disconnection within the amygdala reveals a direct pathway to fear. Learn Mem *16*, 766-768.

Jiménez, G., Shvartsman, S.Y., and Paroush, Z. (2012). The Capicua repressor--a general sensor of RTK signaling in development and disease. J Cell Sci *125*, 1383-1391.

Johansson, C., Velupillai, S., Tumber, A., Szykowska, A., Hookway, E.S., Nowak, R.P., Strain-Damerell, C., Gileadi, C., Philpott, M., Burgess-Brown, N.*, et al.* (2016). Structural analysis of human KDM5B guides histone demethylase inhibitor development. Nature chemical biology *12*, 539-545.

Johnson, M.B., Kawasawa, Y.I., Mason, C.E., Krsnik, Z., Coppola, G., Bogdanovic, D., Geschwind, D.H., Mane, S.M., State, M.W., and Sestan, N. (2009). Functional and evolutionary

insights into human brain development through global transcriptome analysis. Neuron *62*, 494-509.

Jones, W.D., Dafou, D., McEntagart, M., Woollard, W.J., Elmslie, F.V., Holder-Espinasse, M., Irving, M., Saggar, A.K., Smithson, S., Trembath, R.C.*, et al.* (2012). De Novo Mutations in MLL Cause Wiedemann-Steiner Syndrome. American Journal of Human Genetics *91*, 358-364.

Kang, H.J., Kawasawa, Y.I., Cheng, F., Zhu, Y., Xu, X., Li, M., Sousa, A.M., Pletikos, M., Meyer, K.A., Sedmak, G.*, et al.* (2011). Spatio-temporal transcriptome of the human brain. Nature *478*, 483-489.

Katsanis, N., Beales, P.L., Woods, M.O., Lewis, R.A., Green, J.S., Parfrey, P.S., Ansley, S.J., Davidson, W.S., and Lupski, J.R. (2000). Mutations in MKKS cause obesity, retinal dystrophy and renal malformations associated with Bardet-Biedl syndrome. Nat Genet *26*, 67-70.

Keiser, A.A., Turnbull, L.M., Darian, M.A., Feldman, D.E., Song, I., and Tronson, N.C. (2017). Sex Differences in Context Fear Generalization and Recruitment of Hippocampus and Amygdala during Retrieval. Neuropsychopharmacology *42*, 397-407.

Kent-First, M.G., Maffitt, M., Muallem, A., Brisco, P., Shultz, J., Ekenberg, S., Agulnik, A.I., Agulnik, I., Shramm, D., Bavister, B.*, et al.* (1996). Gene sequence and evolutionary conservation of human SMCY. Nat Genet *14*, 128-129.

Kerimoglu, C., Agis-Balboa, R.C., Kranz, A., Stilling, R., Bahari-Javan, S., Benito-Garagorri, E., Halder, R., Burkhardt, S., Stewart, A.F., and Fischer, A. (2013). Histone-methyltransferase MLL2 (KMT2B) is required for memory formation in mice. J Neurosci *33*, 3452-3464.

Kerimoglu, C., Sakib, M.S., Jain, G., Benito, E., Burkhardt, S., Capece, V., Kaurani, L., Halder, R., Agís-Balboa, R.C., Stilling, R.*, et al.* (2017). KMT2A and KMT2B Mediate Memory Function by Affecting Distinct Genomic Regions. Cell Rep *20*, 538-548.

Khomtchouk, B.B., Hennessy, J.R., and Wahlestedt, C. (2017). shinyheatmap: Ultra fast low memory heatmap web interface for big data genomics. PLoS One *12*, e0176334.

Kidder, B.L., Hu, G., and Zhao, K. (2014). KDM5B focuses H3K4 methylation near promoters and enhancers during embryonic stem cell self-renewal and differentiation. Genome Biol *15*, R32.

Kim, B., Colon, E., Chawla, S., Vandenberg, L.N., and Suvorov, A. (2015). Endocrine disruptors alter social behaviors and indirectly influence social hierarchies via changes in body weight. Environ Health *14*, 64.

Kim, H.G., Kim, H.T., Leach, N.T., Lan, F., Ullmann, R., Silahtaroglu, A., Kurth, I., Nowka, A., Seong, I.S., Shen, Y.*, et al.* (2012). Translocations disrupting PHF21A in the Potocki-Shaffer-syndrome region are associated with intellectual disability and craniofacial anomalies. Am J Hum Genet *91*, 56-72.

Klajn, A., Ferrai, C., Stucchi, L., Prada, I., Podini, P., Baba, T., Rocchi, M., Meldolesi, J., and D'Alessandro, R. (2009). The rest repression of the neurosecretory phenotype is negatively modulated by BHC80, a protein of the BRAF/HDAC complex. J Neurosci *29*, 6296-6307.

Kleefstra, T., Kramer, J.M., Neveling, K., Willemsen, M.H., Koemans, T.S., Vissers, L.E., Wissink-Lindhout, W., Fenckova, M., van den Akker, W.M., Kasri, N.N.*, et al.* (2012). Disruption of an EHMT1-associated chromatin-modification module causes intellectual disability. Am J Hum Genet *91*, 73-82.

Klein, B.J., Piao, L., Xi, Y., Rincon-Arano, H., Rothbart, S.B., Peng, D., Wen, H., Larson, C., Zhang, X., Zheng, X.*, et al.* (2014). The histone-H3K4-specific demethylase KDM5B binds to its substrate and product through distinct PHD fingers. Cell Rep *6*, 325-335.

Kleine-Kohlbrecher, D., Christensen, J., Vandamme, J., Abarrategui, I., Bak, M., Tommerup, N., Shi, X.B., Gozani, O., Rappsilber, J., Salcini, A.E.*, et al.* (2010). A Functional Link between the Histone Demethylase PHF8 and the Transcription Factor ZNF711 in X-Linked Mental Retardation. Molecular Cell *38*, 165-178.

Klose, R.J., Yan, Q., Tothova, Z., Yamane, K., Erdjument-Bromage, H., Tempst, P., Gilliland, D.G., Zhang, Y., and Kaelin, W.G. (2007). The retinoblastoma binding protein RBP2 is an H3K4 demethylase. Cell *128*, 889-900.

Koivisto, A.M., Ala-Mello, S., Lemmela, S., Komu, H.A., Rautio, J., and Jarvela, I. (2007). Screening of mutations in the PHF8 gene and identification of a novel mutation in a Finnish family with XLMR and cleft lip/cleft palate. Clin Genet *72*, 145-149.

Kong, A., Gudbjartsson, D.F., Sainz, J., Jonsdottir, G.M., Gudjonsson, S.A., Richardsson, B., Sigurdardottir, S., Barnard, J., Hallbeck, B., Masson, G.*, et al.* (2002). A high-resolution recombination map of the human genome. Nat Genet *31*, 241-247.

Kouzarides, T. (2007). Chromatin modifications and their function. Cell *128*, 693-705.

Kulkarni, N., Tang, S., Bhardwaj, R., Bernes, S., and Grebe, T.A. (2016). Progressive Movement Disorder in Brothers Carrying a GNAO1 Mutation Responsive to Deep Brain Stimulation. J Child Neurol *31*, 211-214.

Lan, F., Collins, R.E., De Cegli, R., Alpatov, R., Horton, J.R., Shi, X., Gozani, O., Cheng, X., and Shi, Y. (2007). Recognition of unmethylated histone H3 lysine 4 links BHC80 to LSD1-mediated gene repression. Nature *448*, 718-722.

Larrieu, T., Cherix, A., Duque, A., Rodrigues, J., Lei, H., Gruetter, R., and Sandi, C. (2017). Hierarchical Status Predicts Behavioral Vulnerability and Nucleus Accumbens Metabolic Profile Following Chronic Social Defeat Stress. Curr Biol *27*, 2202-2210.e2204.

Lauberth, S.M., Nakayama, T., Wu, X., Ferris, A.L., Tang, Z., Hughes, S.H., and Roeder, R.G. (2013). H3K4me3 Interactions with TAF3 Regulate Preinitiation Complex Assembly and Selective Gene Activation. Cell *152*, 1021-1036.

Laumonnier, F., Holbert, S., Ronce, N., Faravelli, F., Lenzner, S., Schwartz, C.E., Lespinasse, J., Van Esch, H., Lacombe, D., Goizet, C.*, et al.* (2005). Mutations in PHF8 are associated with X linked mental retardation and cleft lip/cleft palate. Journal of Medical Genetics *42*, 780-786.

Lee, J.E., Wang, C.C., Xu, S.L.Y., Cho, Y.W., Wang, L.F., Feng, X.S., Baldridge, A., Sartorelli, V., Zhuang, L.N., Peng, W.Q.*, et al.* (2013). H3K4 mono- and di-methyltransferase MLL4 is required for enhancer activation during cell differentiation. Elife *2*.

Lee, J.H., and Skalnik, D.G. (2005). CpG-binding protein (CXXC finger protein 1) is a component of the mammalian set1 histone H3-Lys(4) methyltransferase complex, the analogue of the yeast Set1/COMPASS complex. Journal of Biological Chemistry *280*, 41725-41731.

Lee, M.G., Wynder, C., Cooch, N., and Shiekhattar, R. (2005). An essential role for CoREST in nucleosomal histone 3 lysine 4 demethylation. Nature *437*, 432-435.

Lein, E.S., Hawrylycz, M.J., Ao, N., Ayres, M., Bensinger, A., Bernard, A., Boe, A.F., Boguski, M.S., Brockway, K.S., Byrnes, E.J.*, et al.* (2007). Genome-wide atlas of gene expression in the adult mouse brain. Nature *445*, 168-176.

Leonard, H., and Wen, X. (2002). The epidemiology of mental retardation: challenges and opportunities in the new millennium. Mental retardation and developmental disabilities research reviews *8*, 117-134.

Lessel, D., Gehbauer, C., Bramswig, N.C., Schluth-Bolard, C., Venkataramanappa, S., van Gassen, K.L.I., Hempel, M., Haack, T.B., Baresic, A., Genetti, C.A.*, et al.* (2018). BCL11B mutations in patients affected by a neurodevelopmental disorder with reduced type 2 innate lymphoid cells. Brain *141*, 2299-2311.

Levinson, D.M., Reeves, D.L., and Buchanan, D.R. (1980). Reductions in aggression and dominance status in guinea pigs following bilateral lesions in the basolateral amygdala or lateral septum. Physiol Behav *25*, 963-971.

Li, X., Liu, L., Yang, S., Song, N., Zhou, X., Gao, J., Yu, N., Shan, L., Wang, Q., Liang, J.*, et al.* (2014). Histone demethylase KDM5B is a key regulator of genome stability. Proc Natl Acad Sci U S A *111*, 7096-7101.

Li, Y., Bogershausen, N., Alanay, Y., Simsek Kiper, P.O., Plume, N., Keupp, K., Pohl, E., Pawlik, B., Rachwalski, M., Milz, E.*, et al.* (2011). A mutation screen in patients with Kabuki syndrome. Hum Genet *130*, 715-724.

Liang, Z., Diamond, M., Smith, J.A., Schnell, M., and Daniel, R. (2011). Proliferating cell nuclear antigen is required for loading of the SMCX/KMD5C histone demethylase onto chromatin. Epigenetics Chromatin *4*, 18.

Liao, Y., Smyth, G.K., and Shi, W. (2014). featureCounts: an efficient general purpose program for assigning sequence reads to genomic features. Bioinformatics *30*, 923-930.

Lim, D.A., Huang, Y.C., Swigut, T., Mirick, A.L., Garcia-Verdugo, J.M., Wysocka, J., Ernst, P., and Alvarez-Buylla, A. (2009). Chromatin remodelling factor Mll1 is essential for neurogenesis from postnatal neural stem cells. Nature *458*, 529-U529.

Local, A., Huang, H., Albuquerque, C.P., Singh, N., Lee, A.Y., Wang, W., Wang, C., Hsia, J.E., Shiau, A.K., Ge, K.*, et al.* (2018). Identification of H3K4me1-associated proteins at mammalian enhancers. Nat Genet *50*, 73-82.

Loenarz, C., Ge, W., Coleman, M.L., Rose, N.R., Cooper, C.D., Klose, R.J., Ratcliffe, P.J., and Schofield, C.J. (2010). PHF8, a gene associated with cleft lip/palate and mental retardation, encodes for an Nepsilon-dimethyl lysine demethylase. Hum Mol Genet *19*, 217-222.

Loke, H., Harley, V., and Lee, J. (2015). Biological factors underlying sex differences in neurological disorders. Int J Biochem Cell Biol *65*, 139-150.

Lopez-Bigas, N., Kisiel, T.A., Dewaal, D.C., Holmes, K.B., Volkert, T.L., Gupta, S., Love, J., Murray, H.L., Young, R.A., and Benevolenskaya, E.V. (2008). Genome-wide analysis of the H3K4 histone demethylase RBP2 reveals a transcriptional program controlling differentiation. Mol Cell *31*, 520-530.

Love, M.I., Huber, W., and Anders, S. (2014). Moderated estimation of fold change and dispersion for RNA-seq data with DESeq2. Genome Biol *15*, 550.

Lu, H.C., Tan, Q., Rousseaux, M.W., Wang, W., Kim, J.Y., Richman, R., Wan, Y.W., Yeh, S.Y., Patel, J.M., Liu, X.*, et al.* (2017). Disruption of the ATXN1-CIC complex causes a spectrum of neurobehavioral phenotypes in mice and humans. Nat Genet *49*, 527-536.

Lupo, G., Harris, W.A., and Lewis, K.E. (2006). Mechanisms of ventral patterning in the vertebrate nervous system. Nat Rev Neurosci *7*, 103-114.

Maren, S. (2001). Neurobiology of Pavlovian fear conditioning. Annual review of neuroscience *24*, 897-931.

McCann, K.E., Sinkiewicz, D.M., Rosenhauer, A.M., Beach, L.Q., and Huhman, K.L. (2018). Transcriptomic Analysis Reveals Sex-Dependent Expression Patterns in the Basolateral Amygdala of Dominant and Subordinate Animals After Acute Social Conflict. Mol Neurobiol.

McGregor, A., and Herbert, J. (1992). Differential effects of excitotoxic basolateral and corticomedial lesions of the amygdala on the behavioural and endocrine responses to either sexual or aggression-promoting stimuli in the male rat. Brain Res *574*, 9-20.

McMahon, K.A., Hiew, S.Y., Hadjur, S., Veiga-Fernandes, H., Menzel, U., Price, A.J., Kioussis, D., Williams, O., and Brady, H.J. (2007). Mll has a critical role in fetal and adult hematopoietic stem cell self-renewal. Cell stem cell *1*, 338-345.

Mersman, D.P., Du, H.N., Fingerman, I.M., South, P.F., and Briggs, S.D. (2012). Charge-based Interaction Conserved within Histone H3 Lysine 4 (H3K4) Methyltransferase Complexes Is Needed for Protein Stability, Histone Methylation, and Gene Expression. Journal of Biological Chemistry *287*, 2652-2665.

Micale, L., Augello, B., Fusco, C., Selicorni, A., Loviglio, M.N., Silengo, M.C., Reymond, A., Gumiero, B., Zucchetti, F., D'Addetta, E.V.*, et al.* (2011). Mutation spectrum of MLL2 in a cohort of Kabuki syndrome patients. Orphanet J Rare Dis *6*, 38.

Miczek, K.A., Maxson, S.C., Fish, E.W., and Faccidomo, S. (2001). Aggressive behavioral phenotypes in mice. Behav Brain Res *125*, 167-181.

Milad, M.R., Igoe, S.A., Lebron-Milad, K., and Novales, J.E. (2009). Estrous cycle phase and gonadal hormones influence conditioned fear extinction. Neuroscience *164*, 887-895.

Miller, J.A., Ding, S.L., Sunkin, S.M., Smith, K.A., Ng, L., Szafer, A., Ebbert, A., Riley, Z.L., Royall, J.J., Aiona, K.*, et al.* (2014). Transcriptional landscape of the prenatal human brain. Nature *508*, 199-206.

Mishra, S., Van Rechem, C., Pal, S., Clarke, T.L., Chakraborty, D., Mahan, S.D., Black, J.C., Murphy, S.E., Lawrence, M.S., Daniels, D.L.*, et al.* (2018). Cross-talk between Lysine-Modifying Enzymes Controls Site-Specific DNA Amplifications. Cell *175*, 1716.

Miyake, N., Koshimizu, E., Okamoto, N., Mizuno, S., Ogata, T., Nagai, T., Kosho, T., Ohashi, H., Kato, M., Sasaki, G.*, et al.* (2013). MLL2 and KDM6A Mutations in Patients With Kabuki Syndrome. American Journal of Medical Genetics Part A *161*, 2234-2243.

Miyazaki, T., Hashimoto, K., Uda, A., Sakagami, H., Nakamura, Y., Saito, S.Y., Nishi, M., Kume, H., Tohgo, A., Kaneko, I.*, et al.* (2006). Disturbance of cerebellar synaptic maturation in mutant mice lacking BSRPs, a novel brain-specific receptor-like protein family. FEBS Lett *580*, 4057-4064.

Mohan, M., Herz, H.M., Smith, E.R., Zhang, Y., Jackson, J., Washburn, M.P., Florens, L., Eissenberg, J.C., and Shilatifard, A. (2011). The COMPASS family of H3K4 methylases in Drosophila. Mol Cell Biol *31*, 4310-4318.

Moretti, P., Bouwknecht, J.A., Teague, R., Paylor, R., and Zoghbi, H.Y. (2005). Abnormalities of social interactions and home-cage behavior in a mouse model of Rett syndrome. Hum Mol Genet *14*, 205-220.

Mudunuri, U., Che, A., Yi, M., and Stephens, R.M. (2009). bioDBnet: the biological database network. Bioinformatics *25*, 555-556.

Murphy, G.J., Mostoslavsky, G., Kotton, D.N., and Mulligan, R.C. (2006). Exogenous control of mammalian gene expression via modulation of translational termination. Nature medicine *12*, 1093-1099.

Musselman, C.A., and Kutateladze, T.G. (2011). Handpicking epigenetic marks with PHD fingers. Nucleic Acids Res *39*, 9061-9071.

Nagase, T., Kikuno, R., Ishikawa, K., Hirosawa, M., and Ohara, O. (2000). Prediction of the coding sequences of unidentified human genes. XVII. The complete sequences of 100 new cDNA clones from brain which code for large proteins in vitro. DNA Res *7*, 143-150.

Najmabadi, H., Hu, H., Garshasbi, M., Zemojtel, T., Abedini, S.S., Chen, W., Hosseini, M., Behjati, F., Haas, S., Jamali, P.*, et al.* (2011). Deep sequencing reveals 50 novel genes for recessive cognitive disorders. Nature *478*, 57-63.

Nakamura, K., Kodera, H., Akita, T., Shiina, M., Kato, M., Hoshino, H., Terashima, H., Osaka, H., Nakamura, S., Tohyama, J.*, et al.* (2013). De Novo mutations in GNAO1, encoding a Gαo subunit of heterotrimeric G proteins, cause epileptic encephalopathy. Am J Hum Genet *93*, 496-505.

Network, and Pathway Analysis Subgroup of Psychiatric Genomics, C. (2015). Psychiatric genome-wide association study analyses implicate neuronal, immune and histone pathways. Nature neuroscience *18*, 199-209.

Ng, S.B., Bigham, A.W., Buckingham, K.J., Hannibal, M.C., McMillin, M.J., Gildersleeve, H.I., Beck, A.E., Tabor, H.K., Cooper, G.M., Mefford, H.C.*, et al.* (2010). Exome sequencing identifies MLL2 mutations as a cause of Kabuki syndrome. Nature Genetics *42*, 790-U785.

Ooi, S.K., Qiu, C., Bernstein, E., Li, K., Jia, D., Yang, Z., Erdjument-Bromage, H., Tempst, P., Lin, S.P., Allis, C.D.*, et al.* (2007). DNMT3L connects unmethylated lysine 4 of histone H3 to de novo methylation of DNA. Nature *448*, 714-717.

Ounap, K., Puusepp-Benazzouz, H., Peters, M., Vaher, U., Rein, R., Proos, A., Field, M., and Reimand, T. (2012). A novel c.2T > C mutation of the KDM5C/JARID1C gene in one large family with X-linked intellectual disability. European journal of medical genetics *55*, 178-184.

Outchkourov, N.S., Muino, J.M., Kaufmann, K., van Ijcken, W.F., Groot Koerkamp, M.J., van Leenen, D., de Graaf, P., Holstege, F.C., Grosveld, F.G., and Timmers, H.T. (2013). Balancing of histone H3K4 methylation states by the Kdm5c/SMCX histone demethylase modulates promoter and enhancer function. Cell Rep *3*, 1071-1079.

Park, J., Thomas, S., and Munster, P.N. (2015). Epigenetic modulation with histone deacetylase inhibitors in combination with immunotherapy. Epigenomics *7*, 641-652.

Paré, D., Quirk, G.J., and Ledoux, J.E. (2004). New vistas on amygdala networks in conditioned fear. J Neurophysiol *92*, 1-9.

Paulussen, A.D., Stegmann, A.P., Blok, M.J., Tserpelis, D., Posma-Velter, C., Detisch, Y., Smeets, E.E., Wagemans, A., Schrander, J.J., van den Boogaard, M.J.*, et al.* (2011). MLL2 mutation spectrum in 45 patients with Kabuki syndrome. Hum Mutat *32*, E2018-2025.

Penzes, P., Cahill, M.E., Jones, K.A., VanLeeuwen, J.E., and Woolfrey, K.M. (2011). Dendritic spine pathology in neuropsychiatric disorders. Nat Neurosci *14*, 285-293.

Pletikos, M., Sousa, A.M., Sedmak, G., Meyer, K.A., Zhu, Y., Cheng, F., Li, M., Kawasawa, Y.I., and Sestan, N. (2014). Temporal specification and bilaterality of human neocortical topographic gene expression. Neuron *81*, 321-332.

Poeta, L., Fusco, F., Drongitis, D., Shoubridge, C., Manganelli, G., Filosa, S., Paciolla, M., Courtney, M., Collombat, P., Lioi, M.B.*, et al.* (2013). A regulatory path associated with X-

linked intellectual disability and epilepsy links KDM5C to the polyalanine expansions in ARX. Am J Hum Genet *92*, 114-125.

Potocki, L., and Shaffer, L.G. (1996). Interstitial deletion of 11(p11.2p12): a newly described contiguous gene deletion syndrome involving the gene for hereditary multiple exostoses (EXT2). Am J Med Genet *62*, 319-325.

Qi, H.H., Sarkissian, M., Hu, G.Q., Wang, Z., Bhattacharjee, A., Gordon, D.B., Gonzales, M., Lan, F., Ongusaha, P.P., Huarte, M.*, et al.* (2010). Histone H4K20/H3K9 demethylase PHF8 regulates zebrafish brain and craniofacial development. Nature *466*, 503-507.

Qiao, Y., Liu, X., Harvard, C., Hildebrand, M.J., Rajcan-Separovic, E., Holden, J.J.A., and Lewis, M.E.S. (2008). Autism-associated familial microdeletion of Xp11.22. Clinical Genetics *74*, 134-144.

Qiu, J.H., Shi, G.A., Jia, Y.H., Li, J., Wu, M., Li, J.W., Dong, S., and Wong, J.M. (2010). The X-linked mental retardation gene PHF8 is a histone demethylase involved in neuronal differentiation. Cell Research *20*, 908-918.

Qu, Q., Takahashi, Y.H., Yang, Y., Hu, H., Zhang, Y., Brunzelle, J.S., Couture, J.F., Shilatifard, A., and Skiniotis, G. (2018). Structure and Conformational Dynamics of a COMPASS Histone H3K4 Methyltransferase Complex. Cell *174*, 1117-1126.e1112.

Raiymbek, G., An, S., Khurana, N., Gopinath, S., Trievel, R., Cho, U.-s., and Ragunathan, K. (2019). A non-enzymatic function associated with a putative histone demethylase licenses epigenetic inheritance (BioRxiv).

Ramírez, F., Dündar, F., Diehl, S., Grüning, B.A., and Manke, T. (2014). deepTools: a flexible platform for exploring deep-sequencing data. Nucleic Acids Res *42*, W187-191.

Ramírez, F., Ryan, D.P., Grüning, B., Bhardwaj, V., Kilpert, F., Richter, A.S., Heyne, S., Dündar, F., and Manke, T. (2016). deepTools2: a next generation web server for deep-sequencing data analysis. Nucleic Acids Res *44*, W160-165.

Rao, R.C., and Dou, Y. (2015). Hijacked in cancer: the KMT2 (MLL) family of methyltransferases. Nat Rev Cancer *15*, 334-346.

Ronan, J.L., Wu, W., and Crabtree, G.R. (2013). From neural development to cognition: unexpected roles for chromatin. Nat Rev Genet *14*, 347-359.

Rondinelli, B., Schwerer, H., Antonini, E., Gaviraghi, M., Lupi, A., Frenquelli, M., Cittaro, D., Segalla, S., Lemaitre, J.M., and Tonon, G. (2015). H3K4me3 demethylation by the histone demethylase KDM5C/JARID1C promotes DNA replication origin firing. Nucleic Acids Res *43*, 2560-2574.

Ropers, H.H., and Hamel, B.C. (2005). X-linked mental retardation. Nat Rev Genet *6*, 46-57.

Rossler, T., and Marschalek, R. (2013). An alternative splice process renders the MLL protein either into a transcriptional activator or repressor. Pharmazie *68*, 601-607.

Rothbart, S.B., Krajewski, K., Strahl, B.D., and Fuchs, S.M. (2012). Peptide microarrays to interrogate the "histone code". Methods Enzymol *512*, 107-135.

Ruault, M., Brun, M.E., Ventura, M., Roizes, G., and De Sario, A. (2002). MLL3, a new human member of the TRX/MLL gene family, maps to 7q36, a chromosome region frequently deleted in myeloid leukaemia. Gene *284*, 73-81.

Rujirabanjerd, S., Nelson, J., Tarpey, P.S., Hackett, A., Edkins, S., Raymond, F.L., Schwartz, C.E., Turner, G., Iwase, S., Shi, Y.*, et al.* (2010). Identification and characterization of two novel JARID1C mutations: suggestion of an emerging genotype-phenotype correlation. European journal of human genetics : EJHG *18*, 330-335.

Ruthenburg, A.J., Allis, C.D., and Wysocka, J. (2007). Methylation of lysine 4 on histone H3: intricacy of writing and reading a single epigenetic mark. Mol Cell *25*, 15-30.

S, G., E, M., Y, M.-N., CN, V., RS, P., PM, G., S, I., S, K., and Kalantry, V.O. (2017). Induction of X-chromosome Inactivation by the Histone Demethylase SMCX/KDM5C (biorxiv: Cold Spring Harbor Laboratory).

Santos, C., Rodriguez-Revenga, L., Madrigal, I., Badenas, C., Pineda, M., and Mila, M. (2006). A novel mutation in JARID1C gene associated with mental retardation. European journal of human genetics : EJHG *14*, 583-586.

Santos-Reboucas, C.B., Fintelman-Rodrigues, N., Jensen, L.R., Kuss, A.W., Ribeiro, M.G., Campos, M., Jr., Santos, J.M., and Pimentel, M.M. (2011). A novel nonsense mutation in KDM5C/JARID1C gene causing intellectual disability, short stature and speech delay. Neuroscience letters *498*, 67-71.

Scandaglia, M., Lopez-Atalaya, J.P., Medrano-Fernandez, A., Lopez-Cascales, M.T., Del Blanco, B., Lipinski, M., Benito, E., Olivares, R., Iwase, S., Shi, Y.*, et al.* (2017). Loss of Kdm5c Causes Spurious Transcription and Prevents the Fine-Tuning of Activity-Regulated Enhancers in Neurons. Cell Rep *21*, 47-59.

Schaefer, E., Durand, M., Stoetzel, C., Doray, B., Viville, B., Hellé, S., Danse, J.M., Hamel, C., Bitoun, P., Goldenberg, A.*, et al.* (2011). Molecular diagnosis reveals genetic heterogeneity for the overlapping MKKS and BBS phenotypes. Eur J Med Genet *54*, 157-160.

Schmitz, S.U., Albert, M., Malatesta, M., Morey, L., Johansen, J.V., Bak, M., Tommerup, N., Abarrategui, I., and Helin, K. (2011). Jarid1b targets genes regulating development and is involved in neural differentiation. EMBO J *30*, 4586-4600.

Scibetta, A.G., Santangelo, S., Coleman, J., Hall, D., Chaplin, T., Copier, J., Catchpole, S., Burchell, J., and Taylor-Papadimitriou, J. (2007). Functional analysis of the transcription repressor PLU-1/JARID1B. Mol Cell Biol *27*, 7220-7235.

Shaffer, L.G., Hecht, J.T., Ledbetter, D.H., and Greenberg, F. (1993). Familial interstitial deletion 11(p11.12p12) associated with parietal foramina, brachymicrocephaly, and mental retardation. Am J Med Genet *45*, 581-583.

Shah, R.N., Grzybowski, A.T., Cornett, E.M., Johnstone, A.L., Dickson, B.M., Boone, B.A., Cheek, M.A., Cowles, M.W., Maryanski, D., Meiners, M.J., *et al.* (2018). Examining the Roles of H3K4 Methylation States with Systematically Characterized Antibodies. Molecular cell *72*, 162-177 e167.

Shao, G.B., Chen, J.C., Zhang, L.P., Huang, P., Lu, H.Y., Jin, J., Gong, A.H., and Sang, J.R. (2014). Dynamic patterns of histone H3 lysine 4 methyltransferases and demethylases during mouse preimplantation development. In Vitro Cell Dev Biol Anim.

Shen, E., Shulha, H., Weng, Z., and Akbarian, S. (2014). Regulation of histone H3K4 methylation in brain development and disease. Philos Trans R Soc Lond B Biol Sci *369*.

Shen, H., Xu, W., Guo, R., Rong, B., Gu, L., Wang, Z., He, C., Zheng, L., Hu, X., Hu, Z., *et al.* (2016). Suppression of Enhancer Overactivation by a RACK7-Histone Demethylase Complex. Cell *165*, 331-342.

Shi, Y., Lan, F., Matson, C., Mulligan, P., Whetstine, J.R., Cole, P.A., and Casero, R.A. (2004). Histone demethylation mediated by the nuclear amine oxidase homolog LSD1. Cell *119*, 941-953.

Shi, Y.J., Matson, C., Lan, F., Iwase, S., Baba, T., and Shi, Y. (2005). Regulation of LSD1 histone demethylase activity by its associated factors. Molecular Cell *19*, 857-864.

Shilatifard, A. (2012). The COMPASS family of histone H3K4 methylases: mechanisms of regulation in development and disease pathogenesis. Annu Rev Biochem *81*, 65-95.

Shmelkov, S.V., Hormigo, A., Jing, D., Proenca, C.C., Bath, K.G., Milde, T., Shmelkov, E., Kushner, J.S., Baljevic, M., Dincheva, I., *et al.* (2010). Slitrk5 deficiency impairs corticostriatal circuitry and leads to obsessive-compulsive-like behaviors in mice. Nature medicine *16*, 598-602, 591p following 602.

Shulha, H.P., Cheung, I., Guo, Y., Akbarian, S., and Weng, Z. (2013). Coordinated cell type-specific epigenetic remodeling in prefrontal cortex begins before birth and continues into early adulthood. PLoS Genet *9*, e1003433.

Shulha, H.P., Cheung, I., Whittle, C., Wang, J., Virgil, D., Lin, C.L., Guo, Y., Lessard, A., Akbarian, S., and Weng, Z. (2012a). Epigenetic signatures of autism: trimethylated H3K4 landscapes in prefrontal neurons. Arch Gen Psychiatry *69*, 314-324.

Shulha, H.P., Crisci, J.L., Reshetov, D., Tushir, J.S., Cheung, I., Bharadwaj, R., Chou, H.J., Houston, I.B., Peter, C.J., Mitchell, A.C., *et al.* (2012b). Human-specific histone methylation signatures at transcription start sites in prefrontal neurons. PLoS biology *10*, e1001427.

Siderius, L.E., Hamel, B.C.J., van Bokhoven, H., de Jager, F., van den Helm, B., Kremer, H., Heineman-de Boer, J.A., Ropers, H.H., and Mariman, E.C.M. (1999). X-linked mental retardation associated with cleft lip palate maps to Xp11.3-q21.3. American Journal of Medical Genetics *85*, 216-220.

Simensen, R.J., Rogers, R.C., Collins, J.S., Abidi, F., Schwartz, C.E., and Stevenson, R.E. (2012). Short-term memory deficits in carrier females with KDM5C mutations. Genet Couns *23*, 31-40.

Sirmaci, A., Spiliopoulos, M., Brancati, F., Powell, E., Duman, D., Abrams, A., Bademci, G., Agolini, E., Guo, S., Konuk, B.*, et al.* (2011). Mutations in ANKRD11 cause KBG syndrome, characterized by intellectual disability, skeletal malformations, and macrodontia. Am J Hum Genet *89*, 289-294.

Slavotinek, A.M., Stone, E.M., Mykytyn, K., Heckenlively, J.R., Green, J.S., Heon, E., Musarella, M.A., Parfrey, P.S., Sheffield, V.C., and Biesecker, L.G. (2000). Mutations in MKKS cause Bardet-Biedl syndrome. Nat Genet *26*, 15-16.

Smith, T., Heger, A., and Sudbery, I. (2017). UMI-tools: modeling sequencing errors in Unique Molecular Identifiers to improve quantification accuracy. Genome Res *27*, 491-499.

Soshnikova, N., and Duboule, D. (2008). Epigenetic regulation of Hox gene activation: the waltz of methyls. Bioessays *30*, 199-202.

Stone, D.L., Slavotinek, A., Bouffard, G.G., Banerjee-Basu, S., Baxevanis, A.D., Barr, M., and Biesecker, L.G. (2000). Mutation of a gene encoding a putative chaperonin causes McKusick-Kaufman syndrome. Nat Genet *25*, 79-82.

Strahl, B.D., and Allis, C.D. (2000). The language of covalent histone modifications. Nature *403*, 41-45.

Strom, S.P., Lozano, R., Lee, H., Dorrani, N., Mann, J., O'Lague, P.F., Mans, N., Deignan, J.L., Vilain, E., Nelson, S.F.*, et al.* (2014). De Novo variants in the KMT2A (MLL) gene causing atypical Wiedemann-Steiner syndrome in two unrelated individuals identified by clinical exome sequencing. BMC Med Genet *15*, 49.

Tahiliani, M., Mei, P., Fang, R., Leonor, T., Rutenberg, M., Shimizu, F., Li, J., Rao, A., and Shi, Y. (2007a). The histone H3K4 demethylase SMCX links REST target genes to X-linked mental retardation. Nature *447*, 601-605.

Tahiliani, M., Mei, P.C., Fang, R., Leonor, T., Rutenberg, M., Shimizu, F., Li, J., Rao, A., and Shi, Y.J. (2007b). The histone H3K4 demethylase SMCX links REST target genes to X-linked mental retardation. Nature *447*, 601-+.

Takata, A., Xu, B., Ionita-Laza, I., Roos, J.L., Gogos, J.A., and Karayiorgou, M. (2014). Loss-of-function variants in schizophrenia risk and SETD1A as a candidate susceptibility gene. Neuron *82*, 773-780.

Tan, Y.C., and Chow, V.T. (2001). Novel human HALR (MLL3) gene encodes a protein homologous to ALR and to ALL-1 involved in leukemia, and maps to chromosome 7q36 associated with leukemia and developmental defects. Cancer Detect Prev *25*, 454-469.

Tasic, B., Menon, V., Nguyen, T.N., Kim, T.K., Jarsky, T., Yao, Z., Levi, B., Gray, L.T., Sorensen, S.A., Dolbeare, T.*, et al.* (2016). Adult mouse cortical cell taxonomy revealed by single cell transcriptomics. Nature neuroscience *19*, 335-346.

Taverna, S.D., Li, H., Ruthenburg, A.J., Allis, C.D., and Patel, D.J. (2007). How chromatin-binding modules interpret histone modifications: lessons from professional pocket pickers. Nat Struct Mol Biol *14*, 1025-1040.

Tchessalova, D., and Tronson, N.C. (2019). Memory deficits in males and females long after subchronic immune challenge. Neurobiol Learn Mem.

Tsai, M.C., Manor, O., Wan, Y., Mosammaparast, N., Wang, J.K., Lan, F., Shi, Y., Segal, E., and Chang, H.Y. (2010). Long noncoding RNA as modular scaffold of histone modification complexes. Science *329*, 689-693.

Tsukada, Y., Fang, J., Erdjument-Bromage, H., Warren, M.E., Borchers, C.H., Tempst, P., and Zhang, Y. (2006). Histone demethylation by a family of JmjC domain-containing proteins. Nature *439*, 811-816.

Tsurusaki, Y., Okamoto, N., Ohashi, H., Kosho, T., Imai, Y., Hibi-Ko, Y., Kaname, T., Naritomi, K., Kawame, H., Wakui, K.*, et al.* (2012). Mutations affecting components of the SWI/SNF complex cause Coffin-Siris syndrome. Nat Genet *44*, 376-378.

Tunovic, S., Barkovich, J., Sherr, E.H., and Slavotinek, A.M. (2014). De novo ANKRD11 and KDM1A gene mutations in a male with features of KBG syndrome and Kabuki syndrome. Am J Med Genet A *164*, 1744-1749.

Tzschach, A., Lenzner, S., Moser, B., Reinhardt, R., Chelly, J., Fryns, J.P., Kleefstra, T., Raynaud, M., Turner, G., Ropers, H.H.*, et al.* (2006). Novel JARID1C/SMCX mutations in patients with X-linked mental retardation. Hum Mutat *27*, 389.

Vallianatos, C., Raines, B., Porter, R., Wu, M., Garay, P., Collette, K., Seo, Y., Dou, Y., Keegan, C., Tronson, N.*, et al.* (2019). Amelioration of Brain Histone Methylopathies by Balancing a Writer-Eraser Duo KMT2A-KDM5C (BioRxiv).

Vallianatos, C.N., Farrehi, C., Friez, M.J., Burmeister, M., Keegan, C.E., and Iwase, S. (2018). Altered Gene-Regulatory Function of KDM5C by a Novel Mutation Associated With Autism and Intellectual Disability. Front Mol Neurosci *11*, 104.

Vallianatos, C.N., and Iwase, S. (2015). Disrupted intricacy of histone H3K4 methylation in neurodevelopmental disorders. Epigenomics *7*, 503-519.

van Bokhoven, H. (2011). Genetic and epigenetic networks in intellectual disabilities. Annual review of genetics *45*, 81-104.

Varholick, J.A., Bailoo, J.D., Palme, R., and Würbel, H. (2018). Phenotypic variability between Social Dominance Ranks in laboratory mice. Sci Rep *8*, 6593.

Vermeulen, M., Mulder, K.W., Denissov, S., Pijnappel, W.W., van Schaik, F.M., Varier, R.A., Baltissen, M.P., Stunnenberg, H.G., Mann, M., and Timmers, H.T. (2007). Selective anchoring of TFIID to nucleosomes by trimethylation of histone H3 lysine 4. Cell *131*, 58-69.

Vinogradova, M., Gehling, V.S., Gustafson, A., Arora, S., Tindell, C.A., Wilson, C., Williamson, K.E., Guler, G.D., Gangurde, P., Manieri, W.*, et al.* (2016). An inhibitor of KDM5 demethylases reduces survival of drug-tolerant cancer cells. Nature chemical biology.

Vissers, L.E., de Ligt, J., Gilissen, C., Janssen, I., Steehouwer, M., de Vries, P., van Lier, B., Arts, P., Wieskamp, N., del Rosario, M.*, et al.* (2010). A de novo paradigm for mental retardation. Nat Genet *42*, 1109-1112.

Vogel-Ciernia, A., and Wood, M.A. (2014). Examining object location and object recognition memory in mice. Curr Protoc Neurosci *69*, 8.31.31-17.

Wang, F., Kessels, H.W., and Hu, H. (2014). The mouse that roared: neural mechanisms of social hierarchy. Trends Neurosci *37*, 674-682.

Wang, J., Hevi, S., Kurash, J.K., Lei, H., Gay, F., Bajko, J., Su, H., Sun, W., Chang, H., Xu, G.*, et al.* (2009a). The lysine demethylase LSD1 (KDM1) is required for maintenance of global DNA methylation. Nat Genet *41*, 125-129.

Wang, J., Muntean, A.G., Wu, L., and Hess, J.L. (2012). A subset of mixed lineage leukemia proteins has plant homeodomain (PHD)-mediated E3 ligase activity. J Biol Chem *287*, 43410-43416.

Wang, J.X., Scully, K., Zhu, X., Cai, L., Zhang, J., Prefontaine, G.G., Krones, A., Ohgi, K.A., Zhu, P., Garcia-Bassets, I.*, et al.* (2007). Opposing LSD1 complexes function in developmental gene activation and repression programmes. Nature *446*, 882-887.

Wang, K.C., Yang, Y.W., Liu, B., Sanyal, A., Corces-Zimmerman, R., Chen, Y., Lajoie, B.R., Protacio, A., Flynn, R.A., Gupta, R.A.*, et al.* (2011). A long noncoding RNA maintains active chromatin to coordinate homeotic gene expression. Nature *472*, 120-124.

Wang, P., Lin, C., Smith, E.R., Guo, H., Sanderson, B.W., Wu, M., Gogol, M., Alexander, T., Seidel, C., Wiedemann, L.M.*, et al.* (2009b). Global analysis of H3K4 methylation defines MLL family member targets and points to a role for MLL1-mediated H3K4 methylation in the regulation of transcriptional initiation by RNA polymerase II. Mol Cell Biol *29*, 6074-6085.

Wang, Z., Song, J., Milne, T.A., Wang, G.G., Li, H., Allis, C.D., and Patel, D.J. (2010). Pro isomerization in MLL1 PHD3-bromo cassette connects H3K4me readout to CyP33 and HDAC-mediated repression. Cell *141*, 1183-1194.

Webb, E.A., AlMutair, A., Kelberman, D., Bacchelli, C., Chanudet, E., Lescai, F., Andoniadou, C.L., Banyan, A., Alsawaid, A., Alrifai, M.T.*, et al.* (2013). ARNT2 mutation causes hypopituitarism, post-natal microcephaly, visual and renal anomalies. Brain *136*, 3096-3105.

Whyte, W.A., Bilodeau, S., Orlando, D.A., Hoke, H.A., Frampton, G.M., Foster, C.T., Cowley, S.M., and Young, R.A. (2012). Enhancer decommissioning by LSD1 during embryonic stem cell differentiation. Nature *482*, 221-225.

Wiedemann, H.R. (1989). Genital overgrowth in the EMG syndrome. Am J Med Genet *32*, 255-256.

Wu, J., Ellison, J., Salido, E., Yen, P., Mohandas, T., and Shapiro, L.J. (1994a). Isolation and characterization of XE169, a novel human gene that escapes X-inactivation. Hum Mol Genet *3*, 153-160.

Wu, J., Salido, E.C., Yen, P.H., Mohandas, T.K., Heng, H.H., Tsui, L.C., Park, J., Chapman, V.M., and Shapiro, L.J. (1994b). The murine Xe169 gene escapes X-inactivation like its human homologue. Nat Genet *7*, 491-496.

Wu, M., Wang, P.F., Lee, J.S., Martin-Brown, S., Florens, L., Washburn, M., and Shilatifard, A. (2008). Molecular regulation of H3K4 trimethylation by Wdr82, a component of human Set1/COMPASS. Mol Cell Biol *28*, 7337-7344.

Wynder, C., Stalker, L., and Doughty, M.L. (2010). Role of H3K4 demethylases in complex neurodevelopmental diseases. Epigenomics *2*, 407-418.

Wysocka, J., Swigut, T., Xiao, H., Milne, T.A., Kwon, S.Y., Landry, J., Kauer, M., Tackett, A.J., Chait, B.T., Badenhorst, P.*, et al.* (2006). A PHD finger of NURF couples histone H3 lysine 4 trimethylation with chromatin remodelling. Nature *442*, 86-90.

Xiang, Y., Zhu, Z., Han, G., Ye, X., Xu, B., Peng, Z., Ma, Y., Yu, Y., Lin, H., Chen, A.P.*, et al.* (2007). JARID1B is a histone H3 lysine 4 demethylase up-regulated in prostate cancer. Proc Natl Acad Sci U S A *104*, 19226-19231.

Xie, L., Pelz, C., Wang, W., Bashar, A., Varlamova, O., Shadle, S., and Impey, S. (2011). KDM5B regulates embryonic stem cell self-renewal and represses cryptic intragenic transcription. EMBO J *30*, 1473-1484.

Xu, J., Burgoyne, P.S., and Arnold, A.P. (2002). Sex differences in sex chromosome gene expression in mouse brain. Hum Mol Genet *11*, 1409-1419.

Xu, J., Deng, X., and Disteche, C.M. (2008). Sex-specific expression of the X-linked histone demethylase gene Jarid1c in brain. PloS one *3*, e2553.

Xu, X., Miller, E.C., and Pozzo-Miller, L. (2014). Dendritic spine dysgenesis in Rett syndrome. Front Neuroanat *8*, 97.

Yamane, K., Tateishi, K., Klose, R.J., Fang, J., Fabrizio, L.A., Erdjument-Bromage, H., Taylor-Papadimitriou, J., Tempst, P., and Zhang, Y. (2007). PLU-1 is an H3K4 demethylase involved in transcriptional repression and breast cancer cell proliferation. Mol Cell *25*, 801-812.

Yang, Y.W., Flynn, R.A., Chen, Y., Qu, K., Wan, B., Wang, K.C., Lei, M., and Chang, H.Y. (2014). Essential role of lncRNA binding for WDR5 maintenance of active chromatin and embryonic stem cell pluripotency. Elife *3*, e02046.

Zeleznik-Le, N.J., Harden, A.M., and Rowley, J.D. (1994). 11q23 translocations split the "AT-hook" cruciform DNA-binding region and the transcriptional repression domain from the activation domain of the mixed-lineage leukemia (MLL) gene. Proc Natl Acad Sci U S A *91*, 10610-10614.

Zhang, H., Gayen, S., Xiong, J., Zhou, B., Shanmugam, A.K., Sun, Y., Karatas, H., Liu, L., Rao, R.C., Wang, S.*, et al.* (2016). MLL1 Inhibition Reprograms Epiblast Stem Cells to Naive Pluripotency. Cell stem cell *18*, 481-494.

Zhang, X.Q., Wang, Z.L., Poon, M.W., and Yang, J.H. (2017). Spatial-temporal transcriptional dynamics of long non-coding RNAs in human brain. Hum Mol Genet *26*, 3202-3211.

Zhang, Y., Chen, K., Sloan, S.A., Bennett, M.L., Scholze, A.R., O'Keeffe, S., Phatnani, H.P., Guarnieri, P., Caneda, C., Ruderisch, N.*, et al.* (2014). An RNA-sequencing transcriptome and splicing database of glia, neurons, and vascular cells of the cerebral cortex. J Neurosci *34*, 11929-11947.

Zhang, Y., Liu, T., Meyer, C.A., Eeckhoute, J., Johnson, D.S., Bernstein, B.E., Nusbaum, C., Myers, R.M., Brown, M., Li, W.*, et al.* (2008). Model-based analysis of ChIP-Seq (MACS). Genome biology *9*, R137.

Zhou, B., Wang, J., Lee, S.Y., Xiong, J., Bhanu, N., Guo, Q., Ma, P., Sun, Y., Rao, R.C., Garcia, B.A.*, et al.* (2016). PRDM16 Suppresses MLL1r Leukemia via Intrinsic Histone Methyltransferase Activity. Mol Cell *62*, 222-236.

Zhou, T., Zhu, H., Fan, Z., Wang, F., Chen, Y., Liang, H., Yang, Z., Zhang, L., Lin, L., Zhan, Y.*, et al.* (2017). History of winning remodels thalamo-PFC circuit to reinforce social dominance. Science *357*, 162-168.

Zhu, J., Adli, M., Zou, J.Y., Verstappen, G., Coyne, M., Zhang, X., Durham, T., Miri, M., Deshpande, V., De Jager, P.L.*, et al.* (2013). Genome-wide chromatin state transitions associated with developmental and environmental cues. Cell *152*, 642-654.

Zibetti, C., Adamo, A., Binda, C., Forneris, F., Toffolo, E., Verpelli, C., Ginelli, E., Mattevi, A., Sala, C., and Battaglioli, E. (2010). Alternative splicing of the histone demethylase LSD1/KDM1 contributes to the modulation of neurite morphogenesis in the mammalian nervous system. J Neurosci *30*, 2521-2532.

Zieminvanderpoel, S., Mccabe, N.R., Gill, H.J., Espinosa, R., Patel, Y., Harden, A., Rubinelli, P., Smith, S.D., Lebeau, M.M., Rowley, J.D.*, et al.* (1991). Identification of a Gene, Mll, That Spans the Breakpoint in 11q23 Translocations Associated with Human Leukemias. Proceedings of the National Academy of Sciences of the United States of America *88*, 10735-10739.